https://ntrs.nasa.gov/search.jsp?R=19820012452 2020-03-21T08:38:05+00:00Z

DYNAMIC CHARACTERIZATION AND ANALYSIS OF SPACE SHUTTLE SRM SOLID PROPELLANT

(NASA-CR-161227) DYNAMIC CHARACTERIZATION AND ANALYSIS OF SPACE SHUTTLE SRM SOLID PROPELLANT Final Report (Hufferd (W. L.) and Associates) 216 p HC A10/MF A01 CSCL 21I G3/28

N82-20326

Unclas 16751

By

William L. Hufferd

April 1979

FINAL REPORT

Prepared under Contract No. NAS8-32234

by

W. L. HUFFERD & ASSOCIATES
Consulting Engineers
2826 Devereaux Way
Salt Lake City, Utah 84109

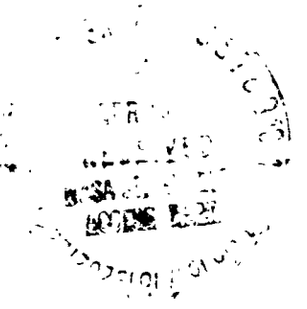

DYNAMIC CHARACTERIZATION AND ANALYSIS OF SPACE SHUTTLE SRM SOLID PROPELLANT

By

William L. Hufferd

April 1979

FINAL REPORT

Prepared under Contract No. NAS8-32234

by

W. L. HUFFERD & ASSOCIATES
Consulting Engineers
2826 Devereaux Way
Salt Lake City, Utah 84109

For

National Aeronautics & Space Administration
George C. Marshall Space Flight Center
Marshall Space Flight Center, Alabama 35812

PREFACE

This report discusses work performed under NASA Contract NAS8-32234 for the George C. Marshall Space Flight Center. The cognizant technical officer was Mr. Frank Bugg, to whom we express our appreciation for his valuable assistance in obtaining the propellant for the dynamic property characterization testing.

ABSTRACT

The results of a research study to characterize the dynamic response properties of the Space Shuttle SRM (TP-H1148) propellant and to establish the expected limits of propellant variability is presented in this final report.

Dynamic shear modulus tests were conducted on six production batches of TP-H1148 at various static and dynamic strain levels over the temperature range from 40°F to 90°F.

A heat conduction analysis and dynamic response analysis of the Shuttle SRM were also conducted.

The dynamic test results show significant dependence on static and dynamic strain levels and considerable batch-to-batch and within-batch variability. However, the results of the SRM dynamic response analyses clearly demonstrate that the stiffness of the propellant has no consequential effect on the overall SRM dynamic response. Only the mass of the propellant needs to be considered in the dynamic analysis of the Shuttle SRM.

Based on the results of the SRM dynamic analysis it is concluded that no special tests are required for quality control of the SRM propellant dynamic response properties.

TABLE OF CONTENTS

LIST OF FIGURES

LIST OF TABLES

NOMENCLATURE

a_T = time-temperature shift function

a = propellant grain inner radius

A = cross-sectional area

A_n = end-fixity parameter

b = propellant grain outer radius

c = specific heat capacity

C = damping coefficient

D = dissipation function

E = tensile modulus

E* = complex tensile modulus

E_o = coefficient in power-law representation of dynamic modulus

E_1 = coefficient in power-law representation of relaxation modulus

E_e = long-time equilibrium relaxation modulus

E_g = short-time glassy relaxation modulus

E_k = coefficients in the Prony series representation of the relaxation modulus

E_{rel} = relaxation modulus

g = acceleration of gravity

G = shear modulus

G* = complex shear modulus

H = heat flow vector

k = coefficient of thermal conductivity

K = bulk modulus

K* = complex bulk modulus

$[K]$ = stiffness matrix

L = propellant grain length

m = exponent in temperature shift-factor representation

$[M]$ = mass matrix

n = acceleration in g's

n = exponent in power-law representation of dynamic modulus

Q = thermal force

$\{r\}$ = nodal point displacement vector

$[R]$ = nodal point force vector

R = strain rate in constant strain rate test

t = case thickness

t = time

T = temperature

T_a = experimentally determined constant in temperature shift-factor representation

T_a = grain inner temperature

T_g = glass transition temperature

T_s = $T_g + 50°C$

T_R = reference temperature

$u(t)$ = Heaviside unit step function

V = thermal potential

ε = dilatation or uniaxial strain

ε^* = complex strain amplitude

δ = loss tangent

κ = thermal diffusivity = $\frac{k}{\rho c}$

ρ = density

τ_o = characteristic time

τ_k = time constant in Prony series representation of relaxation modulus

σ = uniaxial (or shear) stress

σ = standard deviation

σ^* = complex stress amplitude

ν = Poisson's ratio

ω = frequency

Ω_n = circular frequency coefficient

ζ = structural damping coefficient

Superscripts

m = model parameter

' = prime = real part of complex quantity

" = double prime = imaginary part of complex quantity

Subscripts

c = case property

p = propellant property

DYNAMIC CHARACTERIZATION AND ANALYSIS OF SPACE SHUTTLE SRM SOLID PROPELLANT

I. INTRODUCTION

The program objectives were to perform a dynamic shear modulus characterization of TP-H1148 (Space Shuttle) propellant and to investigate the sensitivity of the Shuttle Solid Rocket Motor (SRM) dynamic response to propellant modulus variability associated with batch-to-batch and within-batch casting variations and temperature variations in the SRM.

Specific tasks included:

TASK 1: DYNAMIC SHEAR MODULUS CHARACTERIZATION

A. Examine and analyze existing dynamic response test data for TP-H1148 propellant and other similar solid propellants.

B. Experimentally determine dynamic shear response properties of TP-H1148 propellant as a function of frequency, temperature and strain level.

C. Perform statistical analyses of dynamic shear data obtained to establish probability distributions associated with batch-to-batch and within-batch variability.

D. Extend the SRM propellant dynamic response model to include the effects of propellant variability found in Task 1-B, and strain level, if necessary.

TASK 2: SRM DYNAMIC RESPONSE ANALYSES

Examine the sensitivity of the SRM frequency and mode shape response to the propellant variability expected based on the results of Task 1 and to modulus gradients throughout the grain web associated with a nonuniform temperature distribution and batch-to-batch propellant variability.

TASK 3: IDENTIFY TEST REQUIREMENTS

Based on the results of Tasks 1 and 2, recommend the tests required to characterize the dynamic response of each propellant casting and each SRM segment.

The analysis effort and test data interpretation were carried out by W. L. Hufferd & Associates, and the characterization of TP-H1148 propellant, supplied by Thiokol Corporation, Wasatch Division, was conducted by the Chemical Systems Division (CSD) of United Technologies Corporation under a subcontract from W. L. Hufferd & Associates.

This final report presents the details of the research study. All technical objectives have been accomplished. The complete final report from CSD on the dynamic characterization of TP-H1148 propellant is included as Appendix A to this report.

II. SUMMARY OF ACCOMPLISHMENTS

All technical requirements and objectives of the research study have been met.

2.1 TASK 1: DYNAMIC SHEAR MODULUS CHARACTERICATION

Propellant characterization tests were conducted by CSD on material from one 600 galon batch (TP-H1148-9) and five other batches (TP-H1148-6,-7,-8,-9970096 and -9970115). The dynamic shear modulus of the six SRM solid propellant batches was measured at various static and dynamic strain levels. Constant elongation rate properties were also measured at 2 in/min at 0°F, 40°F, 70°F, 90°F and 120°F, and the viscoelastic relaxation modulus was measured at 40°F, 70°F and 90°F.

The test data show very small batch-to-batch propellant variability and excellent sample-to-sample reproducibility. Dynamic propellant modulus values were sensitive to the static compressive strain level as well as dynamic strain. The test strain levels covered 0.001% to 3% and a correspondingly large modulus range. This strain range should be applicable to the shuttle SRM dynamic loading conditions [1-5]. Specific modulus values for dynamic analyses can be selected from the data presented at the appropriate frequency and strain levels and used with a NASTRAN analysis.

Additional statistical analyses of available test data for similar propellants and for TP-H1148 characterized by Thiokol/Wasatch Division [5-11] were performed to establish expected propellant variability.

Finally, the SRM propellant dynamic response model developed in [4] was extended to include the effects of propellant variability.

2.2 TASK 2: SRM DYNAMIC RESPONSE ANALYSES

Dynamic response analyses of a typical SRM segment were performed to examine the sensitivity of the SRM frequency and mode shape responses to propellant variability and to modulus variations associated with a non-uniform temperature gradient likely to exist in the SRM at the time of launch. It was found that the SRM dynamic response is insensitive to propellant variability and that no significant temperature gradients would exist through the SRM propellant web at the time of launch. The propellant provides most of the mass, but the case provides almost all of the stiffness due to the large differences between the propellant and case moduli at all temperatures, frequency and strain levels of interest in the Shuttle SRM.

2.3 TASK 3: IDENTIFY TEST REQUIREMENTS

Based on the insensitivity of the SRM dynamic response to propellant variability it is concluded that no special quality assurance testing is required for the dynamic response properties of TP-H1148 propellant. The normal quality control tests for ignition, burn rate and static mechanical properties are sufficient to indicate anomalous batch behavior. It must be emphasized, however, that anomalous behavior of one or even several castings of propellant, will still have an insignificant effect on the shuttle SRM dynamic response.

III. DYNAMIC RESPONSE OF RELATED PROPELLANTS

In addition to characterizing TP-H1148 propellant during this program existing published data on TP-H1148 and similar related propellants were reviewed and analyzed to provide a broader data base for subsequent statistical analyses. Dynamic mechanical property tests have been conducted at the University of Utah [7] on the inert UTI-610 PBAN propellant used in the NASA/Langley dynamic model tests [5]. Thiokol/Wasatch has characterized live and inert TP-H1123 PBAN propellant [6], which closely resembles the SRM propellant, as well as TP-H1148 propellant [10,11]. The Space Division of Rockwell International [8,9] has also conducted dynamic tests in support of one-quarter scale model tests; however, these data are difficult to analyze and draw conclusions from since non-standard tests were used and the test procedures are not well documented.

3.1 UNIVERSITY OF UTAH TESTS

Characterization tests were conducted on the inert solid propellant cast in the 1/8 scale models of the space shuttle SRB dynamically tested at the NASA/Langley Research Center [5]. Static and dynamic tests were conducted to evaluate the interconvertibility of static and dynamic response properties according to linear viscoelasticity theory. These tests were carried out at several temperatures and the time (frequency)-temperature superposition principle used to extend the range of applicability of the data. Some tests were also conducted to evaluate

the effects of moisture (i.e., relative humidity) on propellant response and also the effects of static strain level.

The propellant, designated UTI-610, is an inert Polybutadiene Acrylo-Nitrile (PBAN) propellant with ammonium sulfate and sodium chloride replacing the normal oxidizer, ammonium perchlorate. The propellant samples and models were manufactured by the Chemical Systems Division of United Technologies Corporation, Sunnyvale, California.

Propellant for the experimental characterization program was received from Nasa/Langeley Research Center in sealed one-half gallon milk cartons. Specimens 1.27 cm by 1.27 cm by 10.2 cm (0.5 in by 0.5 in by 4.0 in) were machined and wooden tabs bonded to the ends for the static testing, i.e., constant strain-rate and stress relaxation tests. Thin slabs, .1 cm by .3 cm by .2 cm (0.04 in by 0.12 in by 0.8 in) were used for the dynamic tension tests and slabs .15 cm by .15 cm by .3 cm (0.06 in by 0.06 in by 0.12 in) were used for the dynamic shear tests. Test specimen configurations are shown in Figure 1.

A minimum of three and usually four replicate tests were carried out for each condition.

The test methods employed conformed to standard industry-wide practices [12-14]. An Instron Universal testing machine (Figure 2) with Missimer temperature conditioning box was used for static testing and a Rheovibron dynamic tester (Figure 3) was used for the dynamic tests.

Static and dynamic tests were conducted at -18°C (0°F), 4°C (40°F), 25°C (77°F) and 49°C (120°F) and time-temperature superposition used

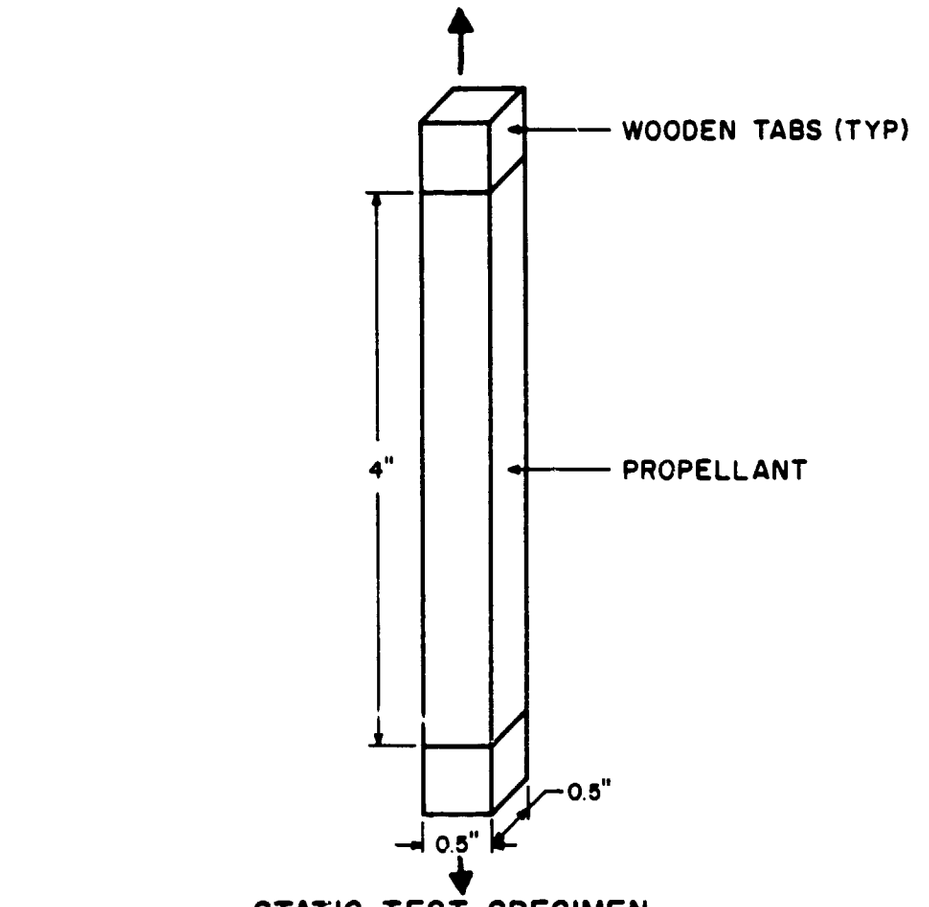

STATIC TEST SPECIMEN

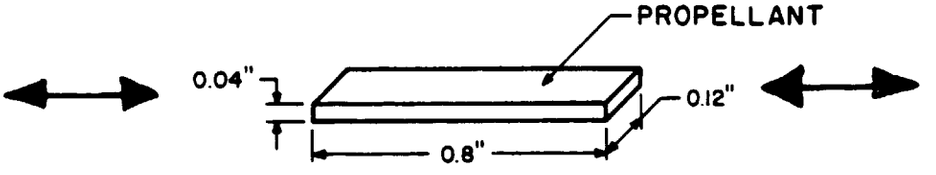

DYNAMIC TENSION TEST SPECIMEN

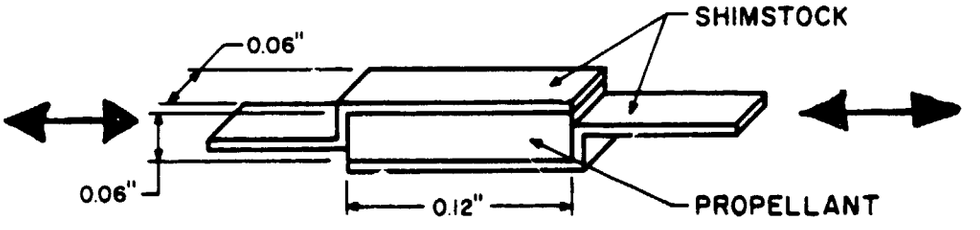

DYNAMIC SHEAR TEST SPECIMEN

FIGURE 1 - Test Specimen Configurations

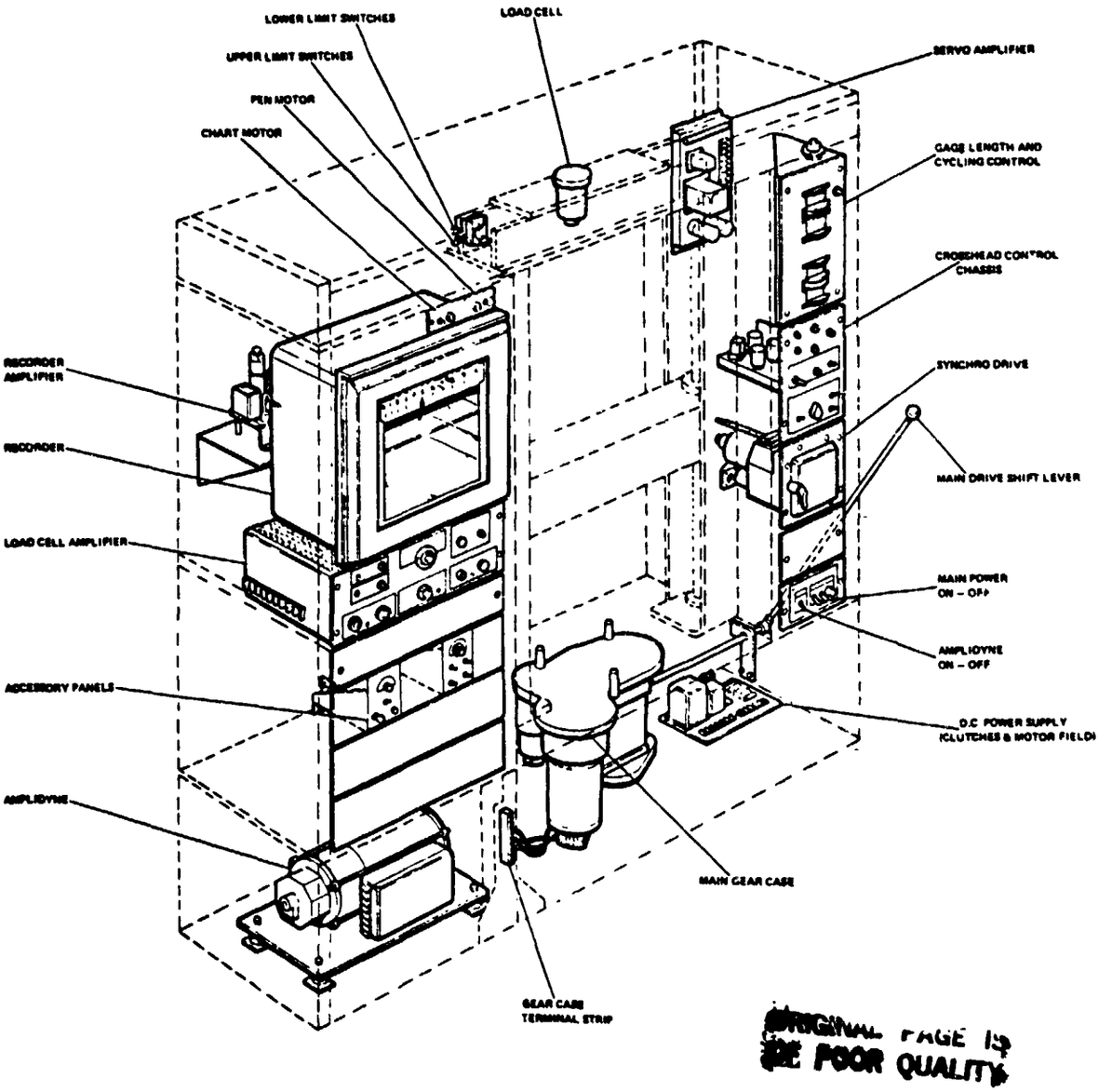

ORIGINAL PAGE IS OF POOR QUALITY

FIGURE 2 - Schematic of Instron
Universal Testing Machine

ORIGINAL PAGE IS
OF POOR QUALITY

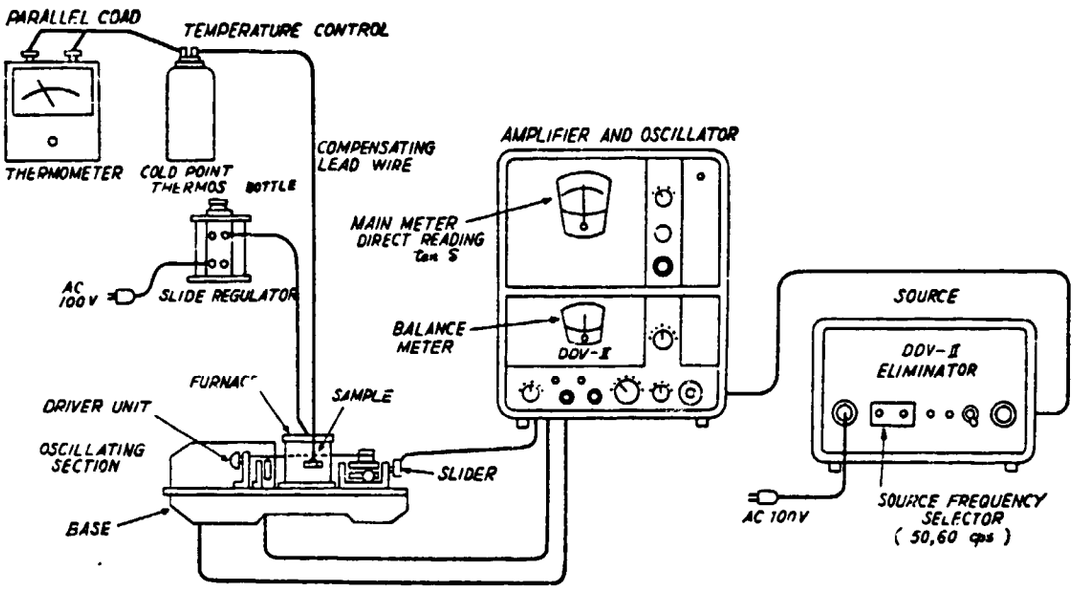

FIGURE 3 - Schematic of Rheovibron Dynamic Tester

to evaluate the response properties at other temperatures and frequencies.[1]

Constant strain rate tests were conducted at the strain rates and temperatures shown in Table I. True stress-strain response is shown in Figure 4.

Stress relaxation tests were conducted according to Table II. Relaxation modulus as a function of log time and strain level is shown in Figure 5. With the exception of the one-percent strain level tests at 4°C the average values of the one and five-percent strain level test data were within the $\pm$ 3σ data band associated with the three-percent strain level tests.

Figure 6 shows the time-temperature shift factor versus temperature as determined from stress-relaxation tests, dynamic tension and

---

[1] It has been widely found that temperature has the effect of expanding or contracting the time scale of response viscoelastic materials and that an equivalence between time or frequency and temperature exists. Time and frequency are roughly the inverse of one another so that short time or high frequency response at one temperature corresponds to lower temperature. The converse holds true at higher temperatures. Thus, by obtaining propellant response at several temperatures, a time-temperature shift function, a_T, relating the equivalence of time or frequency and temperature can be experimentally determined by horizontally "shifting" the test data so that it superimposes to form a single curve at some given reference temperature, usually 21 to 25°C. The resulting curve is known as the "master" response curve and is expressed in terms of temperature-reduced time, t/a_T, in the case of the master-reduced frequency, ωa_T, in the case of the master dynamic moduli curves (See i.e., [12-15]).

Thus, conventional analyses remain valid in terms of the master relaxation and dynamic moduli if time, t, and frequency, ω, are replaced by temperature-reduced time, t/a_T, and frequency-reduced time, ωa_T, respectively.

TABLE I

CONSTANT STRAIN RATE TESTS

Strain Rate $(min)^{-1}$ \ Temperature (°C)	-18	4	25	49
5			X	X
0.5	X	X	X	X
0.05		X	X	
0.005	X		X	

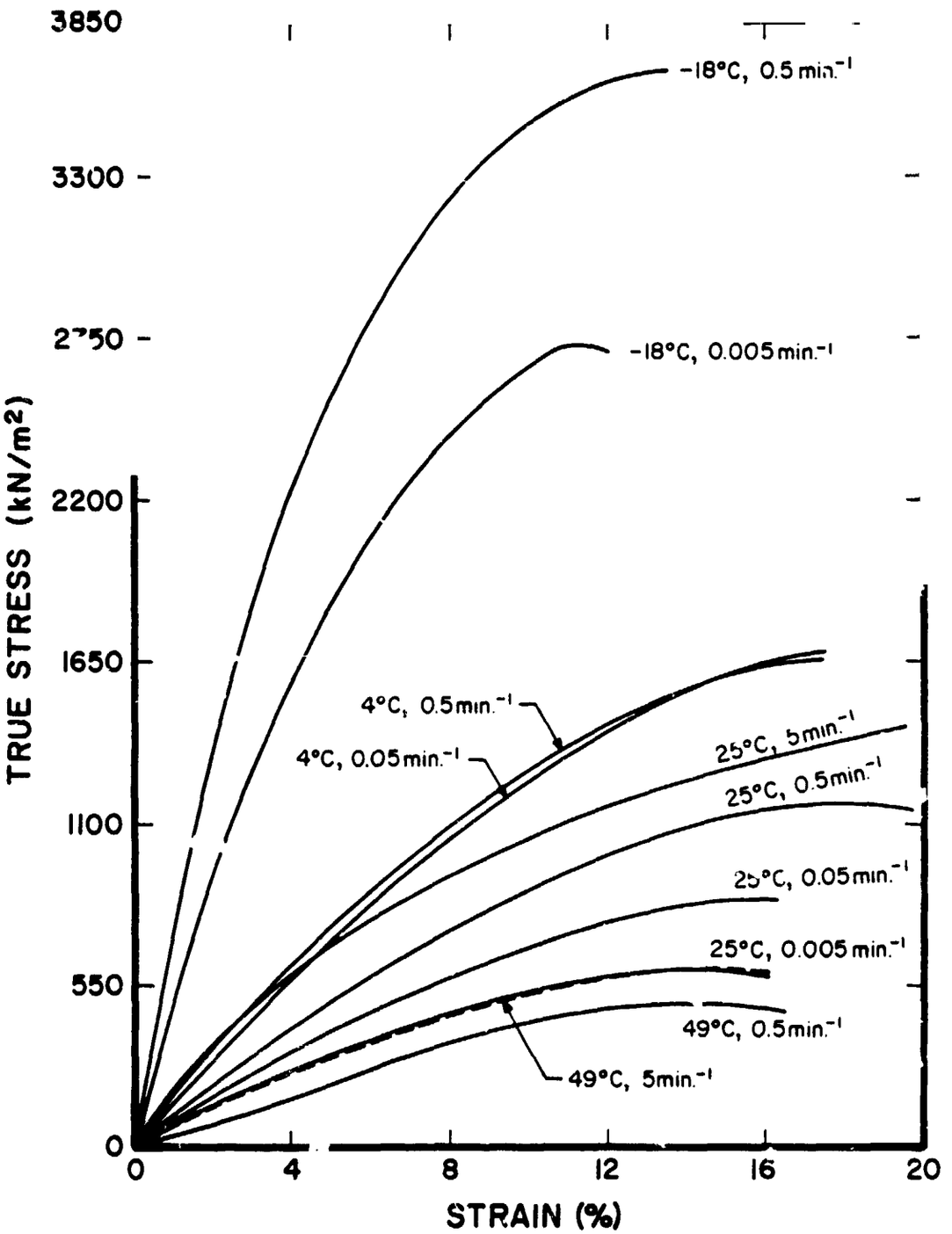

FIGURE 4 - True-Stress-Versus Strain Response

TABLE II

STRESS RELAXATION TESTS

Strain Level (%) \ Temperature (°C)	-18	4	25	49
1		X	X	
3	X	X	X	X
5			X	X

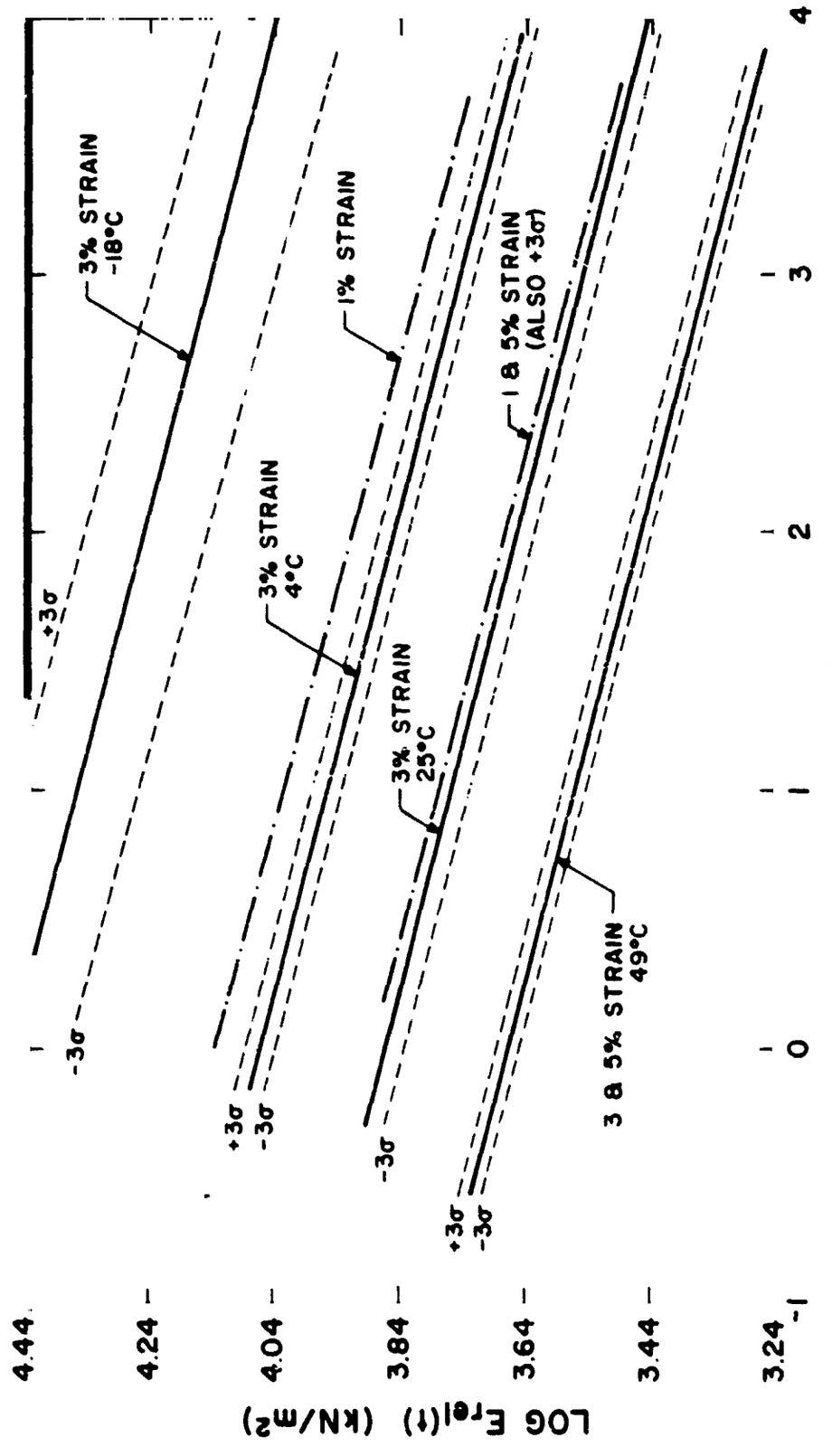

FIGURE 5 - Stress Relaxation Modulus Versus Log Time

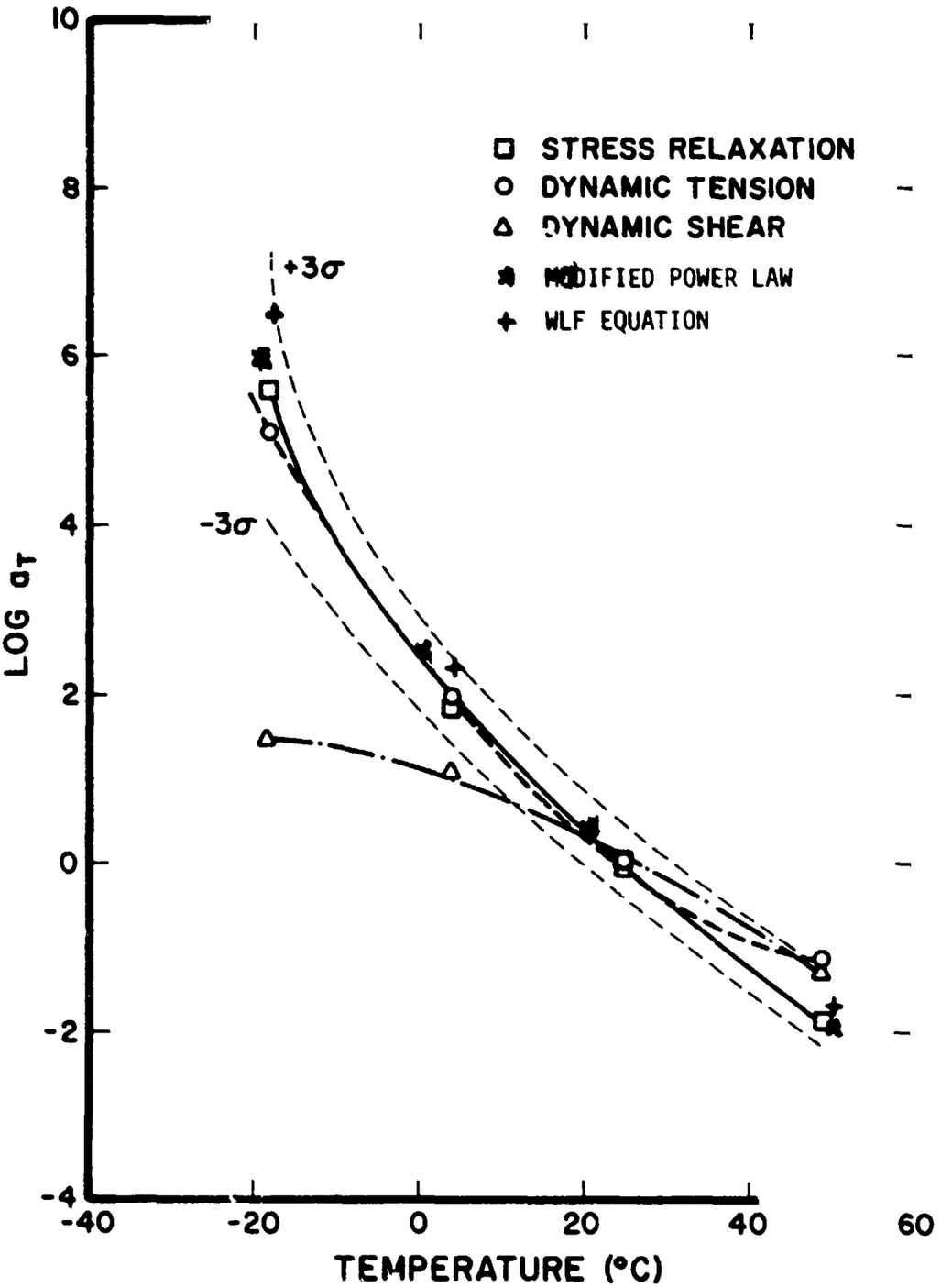

FIGURE 6 - Time-Temperature Shift Factor Versus Temperature

dynamic shear tests. Three-sigma limits are also shown for the stress-relaxation determined shift factors.

Thermorheologically simple material behavior requires time-temperature shift factors to be identical, irrespective of how they were determined. However, it may be noted in Figure 6 that the shift factors determined from dynamic shear tests do not agree with those determined from stress-relaxation or dynamic tension tests, which are in reasonable agreement with each other. The reason for this discrepancy is not known, although it is probably associated with some deficiency in the dynamic shear test procedure. The shift factors associated with the stress relaxation tests were used to superpose the relaxation modulus and dynamic tension test results whereas the shift factors obtained from dynamic shear tests were used to develop a master dynamic shear modulus curve.

Figure 7 presents the master relaxation modulus as a function of temperature-reduced time, t/a_T, a + 25°C. Figure 7 also shows the master relaxation modulus obtained from the constant strain rate test data shown in Figure 4 using the relation [15],

$$E_{rel}(t/a_T) = \frac{d\sigma(t/a_T)}{d\varepsilon}\Bigg|_{\varepsilon=Rt/a_T}$$

where R is the rate of straining. It may be observed that the modulus obtained from the constant strain rate tests is substantially higher than that obtained from stress relaxation tests, particularly at short times or low temperatures. This nonlinear behavior is typically observed of solid propellants.

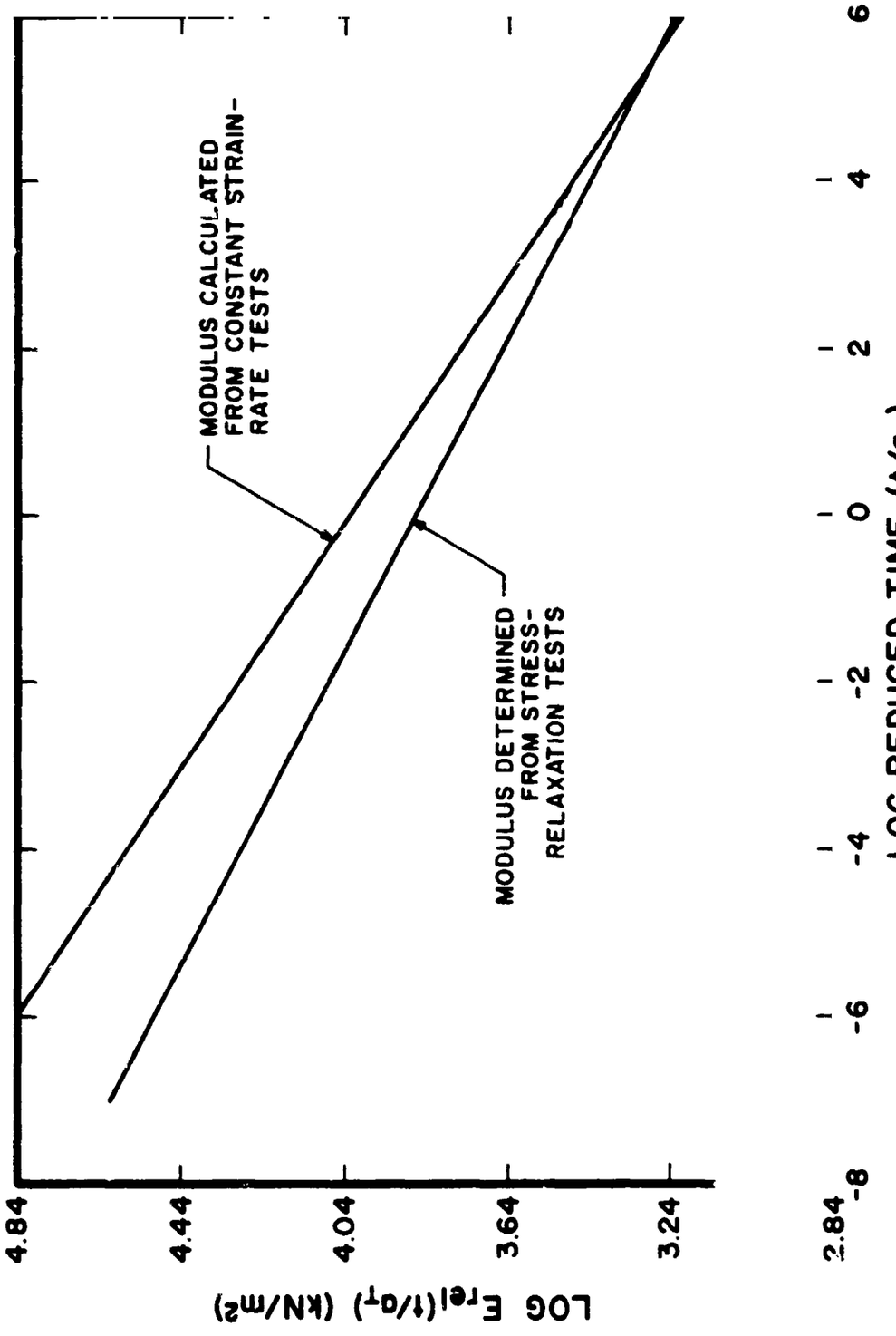

FIGURE 7 - Master Stress Relaxation Modulus Versus Temperature Reduced Time

Dynamic tension tests were conducted at 3.5, 11, 35, and 110 Hz and 0.1, 0.5, 1.0, 2.5, and 5.0 percent static strain levels at 18°C (0°F), 4°C (40°F), 25°C (77°F) and 49°C (120°F). Dynamic shear tests were conducted at the same frequencies and temperatures at pre-imposed static strain levels of 0.5, 1.0, 2.5 and 5.0 percent.

A fixed half-amplitude dynamic displacement of 50 m was used for all dynamic tests. The length of the dynamic specimens for the 0.1 percent strain level tests was 5 cm (2 in) rather than the 2 cm mentioned previously. For this test the dynamic strain level was equal to the imposed static strain of 0.1 percent. In all other dynamic tests the dynamic strain level varied between 0.22 and 0.25 percent.

Dynamic tension results are tabulated in Tables III-a through III-d and dynamic shear results are tabulated in Tables IV-a through IV-d. The notation in Tables III and IV is derived from the following representations for complex modulus:

$$E^*(\omega) = E' + iE''$$

$$G^*(\omega) = G' + iG''$$

$$\tan \delta = \frac{E''}{E'} \text{ or } \frac{G''}{G'}$$

$$|E| = \sqrt{(E')^2 + (E'')^2}$$

$$|G| = \sqrt{(G')^2 + (G')^2}$$

It may be observed from Tables III and IV that a gradual decline or softening of the dynamic stiffness occurs with increasing static

TABLE III-a

DYNAMIC TENSION TEST RESULTS
AT A FREQUENCY OF 3.5 Hz

STATIC STRAIN (%)	TEMPERATURE (°C)	tan δ	$\|E\|$ (MN/m^2)	E' (MN/m^2)	E'' (MN/m^2)
0.1	-18	0.32	313	299	95.1
	4	0.47	65.3	59.0	27.8
	25	0.45	16.5	15.0	6.74
	49	0.38	3.92	3.68	1.36
0.5	-18	0.32	179	170	54.4
	4	0.45	45.6	41.5	18.8
	25	0.43	13.5	12.4	5.3
	49	0.32	5.91	5.58	1.82
1.0	-18	0.33	175	166	53.7
	4	0.45	43.8	40	17.9
	25	0.43	12.6	11.6	4.6,
	49	0.30	5.42	5.17	1.58
2.5	-18	0.34	166	158	52.3
	4	0.45	39.9	36.6	16.3
	25	0.42	11.6	10.53	4.34
	49	0.30	4.68	4.48	1.35
5.0	-18	0.35	138	131	42.3
	4	0.43	34.8	32.1	13.4
	25	0.39	10.9	9.42	3.11
	49	0.26	4.0	3.85	1.09

TABLE III-b

DYNAMIC TENSION TEST RESULTS
AT A FREQUENCY OF 11 Hz

STATIC STRAIN (%)	TEMPERATURE (°C)	tan δ	$\lvert E \rvert$ (MN/m^2)	E' (MN/m^2)	E" (MN/m^2)
0.1	-18	0.34	333	315	107
	4	0.50	70.8	63.3	31.5
	25	0.47	19.7	17.8	8.35
	49	0.42	6.75	6.17	2.72
0.5	-18	0.33	207	197	63.3
	4	0.48	53.8	48.5	23.5
	25	0.48	15.0	13.6	6.49
	49	0.38	5.99	5.6	2.11
1.0	-18	0.33	214	204	66.4
	4	0.49	52.5	47.2	23.2
	25	0.47	14.0	12.6	6.0
	49	0.37	6.22	5.85	2.13
2.5	-18	0.32	213	204	62.6
	4	0.48	55.8	50.33	24.2
	25	0.47	14.7	13.2	6.32
	49	0.36	6.48	6.08	2.24
5.0	-18	0.33	185	177	52.5
	4	0.46	48.5	44.0	20.5
	25	0.44	13.8	12.6	5.64
	49	0.35	5.88	5.54	1.97

TABLE III-c

DYNAMIC TENSION TEST RESULTS
AT A FREQUENCY OF 35 Hz

STATIC STRAIN (%)	TEMPERATURE (°C)	tan δ	$\|E\|$ (MN/m^2)	E' (MN/m^2)	E" (MN/m^2)
0.1	-18	0.42	405	374	153
	4	0.68	71.2	58.9	39.7
	25	1.08	25.0	17.2	18.0
	49	0.64	8.8	7.43	4.72
0.5	-18	0.26	269	260	67.3
	4	0.55	75.2	65.9	36.2
	25	0.62	21.8	18.5	11.4
	49	0.47	8.37	7.56	3.57
1.0	-18	0.26	276	267	69.3
	4	0.55	75.2	65.9	36.2
	25	0.62	21.8	18.5	11.4
	49	0.47	8.37	7.56	3.57
2.5	-18	0.26	263	254	66.1
	4	0.52	76.3	68	34.7
	25	0.58	21.6	18.8	10.7
	49	0.46	8.66	7.85	3.64
5.0	-18	0.27	243	234	61.8
	4	0.48	71	64	30.8
	25	0.50	18.6	16.7	8.24
	49	0.45	7.92	7.23	3.24

TABLE III-d

DYNAMIC TENSION TEST RESULTS
AT A FREQUENCY OF 110 Hz

STATIC STRAIN (%)	TEMPERATURE (°C)	tan δ	$\lvert E \rvert$ (MN/m^2)	E' (MN/m^2)	E'' (MN/m^2)
0.1	-18	0.375	512	482	171
	4	1.1	120	87.2	78.1
	25	1.24	33.5	27.1	24.2
	49	1.25	12.3	8.06	8.94
0.5	-18	0.27	316	304	81.4
	4	0.53	102	90.4	48.0
	25	0.59	30.2	26.0	15.4
	49	0.54	12.2	10.8	5.81
1.0	-18	0.26	328	308	80.7
	4	0.53	105	92.6	49.2
	[illegible]	0.58	31.1	26.8	15.8
	49	0.53	12.2	10.7	5.72
2.5	-18	0.25	324	314	75.8
	4	0.50	108	96.9	47.8
	25	0.56	31.6	27.6	15.5
	49	0.51	12.3	11.3	5.59
5.0	-18	0.26	299	289	73.4
	4	0.48	103	92.0	44.4
	25	0.52	30.3	26.8	14.0
	49	0.48	11.7	10.6	5.12

TABLE IV-a

DYNAMIC SHEAR TEST RESULTS
AT A FREQUENCY OF 3.5 Hz

STATIC STRAIN (%)	TEMPERATURE (°C)	tan δ	$\lvert G \rvert$ (MN/m^2)	G' (MN/m^2)	G" (MN/m^2)
0.5	-18	0.052	11.2	11.2	0.59
	4	0.174	8.06	7.94	1.33
	25	0.29	4.33	4.16	1.18
	49	0.31	1.89	1.81	0.55
1.0	-18	0.061	11.0	11.0	0.67
	4	0.21	7.35	7.16	1.49
	25	0.33	3.44	3.27	1.05
	49	0.31	1.71	1.64	0.51
2.5	-18	0.061	11.1	11.1	0.68
	4	0.21	7.29	7.13	1.48
	25	0.33	3.26	3.12	1.01
	49	0.32	1.59	1.52	0.48
5.0	-18	0.059	11.1	11.1	0.66
	4	0.205	7.35	7.2	1.45
	25	0.33	3.26	3.1	1.01
	49	0.32	1.54	1.47	0.47

TABLE IV-b

DYNAMIC SHEAR TEST RESULTS AT
A FREQUENCY OF 11 Hz

STATIC STRAIN (%)	TEMPERATURE (°C)	tan δ	$\lvert G \rvert$ (MN/m^2)	G' (MN/m^2)	G" (MN/m^2)
0.5	-18	0.023	12.63	12.6	0.30
	4	0.10	10.5	10.4	1.08
	25	0.24	6.5	6.32	1.51
	49	0.31	3.42	3.28	0.99
1.0	-18	0.023	12.8	12.8	0.31
	4	0.1	10.4	10.3	1.14
	25	0.27	6.0	5.78	1.55
	49	0.33	2.99	2.67	0.95
2.5	-18	0.023	12.8	12.8	0.31
	4	0.11	10.5	10.4	1.11
	25	0.27	5.86	5.64	1.59
	49	0.34	2.82	2.67	0.91
5.0	-18	0.023	12.8	12.8	0.30
	4	0.093	10.5	10.4	1.02
	25	0.28	5.55	5.33	1.53
	49	0.34	2.58	2.43	0.85

TABLE IV-c

DYNAMIC SHEAR TEST RESULTS
AT A FREQUENCY OF 35 Hz

STATIC STRAIN	TEMPERATURE (°C)	tan δ	$\|G\|$ (MN/m^2)	G' (MN/m^2)	G" (MN/m^2)
0.5	-18	0.036	14.67	14.67	0.58
	4	0.15	11.5	11.4	1.82
	25	0.31	6.26	5.97	1.85
	49	0.41	2.46	2.29	0.91
1.0	-18	0.045	14.3	14.3	0.68
	4	0.22	9.83	9.58	2.18
	25	0.41	3.8	3.52	1.43
	49	0.42	1.59	1.47	0.61
2.5	-18	0.05	14.0	13.9	0.75
	4	0.23	9.13	8.85	2.16
	25	0.44	3.28	3.01	1.28
	49	0.42	1.23	1.13	0.47
5.0	-18	0.072	13.2	13.2	1.03
	4	0.28	7.8	7.5	2.09
	25	0.45	2.97	2.72	1.23
	49	0.42	0.99	0.91	0.37

TABLE IV-d

DYNAMIC SHEAR TEST RESULTS AT A FREQUENCY OF 110 Hz

STATIC STRAIN (%)	TEMPERATURE (°C)	tan δ	$\lvert G \rvert$ (MN/m^2)	G' (MN/m^2)	G" (MN/m^2)
0.5	-18	0.036	22.0	22.0	0.34
	4	0.12	18.0	17.9	2.13
	25	0.29	10.9	10.4	2.98
	49	0.41	4.99	4.65	1.91
1.0	-18	0.046	22.2	22.2	1.08
	4	0.14	17.6	17.4	2.50
	25	0.34	9.77	9.25	3.08
	49	0.43	4.48	4.12	1.77
2.5	-18	0.046	22.4	22.4	1.12
	4	0.15	17.2	17.0	2.58
	25	0.35	9.33	8.8	3.09
	49	0.45	4.01	3.65	1.66
5.0	-18	0.049	22.0	22.0	1.14
	4	0.16	16.8	16.6	2.66
	25	0.37	8.49	7.96	2.94
	49	0.46	3.07	2.79	1.30

strain level. The maximum dynamic tensile modulus occurs for a static strain of 0.1 percent where the dynamic strain is also equal to this value. Typical of live propellant behavior, dynamic moduli increase for decreasing static strain and/or dynamic strain levels (see, e.g., [4,16,17]).

Figure 8 presents the master dynamic tensile and shear moduli versus temperature reduced frequency at a reference temperature of 25°C. The dynamic tensile modulus, calculated from stress relaxation test data and constant strain rate test data is also shown for comparison. It may be noted that the dynamic moduli calculated in this fashion do not agree with the measured dynamic data. This is typical of solid propellant behavior. The master dynamic shear modulus curve shown in Figure 9 was obtained using the frequency-temperature shift factors developed from the dynamic shear tests and previously presented in Figure 6. Although considerable data scatter exists, it may be seen that the master dynamic shear modulus is approximately one-third of the value of the measured tensile modulus, indicating nearly incompressible material behavior. From bulk compressibility tests conducted by Thiokol/Wasatch, the bulk modulus was experimentally determined to be 267,000 psi (1.84 MN/m^2) implying a Poisson's ratio in the range of 0.4991 to 0.4999 over the frequency range of interest.

The imaginary part of the dynamic tensile and shear modulus, E" and G", are presented in Figure 9 as a function of temperature-reduced frequency. The variability and data scatter in G" indicate that the shear test results are not likely to be truly representative of the

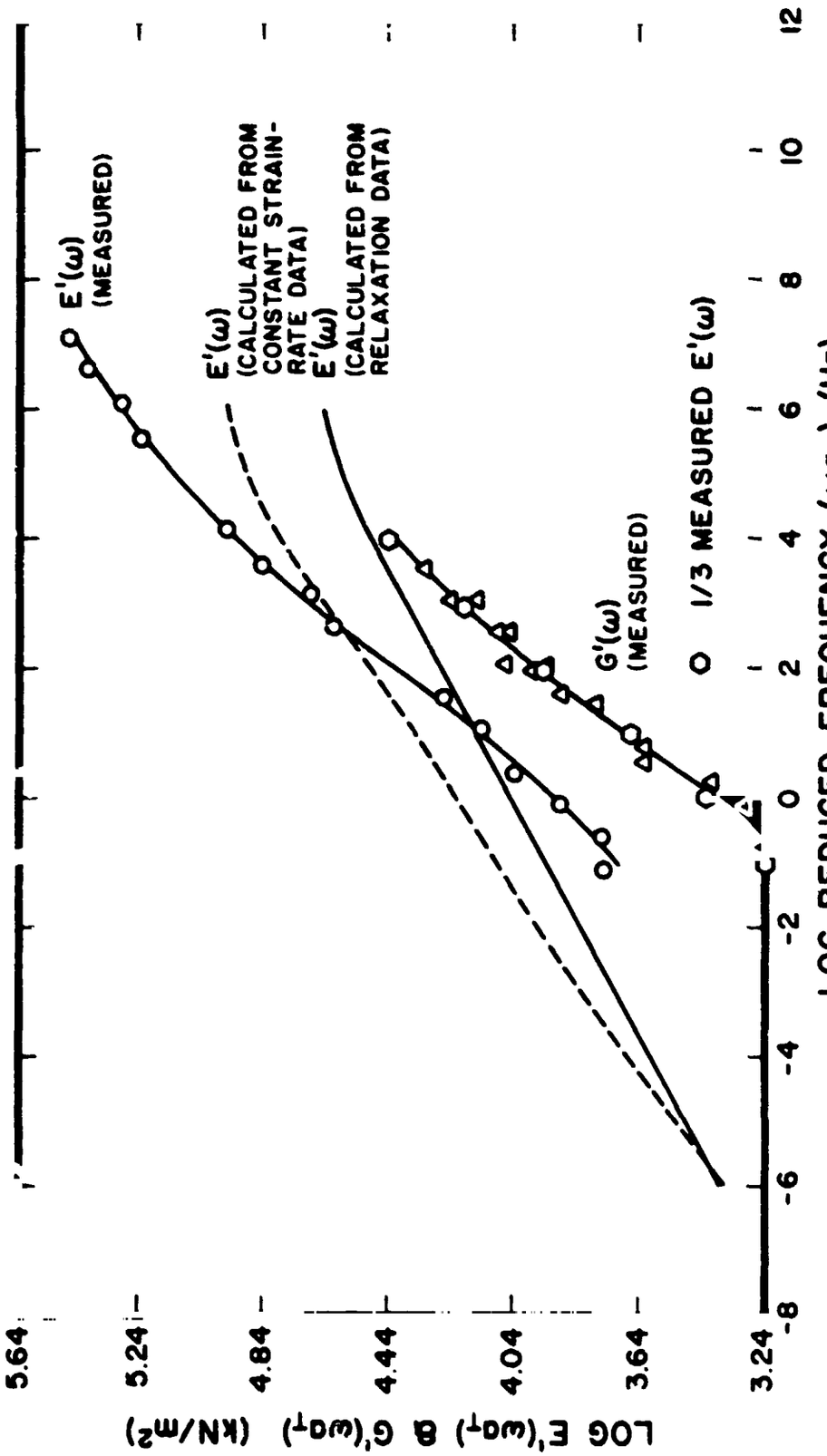

FIGURE 8. Master Dynamic Modulus Versus Temperature Reduced Frequency

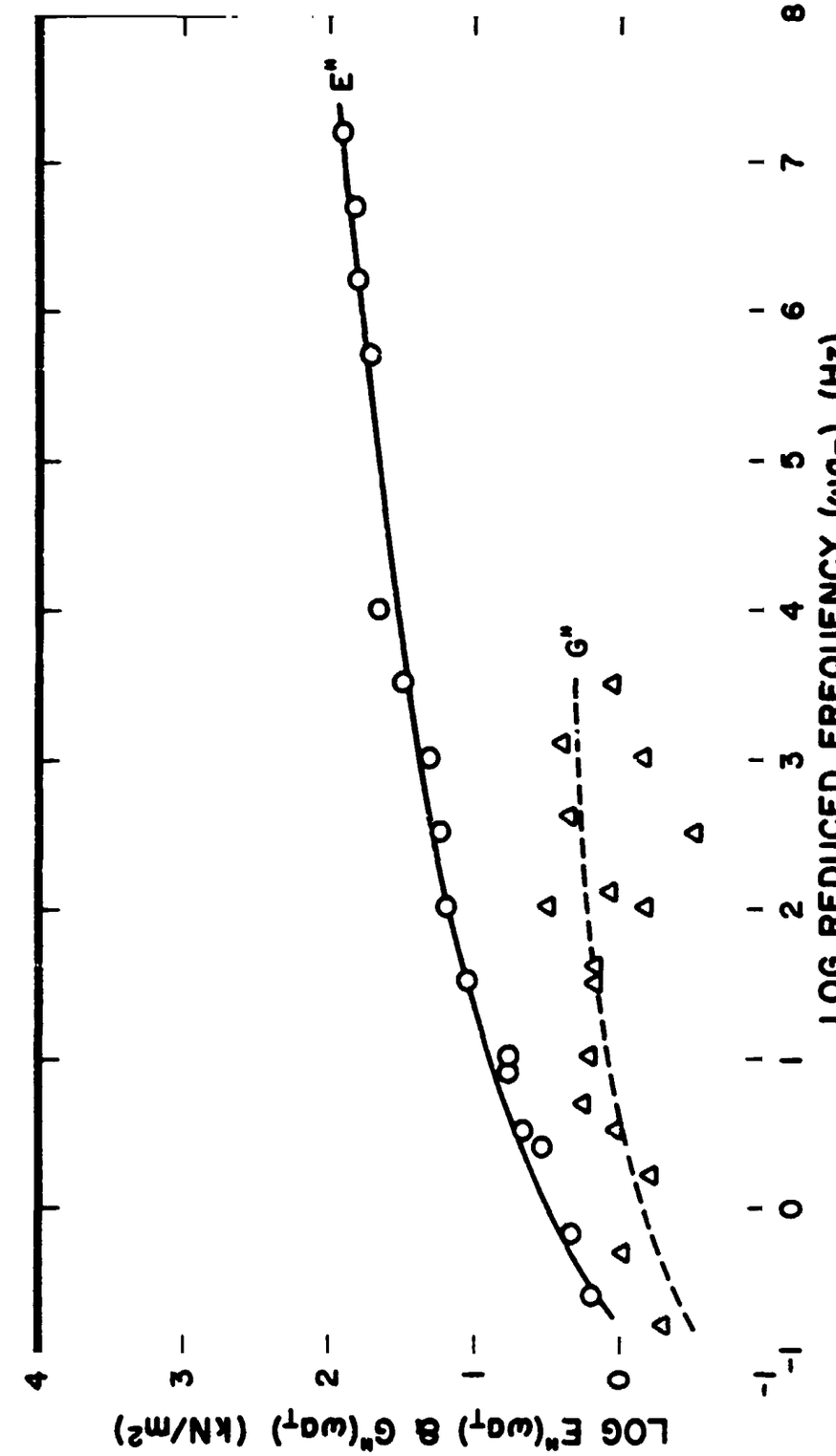

FIGURE 9 - Master Dynamic Loss Modulus Versus Temperature Reduced Frequency

propellant's dynamic stress behavior. The anomalous shear behavior is attributed to coupling between the shim-stock support and glue and the propellant (see Figure 1).

3.2 THIOKOL/WASATCH TESTS

Thiokol has conducted dynamic shear tests on live and inert TP-1123 propellant [6], which, as noted previously, is very similar to TP-H1148, and static and dynamic characterization of TP-H1148 propellant [10,11].

Thiokol conducts dynamic shear tests using a modified Gottenberg disk test technique [12]. The test setup consists of a disk of propellant, bonded to steel outer and center rings (Figure 10), and mechanically loaded at its center with an electromechanical vibrator at a constant displacement. Excitation force, disk center displacement and relative phase angle are measured from which dynamic shear moduli are calculated.

Tests on live and inert TP-H1123 propellant were conducted at frequencies ranging from 10 to 50 Hz at 40°F, 70°F and 90°F. Analytical studies of the Shuttle SRM center segment and the Gottenberg disk test specimen were performed to determine appropriate static and dynamic displacements for the test. A Gottenberg disk static center-body deflection of 0.015 inch was determined to simulate the propellant strains resulting from the Worst case SRM thermal shrinkage, and a vibratory center-body displacement of 0.0006 inch peak-to-peak was required to simulate maximum propellant strains from a 0.5 g peak-to-peak, 2 to 50 Hz, longitudinal, sinusoidal vibration input to the case. Since the above dynamic displacement was below the minimum amplitude limit of

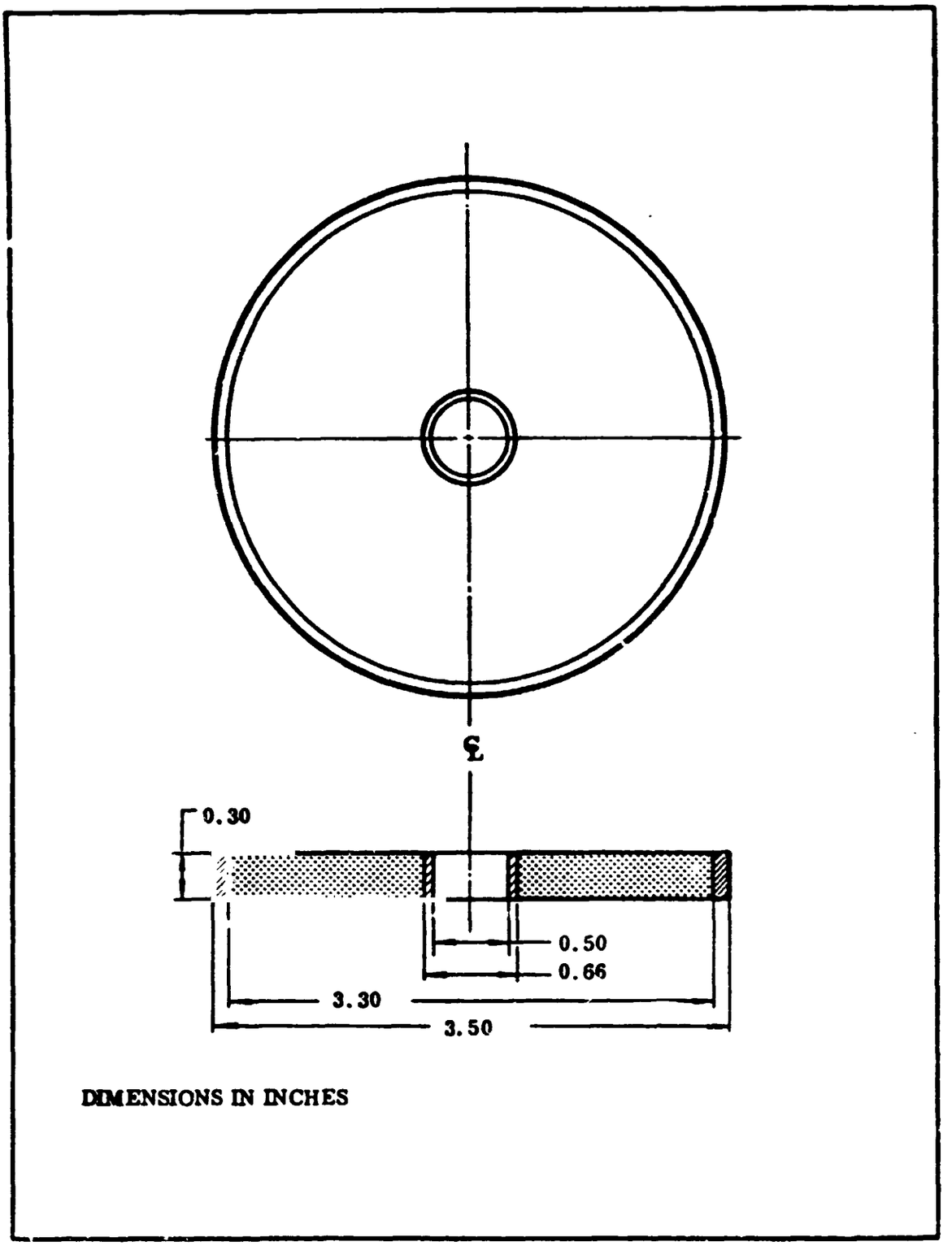

FIGURE 10. Gottenberg Disk Test Specimen

the test apparatus, tests were conducted at dynamic displacement amplitudes ranging from 0.001 to 0.004 inch, and imposed center-body, static displacements ranging from 0.009 to 0.022 inches.

Experimental test results as a function of dynamic displacement are presented in Table V for live TP-H1123 propellant and in Table VII for inert TP-H113 propellant (designated H-13). Similar results are presented in Tables VII and VIII as a function of static displacement. Figure 11 presents the dynamic shear moduli, G' and G", versus temperature reduced frequency for TP-H1123 and H-13 propellants.

While the test data presented in Tables V through VIII indicate a significant influence of temperature and frequency, as expected; a Duncan Multiple Range Test indicated no statistical influence of static or dynamic displacement amplitude over the range studied.

In addition, Thiokol also conducted Gottenberg disk tests on TP-H1123 live propellant in a pressure vessel at ambient, 500 and 1000 psig confining pressures. Their results are presented in Table IX. These data are well within the statistical limits established by the ambient pressure tests previously presented.

Thiokol has also conducted static [10] and dynamic [11] characterization tests of TP-H1148 space shuttle propellant. Dynamic shear tests were conducted on propellant from six mixes (9910-053, -057, -059, -060, -061, -062) at 40, 70 and 90°F and frequencies ranging from 5 to 50 Hz. The tests were conducted using a Gottenberg disk with a dynamic displacement of 0.002 inches. The test data are summarized in Tables X through XV, and analyzed subsequently.

TABLE V

DYNAMIC SHEAR MODULUS OF LIVE TP-H 1123 PROPELLANT
TEST DATA FOR VARIOUS DYNAMIC DISPLACEMENTS

Dynamic Displacement (Inches)	Frequency (Hz)	Temperature (°F)	tanδ	|G| (psi)	G' (psi)	G" (psi)
0.001	50	40	.44	3597	3064	1363
	40		.52	3014	2670	1398
	30		.47	2573	2328	1095
	20		.38	2168	2029	765
	15		.32	1949	1856	596
	10		.25	1757	1705	423
0.002	50	40	.53	3294	2909	1545
		70	.58	1472	1206	704
		90	.62	801	680	423
	40	40	.52	2856	2532	1322
		70	.58	1178	1019	590
		90	.61	660	562	345
	30	40	.47	2426	2196	1030
		70	.53	974	859	457
		90	.57	331	402	262
	20	40	.38	2017	1888	710
		70	.41	782	722	298
		90	.47	414	374	177
	15	40	.32	1824	1737	558
		70	.33	680	656	220
		90	.39	366	334	130
	10	40	.25	1632	1584	393
		70	.24	606	590	140
		90	.28	298	287	79.7
0.0027	50	40	.53	3292	2908	1544
	40		.52	2852	2592	1319
	30		.47	2438	2200	1032
	20		.38	2026	1896	714
	15		.32	1828	1740	558
	10		.24	1655	1608	392

TABLE V (continued)

DYNAMIC SHEAR MODULUS OF LIVE TP-H1123 PROPELLANT
TEST DATA FOR VARIOUS DYNAMIC DISPLACEMENTS

Dynamic Displacement (Inches)	Frequency (Hz)	Temperature (°F)	tanδ	|G| (psi)	G' (psi)	G" (psi)
0.003	50	70	.58	1289	1116	645
		90	.62	793	674	417
	40	70	.58	1089	942	544
		90	.61	655	559	342
	30	70	.53	904	797	425
		90	.57	526	458	259
	20	70	.42	733	676	283
		90	.48	397	357	173
	15	70	.34	699	618	209
		90	.43	322	295	128
	10	70	.24	547	532	127
		90	.30	277	265	80.3
0.004	50	70	.57	1315	1140	656
		90	.52	777	663	406
	40	70	.56	1106	960	542
		90	.61	645	552	335
	30	70	.52	908	807	416
		90	.47	398	360	169
	20	70	.42	726	669	282
		90	.47	398	360	169
	15	70	.35	636	601	208
		90	.39	343	320	125
	10	70	.27	555	539	148
		90	.27	288	278	79.0

TABLE VI

DYNAMIC SHEAR MODULI OF H-13 INERT PROPELLANT
TEST DATA FOR VARIOUS DYNAMIC DISPLACEMENTS

Dynamic Displacement (Inches)	Frequency (Hz)	Temperature (°F)	tanδ	|G| (psi)	G' (psi)	G" (psi)
0.0011	50	40	.52	2504	2220	1153
		70	.64	998	841	538
		90	.77	710	561	430
	40	40	.51	2197	1953	998
		70	.63	836	708	445
		90	.77	599	473	364
	30	40	.50	1909	1707	849
		70	.58	678	588	340
		90	.73	494	397	290
	20	40	.46	1642	1486	689
		70	.47	533	482	227
		90	.63	398	335	211
	15	40	.44	1510	1331	604
		70	.41	462	428	175
		90	.55	349	304	148
	10	40	.41	1382	1277	519
		70	.31	400	382	118
		90	.43	305	280	119
0.002	50	40	.52	2292	2030	1060
		70	.64	995	838	536
		90	.58	616	532	310
	40	40	.51	1981	1764	897
		70	.63	837	708	445
		90	.56	507	443	247
	30	40	.47	1676	1514	714
		70	.57	680	592	336
		90	.5	407	364	182

TABLE VI (continued)

DYNAMIC SHEAR MODULI OF H-13 INERT PROPELLANT
TEST DATA FOR VARIOUS DYNAMIC DISPLACEMENTS

Dynamic Displacement (Inches	Frequency (Hz)	Temperature (°F)	tan	G (psi)	G' (psi)	G" (psi)
0.002	20	40	.43	1391	1277	545
		70	.47	536	484	228
		90	.44	315	288	126
	15	40	.36	1252	1177	422
		70	.31	396	378	116
		90	.33	232	220	72.5
0.003	50	70	.77	946	751	575
	40		.75	796	636	478
	30		.73	648	524	382
	20		.61	506	433	262
	15		.50	439	392	197
	10		.37	371	349	130

TABLE VII

DYNAMIC SHEAR MODULI OF TP-H1123 LIVE PROPELLANT
AS AFFECTED BY VARIOUS STATIC DISPLACEMENTS

Static Displacement (inches)	0.0098	0.0177	0.0217	0.0197
Frequency (Hz)		G'(psi)		
50	1153	1178	1163	1153
40	982	1003	992	982
30	828	850	839	828
20	694	723	718	694
15	627	650	650	627
10	558	588	582	558
		G"(psi)		
50	656	674	663	656
40	551	565	558	551
30	421	433	427	421
15	197	204	204	197
10	122	128	127	122
		|G|(psi)		
50	1327	1357	1339	1327
40	1126	1151	1138	1126
30	929	954	941	923
20	745	777	771	745
15	657	681	681	657
10	571	602	596	871

Note: Tested at 70°F, ambient pressure and a dynamic displacement of 0.002 inch peak to peak.

TABLE VIII

DYNAMIC SHEAR MODULI OF H-13 INERT PROPELLANT
AS AFFECTED BY VARIOUS STATIC DISPLACEMENTS

Static Displacement (inches)	0.0217	0.0098	0.0086	0.0017
Frequency (Hz)			G'(psi)	
50	1046	986	1076	1001
40	899	837	925	853
30	765	706	798	722
20	652	589	675	594
15	588	523	617	535
10	532	477	554	471
			G"(psi)	
50	602	557	624	568
40	506	464	524	475
30	393	359	412	368
20	261	234	271	243
15	195	173	205	177
10	121	108	128	107
			G*(psi)	
50	1207	1132	1244	1151
40	1032	957	1063	976
30	860	792	898	810
20	702	634	727	642
15	619	551	650	564
10	546	489	569	483

Note: Tested at 70°F and ambient pressure.

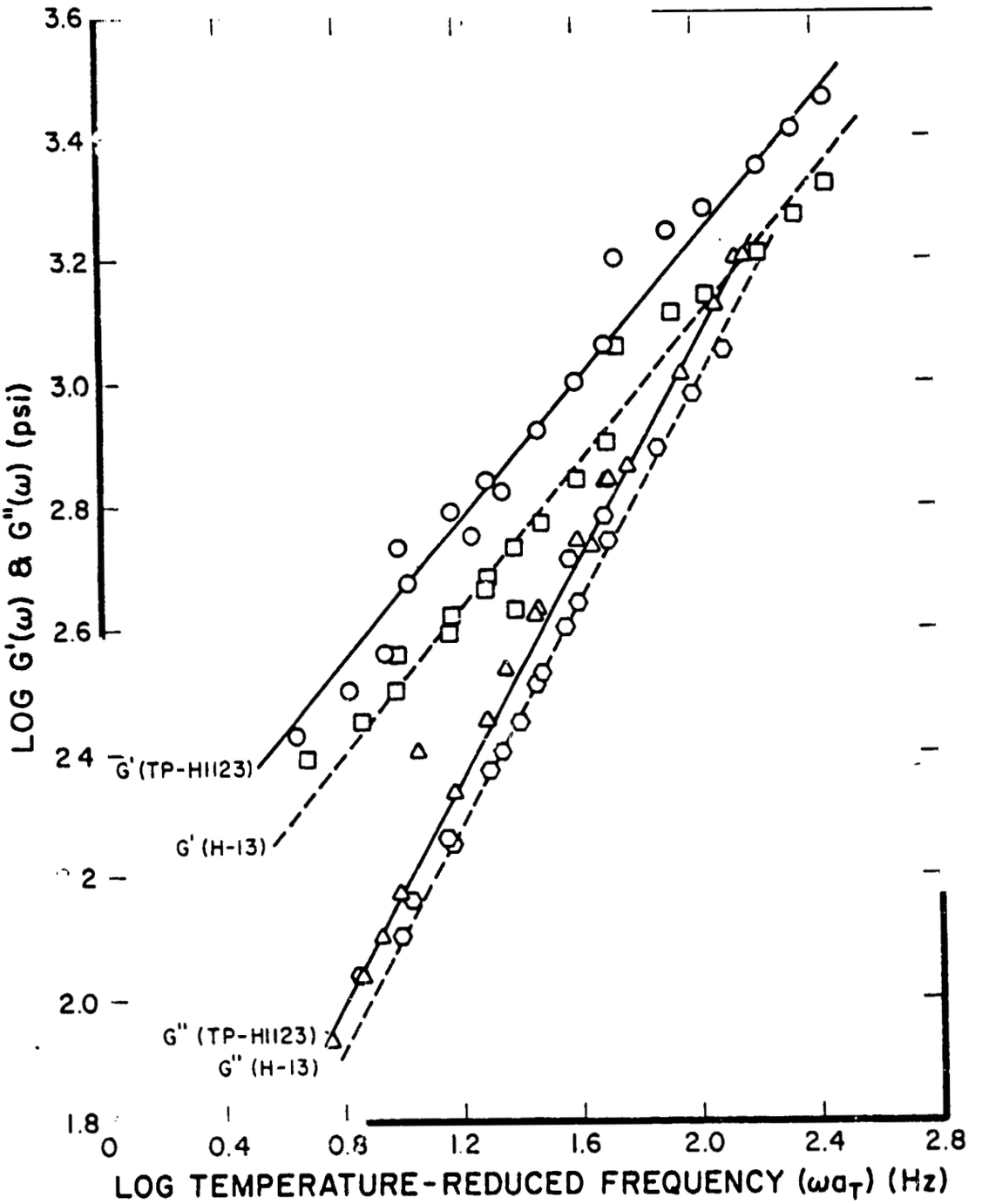

Figure 11 Dynamic Shear Modulus Versus Temperature Reduced Frequency for TP-H1123 and H-13 Propellant

TABLE IX

DYNAMIC SHEAR MODULI OF TP-H1123 LIVE PROPELLANT AS AFFECTED BY PRESSURE

Pressure (psi)	Ambient			500			1000		
Frequency (Hz)									
				G'(psi)					
50	1196	1209	1176	1207	1194	1187	1182	1189	1187
40	986	995	989	982	989	1000	975	989	1000
30	826	841	829	826	826	848	816	826	848
20	678	691	676	671	686	688	680	691	691
				G"(psi)					
50	700	709	685	708	698	693	741	695	693
	565	571	566	562	566	574	600	566	574
30	429	437	430	429	429	441	457	429	441
20	300	305	298	295	303	304	327	305	305
				|G|(psi)					
[illegible]	1386	1402	1361	1399	1383	1374	1395	1377	1374
40	1136	1147	40	1131	1140	1153	1145	1140	1153
30	931	949	934	931	931	956	935	931	956
20	741	755	739	733	750	752	755	755	755

Note: Tested at 70°F and at a dynamic displacement of 0.0045 inch peak to peak.

TABLE X

DYNAMIC SHEAR MODULUS, G', VERSUS FREQUENCY AT 90°F

MIX (9910-)		FREQUENCY (Hz) 5	10	15	20	30	40	50
053		407	525	635	742	965	1190	1450
		455	550	670	782	1020	1160	1590
		328	425	521	625	830	1030	1270
	MEAN	297	500	609	716	938	1160	1440
	STD.DEV.	64	66	78	82	98	118	160
057		298	435	545	660	880	1080	1310
		356	440	535	635	830	1030	1280
		278	365	460	560	749	950	1190
	MEAN	311	413	513	618	820	1020	1260
	STD.DEV.	41	42	46	52	66	66	62
059		291	390	485	587	785	1260	1210
		291	400	480	566	754	1100	1180
		327	420	515	630	840	948	1290
	MEAN	303	403	493	594	793	1100	1230
	STD.DEV.	21	15	19	33	44	156	57
060		416	549	654	785	1030	1090	1530
		340	450	567	669	890	1110	1340
		268	355	450	550	750	1230	1150
	MEAN	341	451	557	668	890	1140	1340
	STD.DEV.	74	97	102	118	140	76	190
061		238	400	520	628	862	1090	1360
		360	449	555	660	883	1110	1400
		429	532	642	760	990	1230	1530
	MEAN	359	460	572	683	912	1140	1430
	STD.DEV.	71	67	63	69	69	76	89
062		357	430	535	647	860	1080	1360
		334	437	538	648	845	1050	1300
		325	410	500	600	800	1000	1220
	MEAN	339	426	524	632	835	1040	1290
	STD.DEV.	17	14	21	27	31	40	70
	GRAND MEAN	342	442	545	652	865	1080	1330
	STD.DEV.	55	59	66	73	88	101	128

TABLE XI

DYNAMIC SHEAR MODULUS, G", VERSUS FREQUENCY AT 90°F

MIX (9910-)		FREQUENCY (Hz) 5	10	15	20	30	40	50
053		243	321	400	500	690	870	1100
		240	320	417	515	718	925	1170
		177	210	294	375	555	730	931
	MEAN	220	284	370	463	654	842	1070
	STD.DEV.	37	64	67	77	87	101	123
057		167	235	315	409	590	785	1000
		235	280	350	430	595	760	941
		156	195	260	340	500	670	858
	MEAN	186	237	308	393	562	738	933
	STD.DEV.	43	43	45	47	53	60	71
059		176	219	280	360	530	700	878
		160	217	281	343	505	692	878
		175	225	305	395	525	760	954
	MEAN	170	220	289	366	537	717	903
	STD.DEV.	9	4	14	27	35	37	44
060		180	275	370	465	661	860	1060
		175	230	312	405	600	797	1000
		151	200	265	350	510	682	851
	MEAN	169	235	316	407	590	780	970
	STD.DEV.	16	38	53	53	76	90	108
061		136	215	305	400	590	770	990
		149	205	290	385	580	777	1020
		186	262	355	455	646	850	1060
	MEAN	157	227	317	413	605	799	1020
	STD.DEV.	26	30	34	37	36	44	35
062		165	249	317	395	563	747	975
		165	220	300	380	552	726	920
		156	220	290	370	540	700	890
	MEAN	162	230	302	382	552	724	928
	STD.DEV.	5	17	14	13	12	24	43
	GRAND MEAN	177	239	317	404	583	967	971
	STD.DEV.	31	38	44	51	62	72	88

TABLE XII

DYNAMIC SHEAR MODULUS, G', VERSUS FREQUENCY AT 70°F

MIX (9910-)		FREQUENCY (Hz) 5	10	15	20	30	40	50
053		597	775	910	1060	1350	1640	2000
		575	725	912	1080	1360	1750	1950
		680	875	1050	1220	1530	1850	2240
	MEAN	617	792	960	1120	1410	1710	2060
	STD.DEV.	55	76	78	87	101	118	155
057		570	714	850	1000	1270	1570	1920
		550	750	900	1050	1350	1670	2000
		634	740	890	1050	1350	1670	2020
	MEAN	585	735	880	1030	1320	1640	1980
	STD.DEV.	44	19	26	29	46	58	53
059		484	650	812	950	1250	1550	1940
		597	740	875	1025	1300	1580	1890
		650	827	1000	1160	1500	1830	2230
	MEAN	577	739	896	1040	1350	1650	2020
	STD.DEV.	85	89	96	106	132	154	184
060		616	800	950	1100	1420	1740	2130
		604	790	960	1120	1440	1750	2100
		544	680	830	970	1280	1580	1940
	MEAN	588	757	913	1068	1380	1690	2060
	STD.DEV.	39	67	72	81	87	95	102
061		564	739	900	1080	1410	1750	2200
		582	700	840	990	1280	1580	1950
		690	900	1080	1260	1600	1940	2350
	MEAN	612	780	940	1110	1430	1760	2170
	STD.DEV.	68	106	125	137	161	180	202
062		611	750	875	1020	1320	1620	1900
		546	700	860	1020	1320	1640	2020
		551	705	867	1010	1300	1620	2000
	MEAN	569	718	867	1020	1310	1630	1970
	STD.DEV.	36	28	8	6	12	12	64
	GRAND MEAN	591	753	909	1060	1370	1680	2040
	STD.DEV.	51	65	74	83	97	109	135

TABLE XIII

DYNAMIC SHEAR MODULUS, G", VERSUS FREQUENCY AT 70°F

MIX (9910-)		FREQUENCY (Hz) 5	10	15	20	30	40	50
053		350	525	660	792	1020	1250	1450
		347	430	560	675	925	1180	1460
		403	514	650	775	1040	1280	1580
	MEAN	367	490	623	747	995	1240	1500
	STD.DEV.	32	52	55	63	61	51	72
057		264	367	475	600	850	1114	1385
		225	356	475	600	850	1125	1400
		310	400	525	640	900	1190	1550
	MEAN	266	374	492	613	867	1140	1440
	STD.DEV.	43	23	29	23	29	41	95
059		220	340	466	575	825	1070	1350
		259	350	460	575	820	1060	1350
		300	440	570	720	973	1250	1520
	MEAN	260	377	499	623	873	1130	1410
	STD.DEV.	40	55	62	84	87	107	98
060		267	415	545	675	930	1200	1500
		275	410	550	680	950	1230	1570
		247	350	465	580	840	1090	1360
	MEAN	263	392	520	645	907	1170	1460
	STD.DEV.	14	36	48	56	59	74	84
061		256	400	540	690	955	1240	1540
		252	325	440	550	800	1040	1310
		300	440	575	715	1000	1290	1620
	MEAN	269	388	518	652	918	1190	1490
	STD.DEV.	27	58	70	89	105	132	161
062		278	370	482	624	860	1120	1410
		250	343	465	600	850	1120	1420
		239	356	480	624	890	1180	1480
	MEAN	256	356	476	616	867	1140	1440
	STD.DEV.	20	14	9	14	21	35	38
	GRAND MEAN	280	396	521	649	904	1170	1460
	STD.DEV.	48	57	65	70	73	79	79

TABLE XIV

DYNAMIC SHEAR MODULU G', VERSUS FREQUENCY AT 40°F

MIX (9910-)	FREQUENCY (Hz) 5	10	15	20	30	40	50
053	1480	1770	2100	2440	3100	3800	4820
	1530	1940	2300	2620	3260	3900	4850
	1550	1920	2290	2540	3340	4060	4920
MEAN	1520	1880	2230	2570	3230	3920	4860
STD.DEV.	36	93	113	110	122	131	51
057	1540	1880	2220	2560	3260	4000	5040
	1480	1790	2130	2450	3180	3880	5000
	1560	1930	2270	2590	3280	4060	5020
MEAN	1530	1870	2210	2530	3240	3980	5020
STD.DEV.	42	71	71	74	53	92	20
059	1410	1760	2100	2420	3110	3860	4800
	1580	1960	2300	2640	3400	4140	5160
	1540	1920	2280	2640	3410	4180	5120
MEAN	1510	1880	2230	2570	3310	4060	5030
STD.DEV.	89	106	110	127	170	174	197
060	1740	2110	2480	2850	3580	4280	5120
	1670	2050	2430	2820	3540	4280	5240
	1400	1720	2070	2420	3120	3930	4860
MEAN	1600	1960	2330	2700	3410	4160	5070
STD.DEV.	180	210	224	240	255	202	194
061	1620	2000	2380	2740	3510	4280	5250
	1660	2080	2470	2830	2570	4460	5400
	1600	1990	2380	2780	3420	4150	5700
MEAN	1630	2020	2410	2780	3500	4300	5250
STD.DEV.	31	49	52	45	75	156	150
062	1590	1940	2300	2700	3530	4370	5300
	1610	1990	2340	2710	3400	4090	5000
	1470	1810	2160	2500	3250	4400	5030
MEAN	1560	1910	2270	2640	3390	4190	5110
STD.DEV.	76	93	95	118	140	159	165
GRAND MEAN	1560	1920	2280	2630	3350	4100	5060
STD.DEV.	89	113	127	144	161	186	171

TABLE XV

DYNAMIC SHEAR MODULUS, G", VERSUS FREQUENCY AT 40°F

MIX (9910-)		FREQUENCY (Hz) 5	10	15	20	30	40	50
053		626	832	1030	1240	1640	2040	2440
		633	870	1070	1280	1690	2100	2520
		640	890	1100	1310	1710	2100	2490
	MEAN	633	864	1070	1280	1680	2080	2480
	STD.DEV.	7	29	35	36	36	35	40
057		606	820	1030	1240	1660	2080	2570
		601	850	1050	1280	1720	2160	2660
		730	915	1120	1330	1760	2170	2720
	MEAN	646	862	1070	1280	1710	2140	2650
	STD.DEV.	73	49	47	45	50	49	75
059		565	796	1000	1220	1680	2100	2640
		672	910	1120	1340	1780	2200	2680
		630	913	1140	1380	1820	2250	2730
	MEAN	622	873	1090	1320	1760	2180	2680
	STD.DEV.	54	67	76	87	72	76	45
060		685	950	1170	1400	1810	2220	2650
		660	900	1040	1380	1820	2260	2810
		577	792	1020	1220	1680	2120	2660
	MEAN	641	881	1110	1330	1770	2200	2710
	STD.DEV.	56	81	79	99	78	72	90
061		637	849	1070	1290	1730	2160	2670
		652	850	1050	1280	1720	2170	2720
		610	800	1000	1210	1610	2020	2510
	MEAN	633	833	1040	1260	1690	2120	2633
	STD.DEV.	21	29	36	44	67	84	45
062		625	885	1110	1340	1800	2240	2250
		659	930	1150	1340	1780	2060	2400
		609	810	1020	1240	1650	2070	2550
	MEAN	631	875	1090	1310	1740	2120	2570
	STD.DEV.	26	61	67	58	81	101	176
	GRAND MEAN	634	865	1080	1730	1730	2140	2630
	STD.DEV.	39	50	55	66	66	74	111

3.3 ROCKWELL INTERNATIONAL TESTS

The Space Division of Rockwell International has conducted dynamic shear modulus tests in support of the Quarter Scale GVT, program [8,9]. The propellant, which is inert, is designated UTI-610A and was supplied by CSD.

The specimen dimensions were 4 inch by 4 inch by 1 inch thick. The four inch square surfaces were bonded to aluminum plates. One of the plates was clamped to a rigid, fixed support and the other plate was subjected to controlled sinusoidal forces. Tests were conducted at 67°F from 10 to 200 Hz with force amplitudes of ± 1, ± 2, ± 4 and ± 8 pounds (i.e., average shear stresses of 0.0625, 0.125, 0.250 and 0.500 psi). Test data was obtained from accelerometers used to measure the motion of the specimen along all three axes and rotation about the three axes. Test results are presented in Table XVI as a function of frequency and load and in Table XVII as a function of frequency and dynamic shear strain level. The results show significant nonlinearities at the strain levels tested.

TABLE XVI

UTI-610A DYNAMIC SHEAR MODULUS VERSUS FREQUENCY AT 67°F

Sinusoidal Force / Frequency (Hz)	± 1 lb		± 2 lb		± 4 lb		± 8 lb	
	G'	G"	G'	G"	G'	G"	G'	G"
10	2280	805	2070	800	2070	800	1900	790
20	2980	1100	2730	1000	2600	980	2330	905
40	3930	1540	3570	1410	3330	1370	2920	1250
70	4800	2000	4310	1830	4010	1750	3470	1590
100	5360	2300	4840	2120	4450	2030	3850	1830
150	6040	2700	5440	2500	4990	2380	4290	2140
200	6500	3000	5890	2740	5350	2640	4600	2370

TABLE XVII

UTI-610A DYNAMIC SHEAR MODULUS, G', VERSUS DYNAMIC SHEAR STRAIN AT 67°F

Frequency (Hz) / Strain (%)	20	40	70	100	150
0.001	3000	4000	4800	5450	5950
0.002	2950	3850	4600	5200	5550
0.005	2750	3550	4100	4600	4850
0.01	2550	3150	3650	4000	4170
0.02	2250	2650	3000	3300	3450

IV. DYNAMIC CHARACTERIZATION OF TP-H1148 PROPELLANT

Static and dynamic mechanical characterization tests were conducted by CSD under sub-contract to W. L. Hufferd & Associates. Dynamic shear, constant rate to failure and stress relaxation properties were measured on six batches of the Space Shuttle SRM solid propellant (-6,-7,-8,-9, -9970096, -9970115) supplied to CSD by Thiokol/Wasatch Division. The final report for this work [18] is included as Appendix A to this report. The dynamic shear modulus test results are summarized in the following sub-sections.

4.1 TEST EQUIPMENT AND TEST PROCEDURE

Small strain dynamic shear properties of solid propellants and other low modulus materials are routinely measured at CSD using a piezoelectric transducer device. Illustrations of the dynamic test device and the associated electrical equipment are presented in Figures 12 through 14. The device employs a stack of piezoelectric crystals as the dynamic driver source. This dynamic strain is transmitted through the solid propellant sample as shear and the output load is measured using a single piezoelectric crystal which functions as a load cell.

The dynamic shear test device provides a direct measurement of dynamic properties as a function of frequency and test temperature. Equipment is calibrated using stainless steel rings inserted between the piezoelectric driver stack (Figure 13) and the readout crystal to

ORIGINAL PAGE
BLACK AND WHITE PHOTOGRAPH

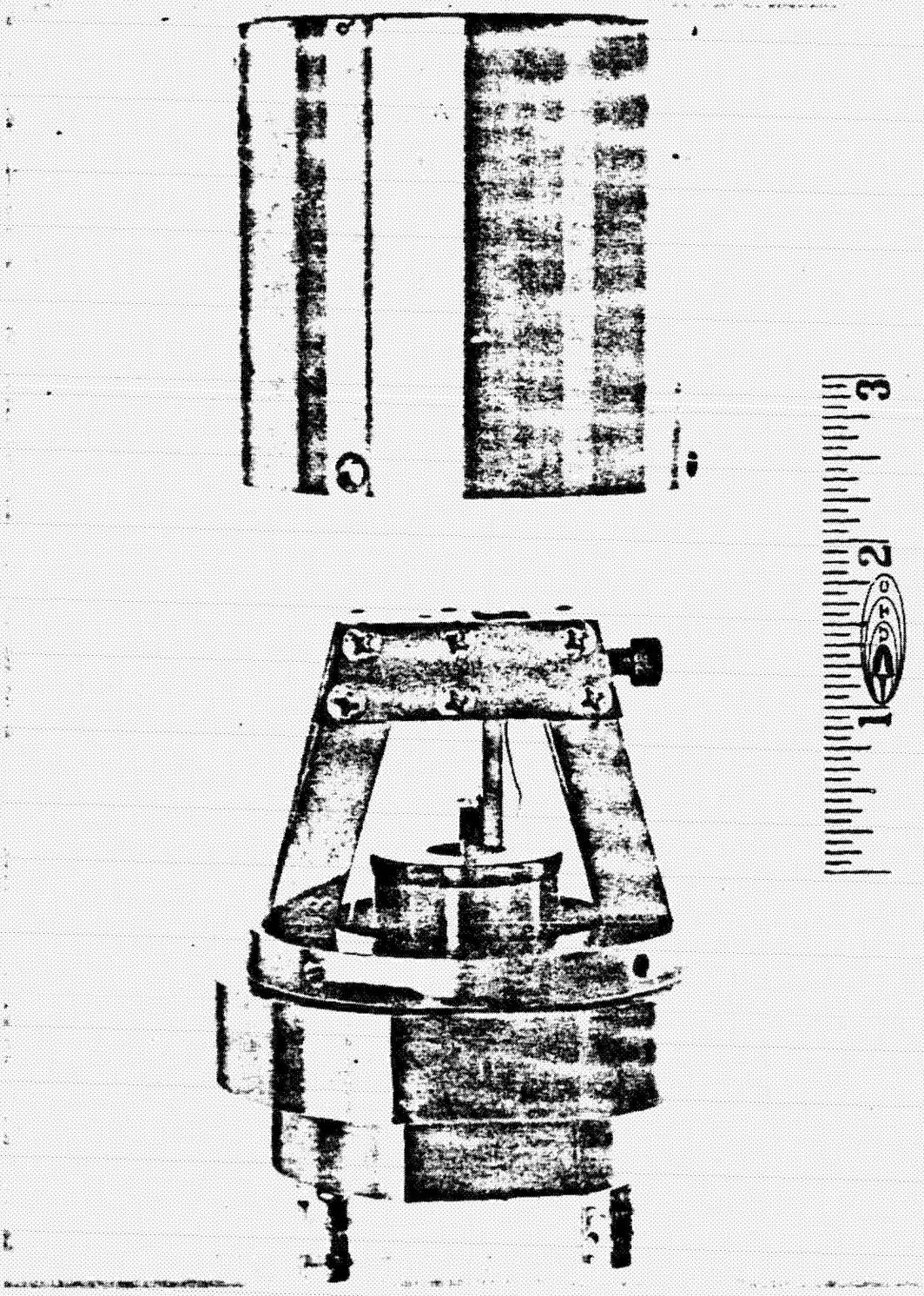

FIGURE 12. Dynamic Shear Test Apparatus and Isolation Cover

ORIGINAL PAGE IS
OF POOR QUALITY

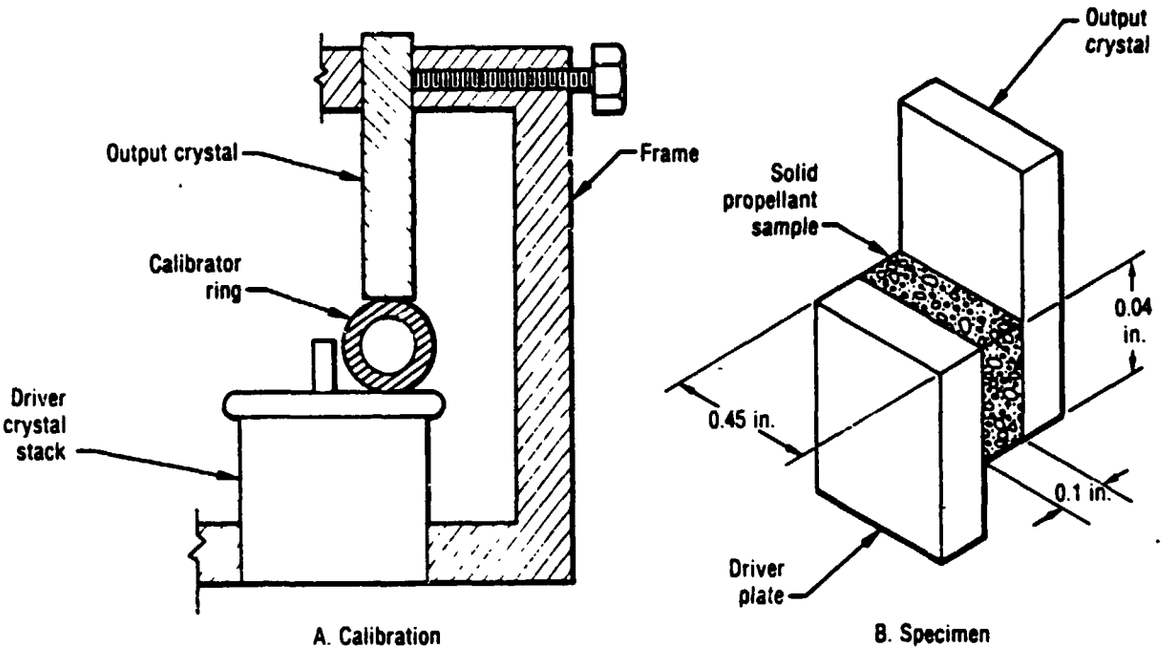

Figure 13. Schematic of Calibration Setup and Specimen

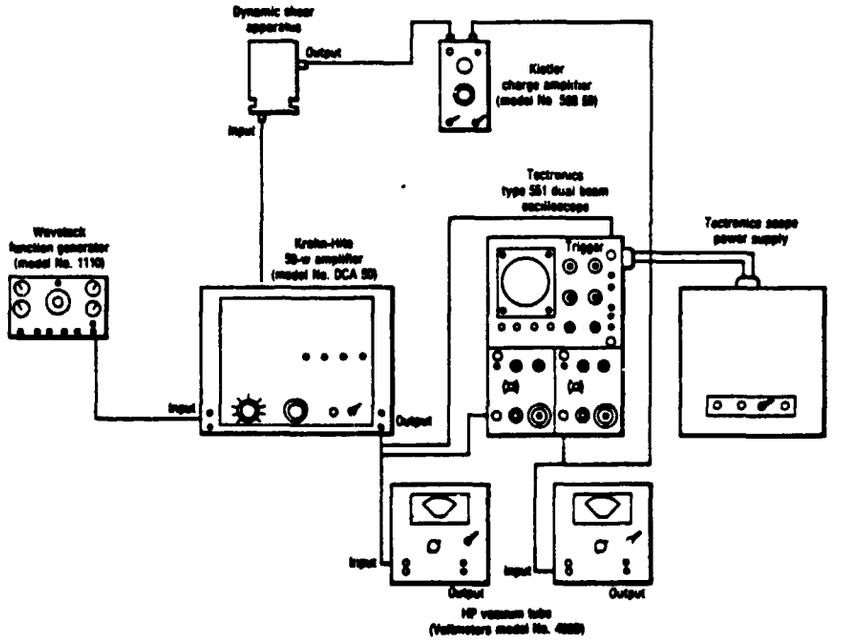

Figure 14. Electrical Equipment for Dynamic Shear Test

calibrate the test device over a wide frequency range. During propellant tests the output signal and the phase angle are measured to determine the dynamic properties of the propellant over the desired frequency and test temperature ranges.

Both the dynamic strain amplitude and the static compressive strain levels can be varied to determine the modulus sensitivity to various loading conditions.

4.2 TP-H1148 PROPELLANT DATA

Dynamic shear modulus behavior was measured for each of the six batches of Shuttle SRM propellant. Production batch No. TP-H1148-9 was evaluated at three static and three dynamic strain levels. Test data for one strain level were obtained for each batch of propellant at 90°, 72° and 40° F.

Dynamic modulus curves are presented in Figures 15, 16, and 17 for batch No. TP-H1148-9 at 0.001% dynamic strain and static strain levels of 3%, 6% and 12%. A comparison of G' curves for each of these tests is presented in Figure 18. Static strain sensitivity at 100 Hz for batch No. TP-H1148-9 illustrates the dynamic modulus increase with compressive static strain levels:

Compressive Strain, %	G', psi
3	2,070
5.8	2,950
12	6,250

where temperature = 72° F, and dynamic strain = 0.001%.

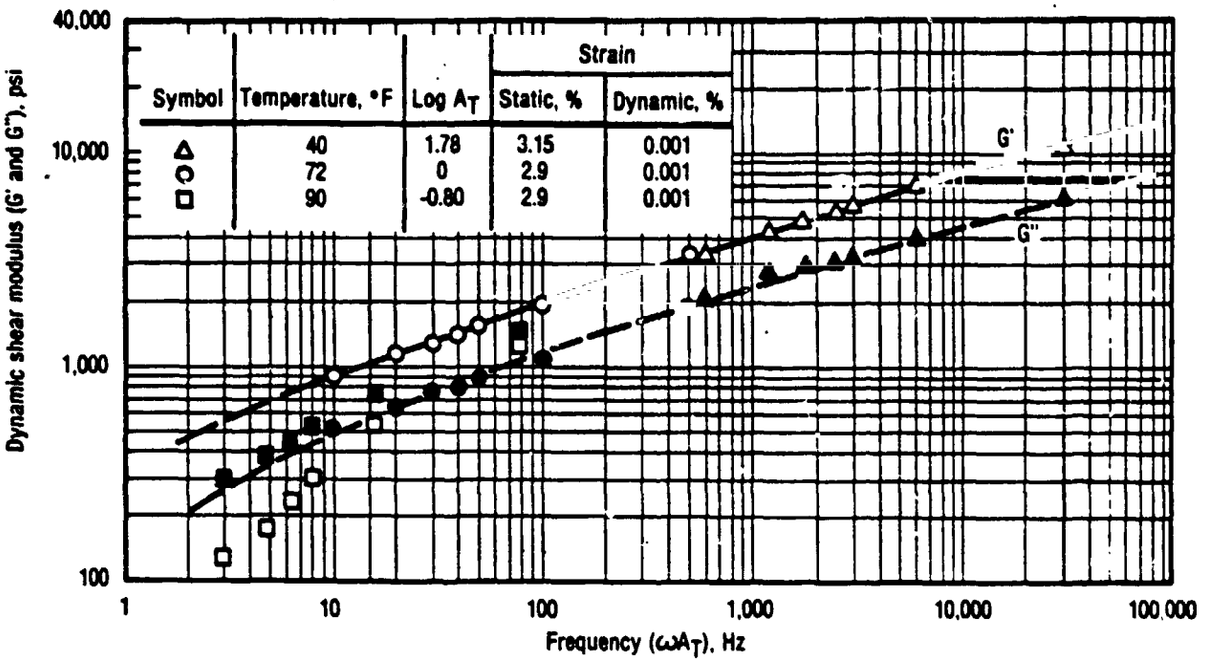

Figure 15. Master Dynamic Shear Modulus for Batch No. TP-H1148-9 at 3% Static and 0.001 Dynamic Strains

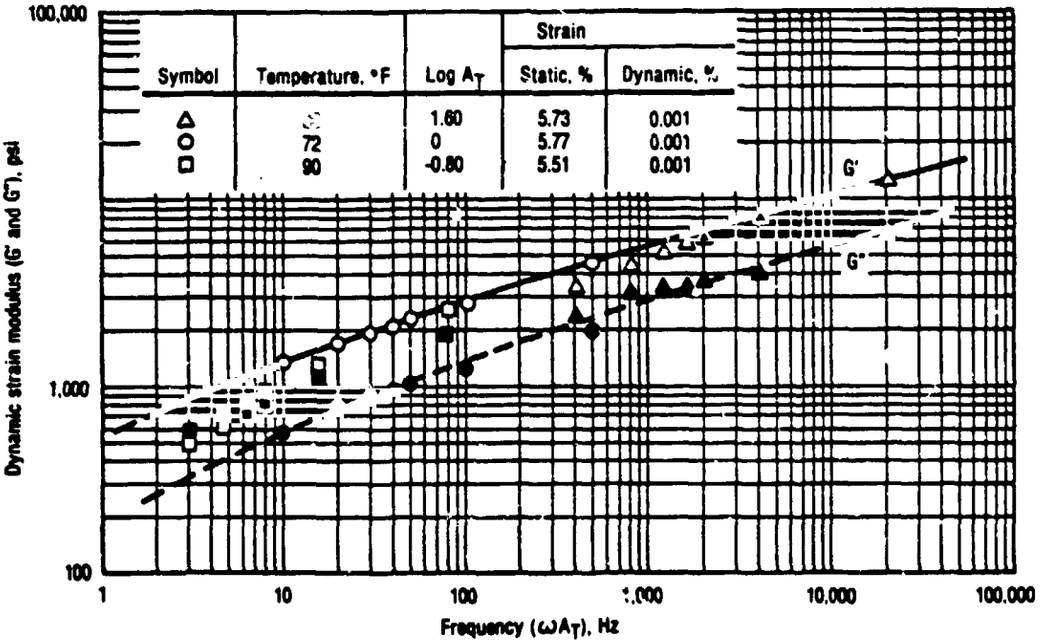

Figure 16. Master Dynamic Shear Modulus for Batch No. TP-H1148-9 at 6% Static and 0.001% Dynamic Strains

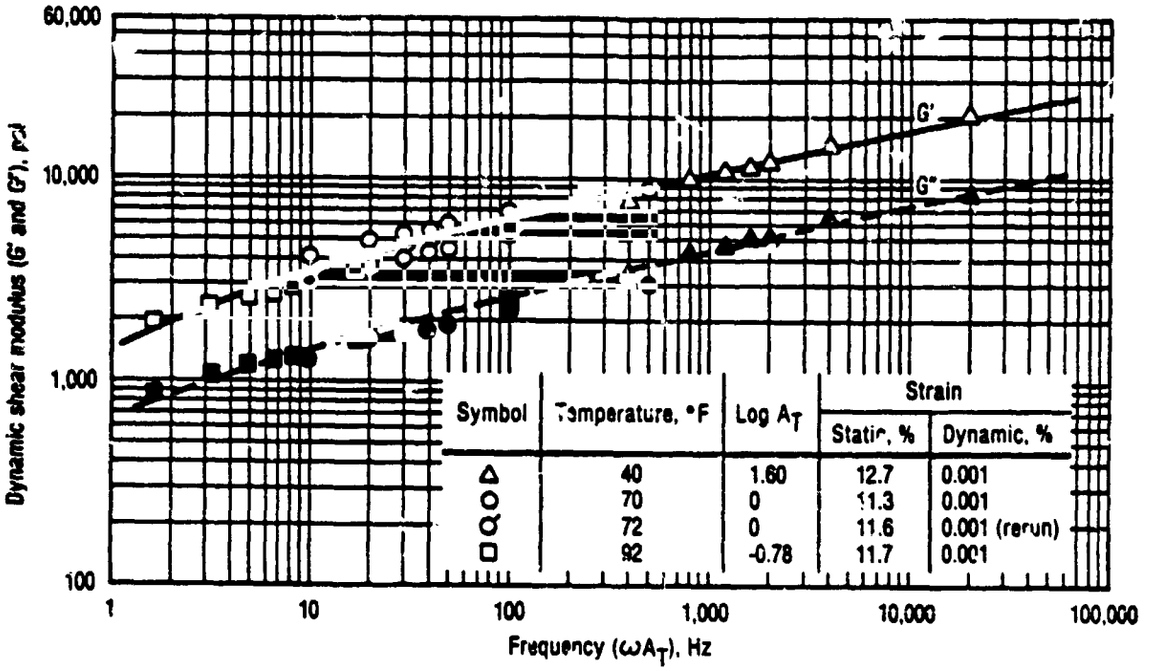

Figure 17. Master Dynamic Shear Modulus for Batch No. TP-H1148-9 at 12% Static and 0.001% Dynamic Strains

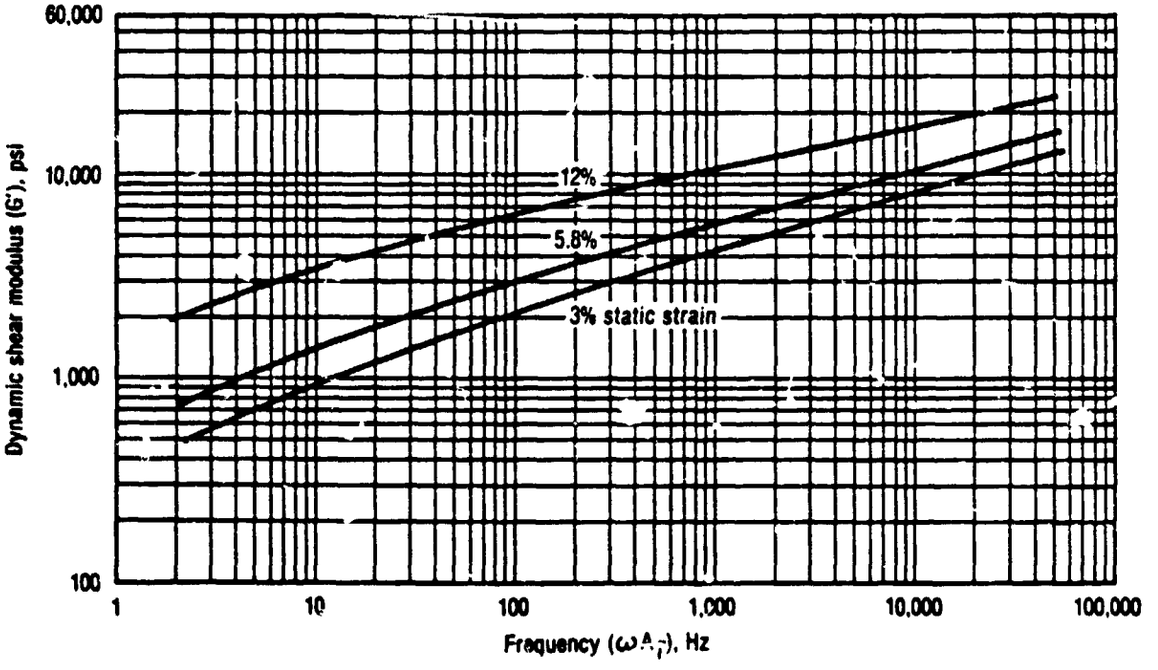

Figure 18. Comparison of Static Strain Levels for Batch No. TP-H1148-9

Test data in Figures 15, 16 and 17 shows that G' actually drops lower than G" at the 90°F test temperature for the 3% and 6% static strains. The soft propellant at 90°F is absorbing a larger percentage of the energy input to the sample.

Empirical shift factors for the three temperatures worked well at all three strain levels (Figure 19).

Dynamic shear moduli as a function of dynamic strain level was measured and is presented in Figures 20 through 23. The real part of the dynamic modulus increases with decreasing strain level but the total range in modulus is less than a 50% variation. This is a much smaller amplitude change than experienced with static strain variations.

Dynamic modulus test results for the other batches of TP-H1148 propellant are presented in Figures 24 through 28. These batches were very similar to the major batch (-9). The real part of the dynamic modulus for each of the six batches is presented in Figure 29.

The real part of the dynamic modulus for each batch at 100 Hz is given below:

Batch No.	G', psi at 100 Hz
9970115	3,100
-9	2,120
-7	2,120
-8	2,100
9970096	1,900
-6	1,800

Batch No. 9970115 has the highest dynamic modulus with the others being close together; batch No. TP-H1148-6 is the lowest.

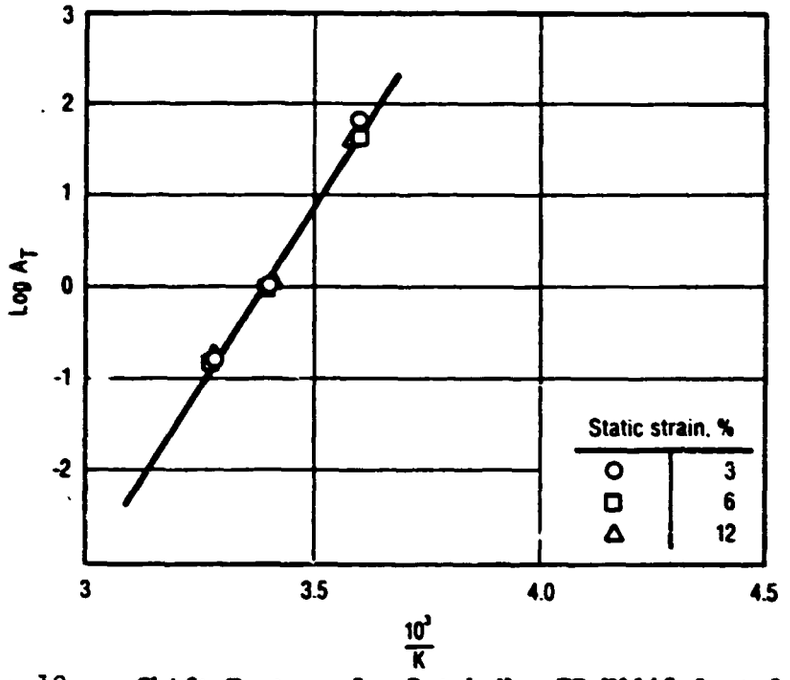

Figure 19. Shift Factors for Batch No. TP-H1148-9 at 0.001% Dynamic and 3% Static Strain Levels

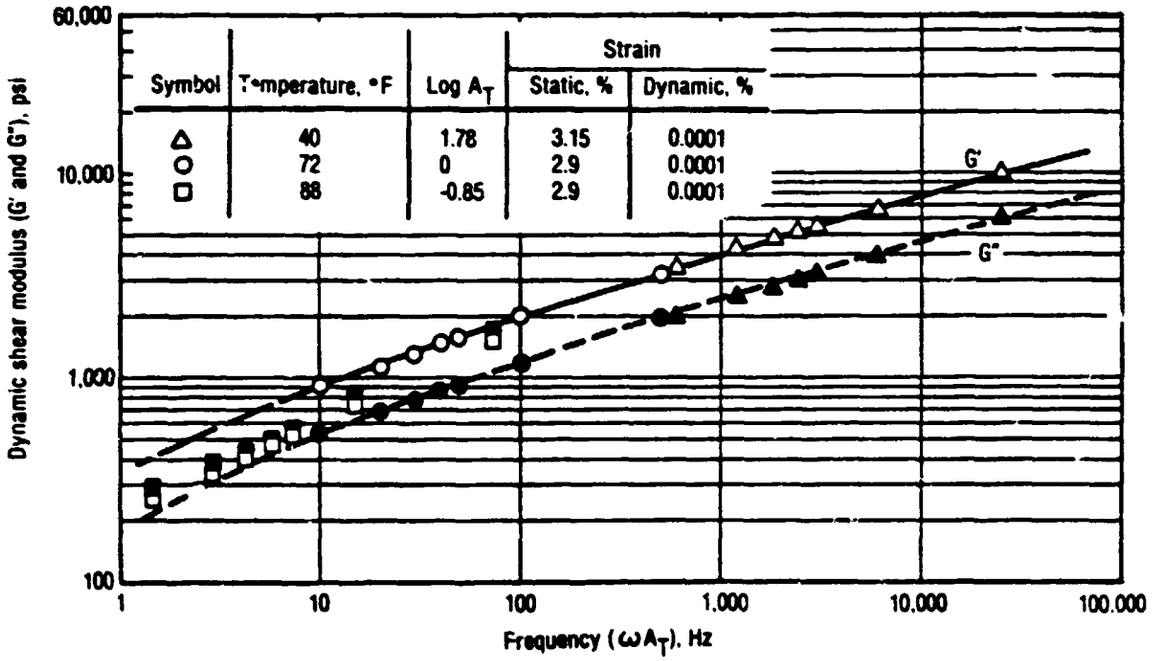

Figure 20. Master Dynamic Shear Modulus for Batch No. TP-H1148-9 at 3% Static and 0.0001% Dynamic Strain

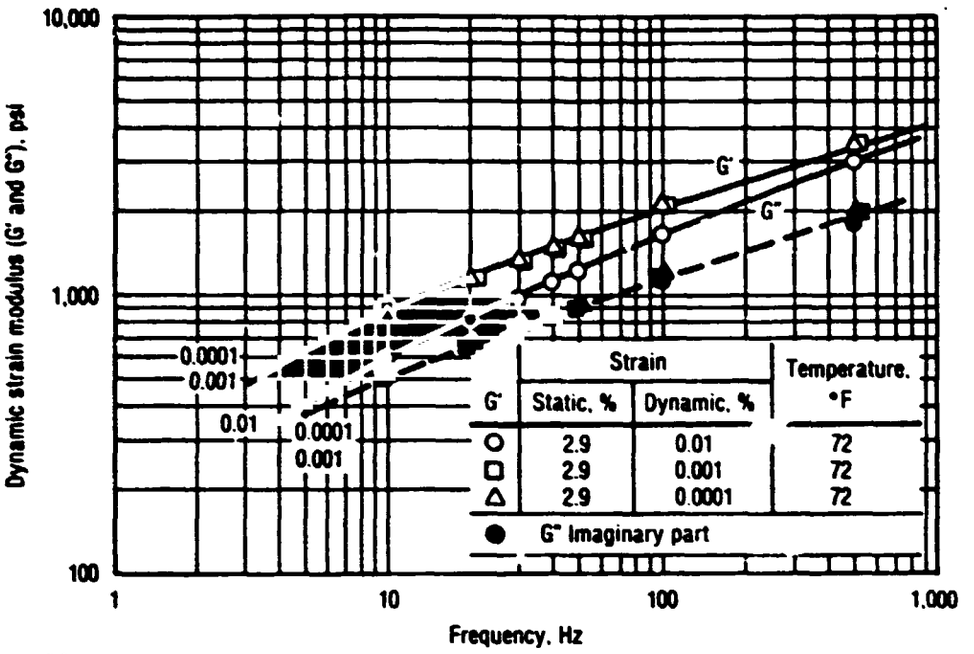

Figure 21. Comparison of Shear Modulus for Batch No. TP-H1148-9 at 2.9% Static and Different Dynamic Strain Levels

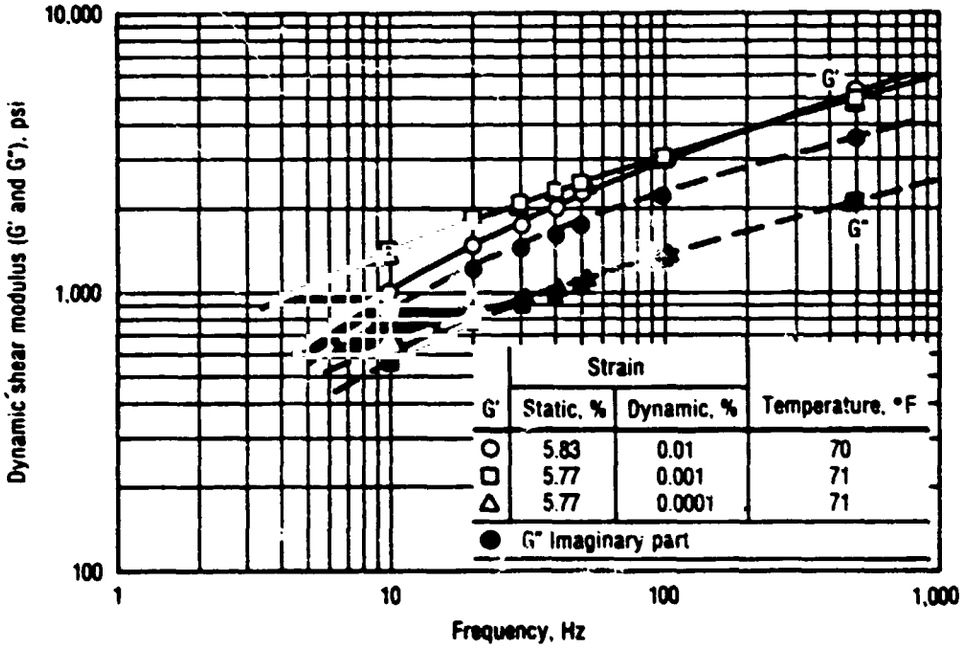

Figure 22. Comparison of Shear Modulus for Batch No. TP-H1148-9 at 5.8% Static and Different Dynamic Strain Levels

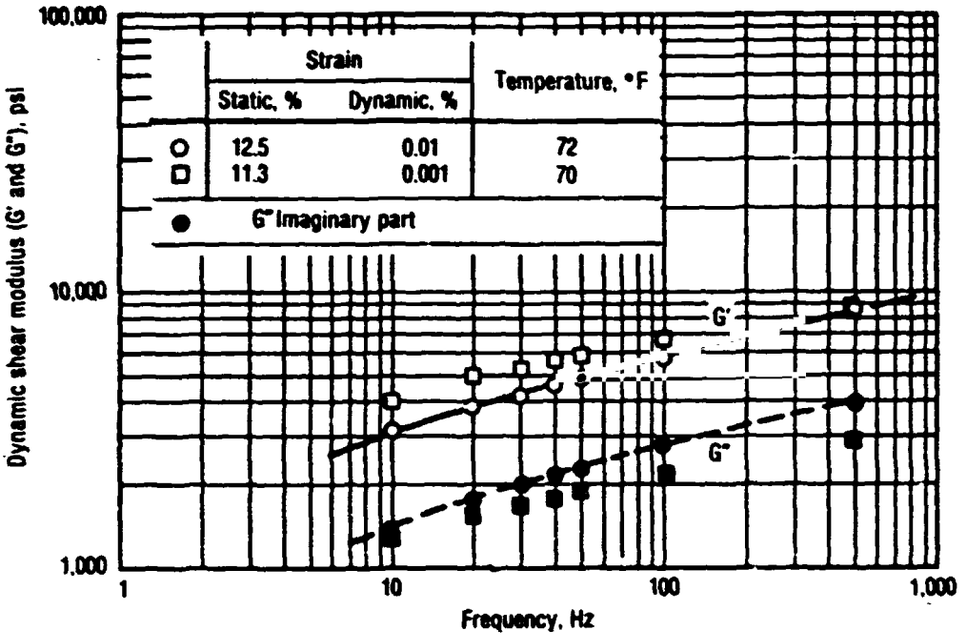

Figure 23. Comparison of Shear Modulus for Batch No. TP-H1148-9 at 12% Static and Different Dynamic Strain Levels

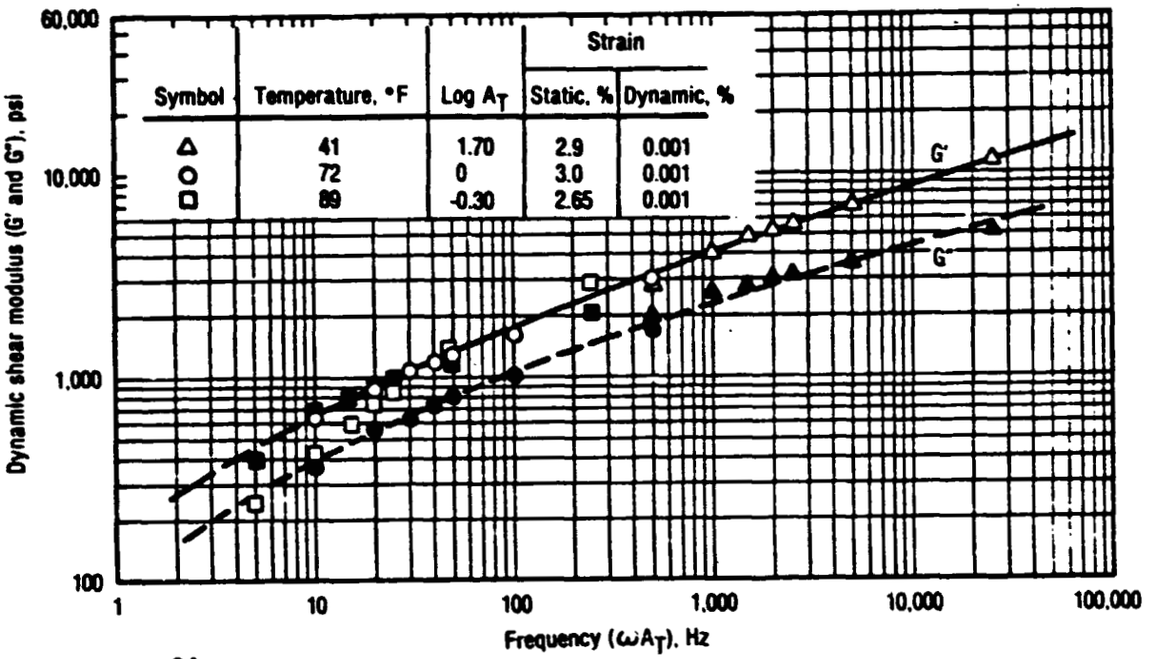

Figure 24. Master Dynamic Shear Modulus for Batch No. TP-H1148-6 at 3% Static and 0.001% Dynamic Strains

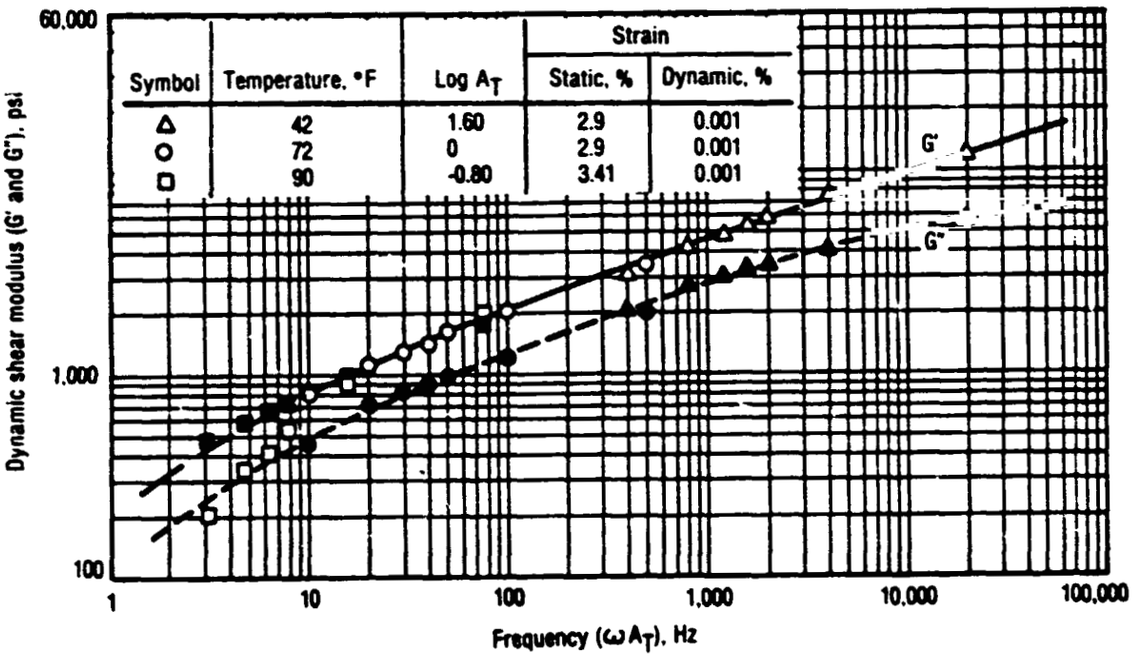

Figure 25. Master Dynamic Shear Modulus for Batch No. TP-H1148-7 at 3% Static and 0.001% Dynamic Strains

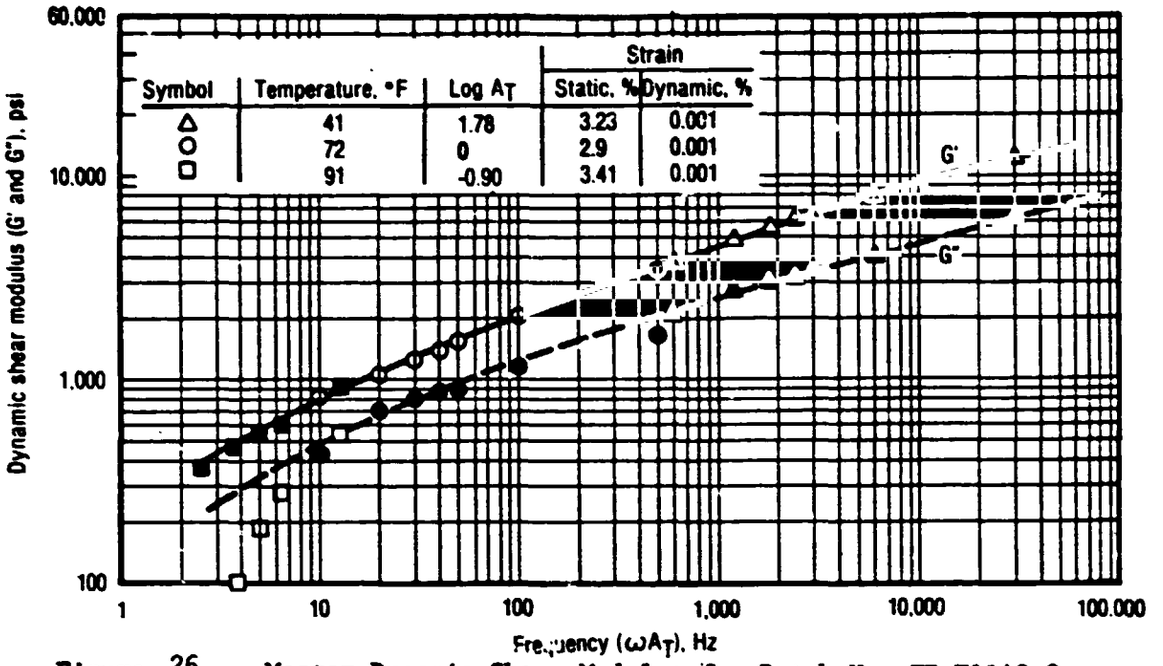

Figure 26. Master Dynamic Shear Modulus for Batch No. TP-H1148-8 at 3% Static and 0.001% Dynamic Strains

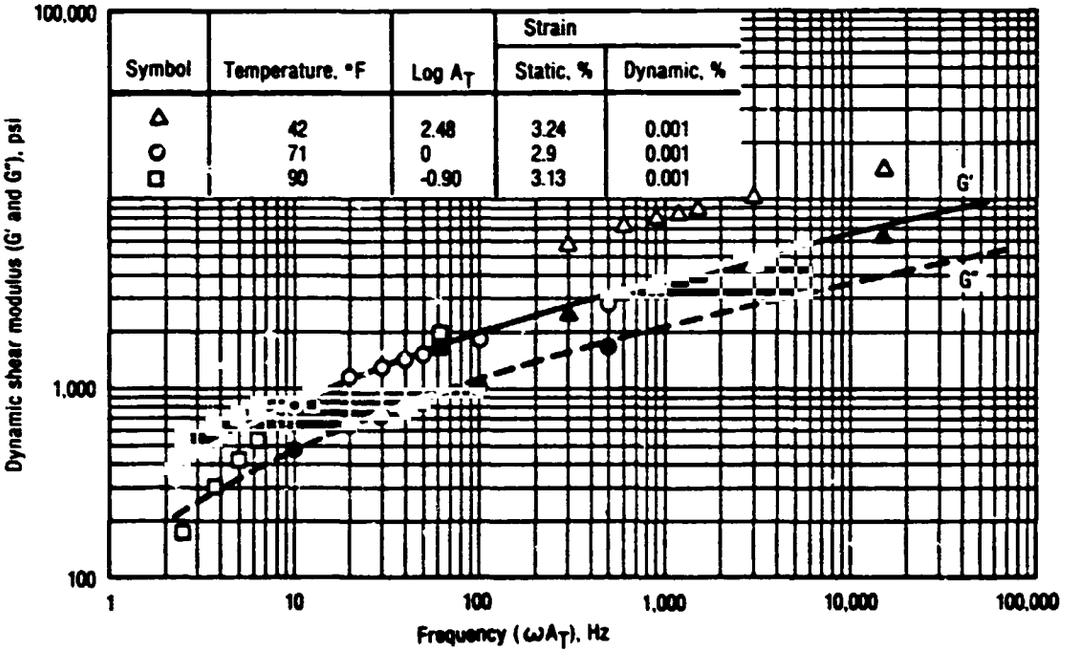

Figure 27. Master Dynamic Shear Modulus for Batch No. TP-H1148-9970096 at 3% Static and 0.001% Dynamic Strains

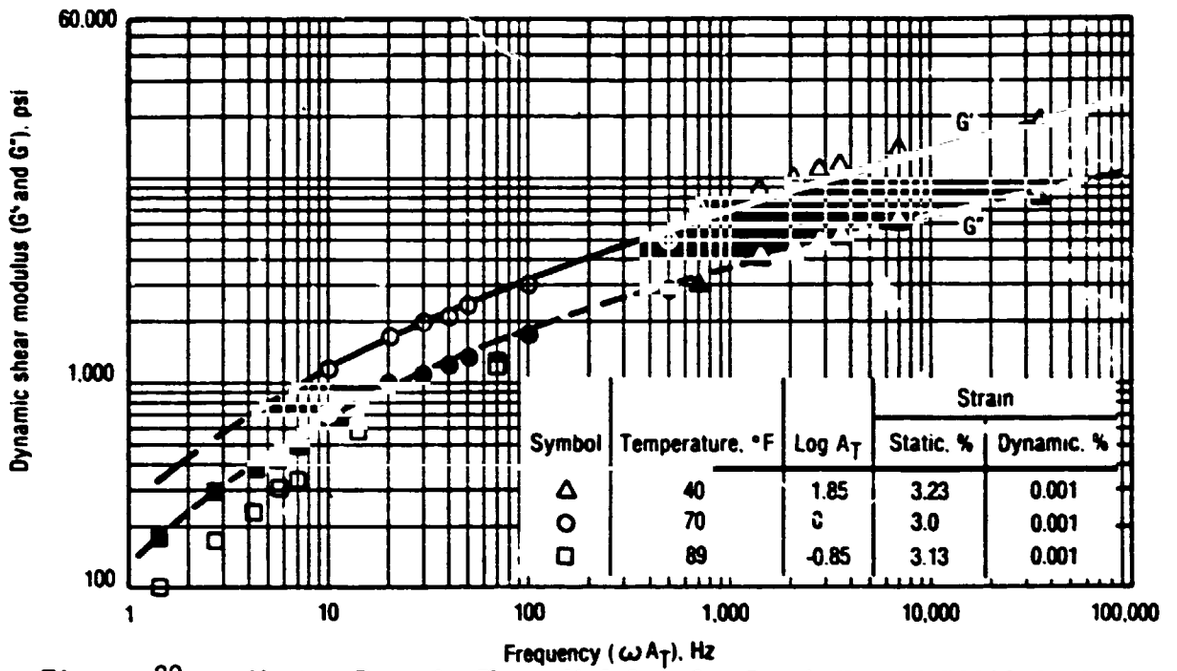

Figure 28. Master Dynamic Shear Modulus for Batch No. TP-H1148-9970115 at 3% Static and 0.001% Dynamic Strains

14299

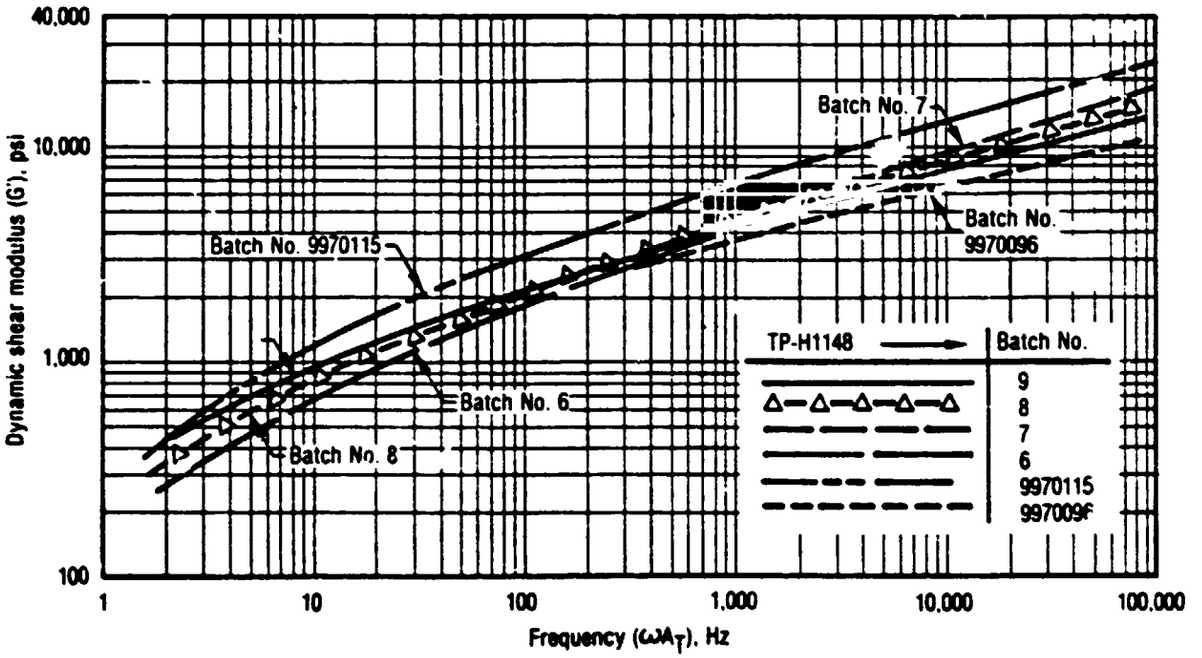

Figure 29. Between Batch Comparison of Propellant TP-H1148 Real Part of Dynamic Shear Modulus at 3% Static and 0.001% Dynamic Strains

The real and imaginary part of the dynamic shear modulus values at 50 Hz are given in Table XVIII for batch -9 and Table XIX for the other five batches. Individual values are listed along with mean values.

4.3 DISCUSSION OF TEST RESULTS

The test data obtained show very small batch-to-batch propellant variability and excellent sample-to-sample reproducibility. Dynamic modulus values are sensitive to the static compressive strain level as well as dynamic strain. Some fuel pockets and voids were observed in the small strain dynamic shear test specimens which may explain the larger data variability than observed with the larger test specimens used for the other test modes.

The test strain levels covered 0.001% to 3% and, correspondingly, a large modulus range. This strain range should be applicable to the Shuttle SRM dynamic loading conditions. Specific modulus values for dynamic analyses can be selected from the available data by defining the propellant strain range and then used with available NASTRAN computer analysis results.

The compressive strain condition of the dynamic shear sample resembles the SRM motor loading during ignition as the propellant grain will be in compression from the internal pressure and a shear load will be superposed due to gravity, loading and acceleration. This particular dynamic shear test [19,20] is more appropriate for determining propellant dynamic properties than the Gottenberg disk and other dynamic

TABLE XVIII. REAL AND IMAGINARY DYNAMIC SHEAR MODULUS FOR BATCH NO. TP-H1148-9 COMPARED AT 50 Hz

Test	G'	G"	Test	G'	G"	Test	G'	G"	Test	G'	G"	Test	G'	G"
S 2.9%	1237	899	S 5.83%	2292	1665	S 12.52%	4544	2624	S 2.9%	312	540	S 3.15%	5727	3306
D 0.01	1202	873	D 0.01%	2228	1741	D 0.01%	4592	2651	D 0.001%	304	527	D 0.001%	5773	3333
T 72°F	1219	886	T 70°F	2287	1662	T 72°F	4724	2407	T 90°F	302	522	T 40°F	5864	3386
	1096	796		2124	1782		4945	2202		302	522		5910	3412
	1113	809		2166	1817		4929	2194		305	528		5818	3359
	1379	1002		2124	1782		4929	2194						
	1273	925		2220	1613		4787	2131						
	1273	925		2119	1655		4787	2131	S 2.9%	524	582	S 3.15%	5131	2962
	1132	822		2097	1638		4787	2131	D 0.0001%	524	582	D 0.0001%	5360	3095
	1252	909		2153	1564		4812	2142	T 88°F	524	582	T 40°F	5487	3168
Mean	1190	885		2181	1692		4784	2281		524	582		5487	3168
										524	582		5366	3098
S 2.9%	1566	904	S 5.77%	2540	1131	S 11.3%	5659	1839						
D 0.001%	1427	824	D 0.001%	2492	1110	D 0.001%	5711	1856						
T 72°F	1518	876	T 71°F	2324	1035	T 70°F	5763	1873						
	1674	966		2139	952		5763	1873	S 5.51%	827	905	S 5.73%	6326	3652
	1304	753		2514	1119		5659	1839	D 0.001%	825	917	D 0.001%	6476	3739
	1727	997		2275	1013		5804	1886	T 90°F	825	917	T 39°F	6463	3731
	1612	931		2275	1013		5649	1836		827	919		6450	3724
	1499	866		2469	1099		5649	1836		826	914		6429	3712
	1542	957		2109	939		5701	1852						
	1554	908		2334	982		5752	1869						
Mean	1542	898		2347	1039		5711	1856						
S 2.9%	1589	917	S 5.77%	2444	1088				S 11.67%	2707	1205	S 12.73%	11042	4916
D 0.0001%	1495	863	D 0.0001%	1965	875	S 11.6%	4480	1456	D 0.001%	2913	1297	D 0.001%	11955	5322
T 72°F	1774	1024	T 71°F	2051	1184	D 0.001%	4380	1423	T 92°F	3008	1339	T 40°F	11115	4949
	1706	985		2536	1129	T 72°F	4206	1367		3056	1361		11695	5207
	1541	890		2323	1034		4355	1415		2921	1300		11452	5098
	1696	979		2299	1023	Rerun								
	1352	790		2205	982									
	1499	866		2548	1134									
	1499	866		2163	963									
	1566	901		2279	1042									
Mean	1572	907		2282	1045									

Notes S = Static Strain
D = Dynamic Strain
T = Temperature

TABLE XIX. **REAL AND IMAGINARY DYNAMIC SHEAR MODULUS FOR OTHER BATCHES OF TP-H1148 PROPELLANT COMPARED AT 50 Hz**

T3183

Notes: T = Temperature
D = Dynamic Strain
S = Static Strain

Batch -6			Batch -7			Batch -8			Batch 9970096			Batch 9970115		
Test	G'	G"	Test	G'	G"	Test	G'	G"	Test	G'	G"	Test	G'	G"
S 29%	5761	2936	S 2.9%	6252	3610	S 3.23%	6020	3067	S 3.24%	8340	3713	S 3.05%	11100	4942
D 0.001%	5511	3182	D 0.001%	6160	3556	D 0.001%	5806	2958	D 0.001%	8423	3750	D 0.001%	11183	4979
T 41°F	5729	2919	T 42°F	6009	3469	T 41°F	6260	3190	T 42°F	8455	3765	T 40°F	11108	4946
	5486	3167		5963	3442		6576	3351		8854	3942		11235	5002
	5693	2901		5963	3442		6651	3389		8912	3968		11138	4959
	5571	3216		5963	3442		6664	3396		8929	3975		11508	5123
	5589	3227		5894	3403		6651	3389		9293	4137		11077	4932
	5566	3214		5789	3342		6638	3382		8848	3939		11055	4922
	5519	3187		5778	3336		6728	3428		9374	4174		11055	4922
	5566	3214		5858	3382		6678	3402		9234	4111		10981	4889
Mean	5599	3116		5963	3442		6467	3294		8866	3947		11144	4962
S 3.00%	1230	799	S 2.89%	1317	855	S 2.89%	1490	860	S 2.9%	1561	902	S 3.00%	2176	1256
D 0.001%	1404	912	D 0.001%	1674	966	D 0.001%	1535	866	D 0.001%	1443	833	D 0.001%	2312	1335
T 73°F	1291	839	T 72°F	1447	836	T 73°F	1490	860	T 71°F	1490	861	T 70°F	2382	1375
	1212	787		1719	992		1628	940		1492	862		2410	1397
	1212	787		1447	836		1538	888		1511	873		2405	1388
	1313	853		1523	989		1595	921		1511	873		2419	1397
	1269	824		1498	973		1572	908		1497	864		2419	1397
	1173	762		1498	973		1458	842		1511	873		2428	1402
	1051	682		1564	1016		1365	788		1511	873		2475	1429
	1214	788		1527	947		1365	788		1511	873		2452	1415
Mean	1237	803		1521	938		1504	868		1504	869		2389	1379
S 2.65%	1039	1154	S 3.41%	549	756	S 3.41%	237	616	S 3.13%	345	598	S 3.13%	302	416
D 0.001%	875	972	D 0.001%	543	747	D 0.001%	266	598	D 0.001%	389	674	D 0.001%	330	455
T 89°F	875	972	T 90°F	540	744	T 91°F	273	546	T 91°F	433	751	T 89°F	334	460
	875	972		540	744		279	626		549	756		337	464
	862	958		539	742		275	618		568	782		344	473
	868	964		545	751		279	627		489	846		340	369
	850	944		539	742		288	646		502	869		350	481
	847	941		545	751		290	651		596	820		356	490
	844	937		542	746		288	646		714	793		356	490
	840	933		545	751		292	655		777	863		359	494
Mean	878	975		543	747		277	623		536	775		341	469

tests inasmuch as large strain gradients exist through the test sample which are not representative of the Space Shuttle SRM conditions.

V. SRM PROPELLANT DYNAMIC RESPONSE MODEL

When considering the stress-strain relation of an elastic material, it is evident that for a particular value of stress there is associated a particular value of strain, and regardless of the length of time that the stress acts on the body, or what path was followed in applying it, the strain remains constant. In viscoelastic materials, on the other hand, when a stress is applied to the body, the strain state depends upon the manner in which the stress is applied; that is, whether the load is applied rapidly or slowly. Thus, the history of loading, as well as the magnitude of the load must be considered in describing the response of a viscoelastic material. In addition, a viscoelastic body will not maintain a constant deformation under a constant stress, regardless of the loading pattern; rather, it will deform or creep with time. Also, if such a body is constrained at constant deformation, the stress necessary to hold it constrained gradually diminishes or relaxes with time.

The stresses and strains at a point in a viscoelastic body may thus be expected to vary with time, or the frequency of loading. And consequently, also with temperature, as will become evident.

The following paragraphs discuss procedures for representing the viscoelastic response properties of solid propellants in general and TP-H1148 in particular. Additional details and justification of the applicability of the procedures to solid propellants are presented in References 12 to 15. The development herein is in terms of the modulus

of the material. Completely analogous results can be obtained employing the creep compliance representation of the response.

5.1 ISOTHERMAL RESPONSE

A convenient representation for the uniaxial (or shear) stress, σ, in a linear viscoelastic material is the so-called integral or relaxation formulation which, for the isothermal case, has the form

$$\sigma(t) = \int_{-\infty}^{t} E_{rel}(t-\tau) \frac{d\varepsilon(\tau)}{d\tau} d\tau \tag{1}$$

where $E_{rel}(t-\tau)$ is the relaxation modulus in tension (or shear) and $\varepsilon(t)$ is the imposed strain history.

The relaxation modulus is defined as the stress decay associated with a step input strain ε_o. With $\varepsilon = \varepsilon_o H(\tau)$, Equation (1) becomes

$$\sigma(t) = \int_{-\infty}^{t} E_{rel}(t-\tau)\, \varepsilon_o\, \delta(\tau)\, d\tau \tag{2}$$

or

$$\frac{\sigma(t)}{\varepsilon_o} = E_{rel}(t) \tag{3}$$

where $H(\tau)$ is the Heaviside unit step function and $\delta(\tau)$ is the Dirac delta function.

For a constant strain rate test, with strain rate R ($\varepsilon = Rt$), Equation (1) yields

$$\sigma(t) = R \int_{o}^{t} E_{rel}(t-\tau)\, d\tau \tag{4}$$

Differentiating Equation (4) with respect to time, t, gives

$$\frac{d\sigma(\tau)}{dt} = R\,E_{rel}(0) + R\int_0^t \frac{dE_{rel}(t-\tau)}{dt}\,d\tau$$

$$= R\,E_{rel}(0) - R\int_0^t \frac{dE_{rel}(t-\tau)}{dt}\,d\tau$$

$$= R\,E_{rel}(t)$$

or

$$\left.\frac{d\sigma(t)}{d\varepsilon}\right|_{\varepsilon = Rt} = E_{rel}(t) \qquad (5)$$

Thus, the relaxation modulus for a linear viscoelastic material can be deduced from differentiation of the stress-strain curve in a constant rate test.

An alternative method of measuring, and expressing, viscoelastic behavior is by considering steady-state response to forced vibrations. Creep and relaxation experiments are not capable of providing complete information concerning the mechanical behavior of viscoelastic solids. In certain cases the response of a structure is sought to a loading for times substantially shorter than the lower limit of time of usual creep or relaxation experiments.

For a linear system, both stress and strain will vary sinusoidally with the same frequency as the forcing frequency:

$$\varepsilon(t) = \varepsilon_0 e^{i\omega t} \rightarrow \sigma^*(\omega)e^{i\omega t}$$

$$\sigma(t) = \sigma_0 e^{i\omega t} \rightarrow \varepsilon^*(\omega)e^{i\omega t}$$

If the input to a linearly viscoelastic material is an oscillatory stress.

$$\sigma(t) = \sigma_0 e^{i\omega t} \tag{6}$$

then the strain response will be an oscillation at the same frequency as the stress, but lagging behind by a phase angle δ. Thus,

$$\varepsilon(\omega) = \varepsilon_0 e^{i(\omega t-\delta)} \tag{7}$$

where ε_0 is the strain amplitude. The phase angle, δ, is often called the loss angle and is a function of the internal friction. It is convenient to write Equation (7) in the form

$$\varepsilon(\omega) = (\varepsilon_0 e^{-i\delta})e^{i\omega t} = \varepsilon^* e^{i\omega t} \tag{8}$$

where ε^* is the complex strain amplitude defined by

$$\varepsilon^* = \varepsilon_0 e^{-i\gamma} = \varepsilon_0(\cos\delta - i\sin\delta)$$

$$= \frac{\varepsilon_0}{\cos\delta + i\sin\delta} \tag{9}$$

If the input is an oscillatory strain,

$$\varepsilon(t) = \varepsilon_0 e^{i\omega t} \tag{10}$$

then the stress response will lead the strain by the phase angle δ,

$$\sigma(\omega) = \sigma_0 e^{i(\omega t + \delta)} = \sigma^* e^{i\omega t} \tag{11}$$

where

$$\sigma^* = \sigma_0 e^{i\delta} = \sigma_0(\cos\delta + i \sin\delta) \tag{12}$$

The complex dynamic modulus is defined as the oscillatory stress response to an oscillatory strain input; that is,

$$E^*(\omega) \quad \frac{\sigma^*}{\varepsilon_0} = \frac{\sigma_0 e^{i\delta}}{\varepsilon_0}$$

$$= \frac{\sigma_0}{\varepsilon_0} (\cos\delta + i \sin\delta)$$

$$\equiv E'(\omega) + i E''(\omega) \tag{13}$$

where $E'(\omega)$ is in phase with the strain and is called the storage modulus

$$E'(\omega) = \frac{\sigma_0}{\varepsilon_0} \cos\delta \tag{14}$$

For low or medium damping materials E' is nearly equal to the relaxation modulus.

The second term of the last line of Equation (13), $E''(\omega)$, is often called the loss modulus and is defined by

$$E''(\omega) = \frac{\sigma_0}{\varepsilon_0} \sin\delta \tag{15}$$

Equation (13) may also be written in the form

$$E^*(\omega) = |E^*| \, e^{i\delta} \tag{16}$$

where

$$|E^*| = \sqrt{(E')^2 + (E'')^2} = \sigma_0/\varepsilon_0 \tag{17}$$

and

$$\delta = \tan^{-1} \left(\frac{E''}{E'}\right) \tag{18}$$

The ratio defining tan δ is called the loss tangent or mechanical loss. It gives a direct measure of the energy dissipation or damping characteristics of the materials. For an elastic material $\delta = 0$, and $E'' = 0$ giving rise to an instantaneous response. For a viscous fluid $\delta = \infty$ and $E' = 0$ with the response 90 degrees out of phase. A viscoelastic solid has a loss tangent between these limits; i.e., $0 < \delta < \infty$.

A representation for the complex dynamic modulus can be obtained in terms of the stress relaxation modulus by substituting Equation (10) into Equation (2). Then,

$$\sigma(t) = \varepsilon_0 \, i\omega \int_{-\infty}^{t} E_{rel} \, (t-\tau) \, e^{i\omega\tau} \, d\tau \tag{19}$$

Performing a change of variables by letting $u = t - \tau$, Equation (19) becomes

$$\sigma(t) = \varepsilon_o \, i\omega \, e^{i\omega t} \int_o^\infty E_{rel}(u) \, e^{-i\omega u} \, du \tag{20}$$

or

$$E^*(\omega) = \frac{\sigma(t)}{\varepsilon_o e^{i\omega t}} = i\omega \int_o^\infty E_{rel}(u) \, e^{-i\omega u} \, du \tag{21}$$

Recalling the definition of the Laplace Transform, Equation (21) is seen to be

$$E^*(\omega) = i\omega \mathcal{L}[E_{rel}(u)] \Big|_{u=i\omega} \tag{22}$$

Thus, if the stress relaxation modulus is known, the dynamic modulus can be obtained by taking the Laplace transform, setting the transform variable equal to $(i\omega)$ and multiplying the result by $(i\omega)$. This observation is particularly useful if an exponential series (Prony Series or Dirichlet Series) is used to represent the relaxation modulus in this case,

$$E_{rel}(t) = E_e + \sum_{k=1}^{n} E_k \exp(-t/\tau_k) \tag{23}$$

where E_e is the equilibrium relaxation modulus, and E_k and τ_k are constants chosen to fit the experimental data. E' and E" are readily determined from Equation (23) to be

$$E'(\omega) = E_e + \sum_{k=1}^{n} \frac{E_k (\omega\tau_k)^2}{1 + (\omega\tau_k)^2} \tag{24}$$

and

$$E''(\omega) = \sum_{k=1}^{n} \frac{E_k (\omega\tau_k)}{1 + (\omega\tau_k)^2} \tag{25}$$

However, this conversion does not work well for solid propellants which usually exhibit nonlinear modulus variations [7,16,17].

Inasmuch as the conversion of static to dynamic material properties does not work well for solid propellants and also due to the fact that most propellant data, including the shuttle propellant, exhibit log-linear behavior over most of the time or frequency range of interest, it is often more convenient to represent the relaxation and dynamic moduli as power laws,

$$E(t) = E_0 t^{-n}$$

$$E'(\omega) = E_0' \omega^{n'}$$

$$E''(\omega) = E_0'' \omega^{n''} \tag{26}$$

where the exponent represents the slope of the modulus versus log time or log frequency plot. Equation (26) describes the dynamic response

of the space shuttle propellant particularly well since we are concerned only with the response over a narrow temperature and frequency range.

5.2 TIME-TEMPERATURE SUPERPOSITION

The analyses of the previous section apply to isothermal conditions, i.e., constant temperature conditions, In practice, it is impossible to obtain either relaxation data or dynamic data over the time scales and frequency ranges of practical interest in a solid rocket motor. In order to obtain data in these ranges the concept of time-temperature superposition is routinely employed. (See References 12 to 15 for a general discussion.)

It has been widely found that temperature has the effect of expanding or contracting the time scale of response viscoelastic materials and that an equivalence between time or frequency and temperature exists. Time and frequency are roughly the inverse of one another so that short time or high frequency response at one temperature corresponds to longer time or lower frequency response at a lower temperature. The converse holds true at higher temperatures. Thus, by obtaining the propellant response at several temperatures, a time-temperature shift function, a_T, relating the equivalence of time or frequency and temperature can be experimentally determined by horizontally "shifting" the test data so that it superimposes to form a single curve at some given reference temperature, usually 21 to 25°C. The resulting curve is known as the "master" response curve and is expressed in terms of temperature-reduced time, t/a_T, in the case of the master relaxation modulus curve,

or in terms of temperature-reduced frequency, ωa_T, in the case of the master dynamic moduli curves.

Thus, the previous analyses remain valid in terms of the master relaxation and dynamic moduli if time, t, and frequency, ω, in the previous expressions are replaced by temperature-reduced time, t/a_T, and temperature-reduced frequency, ωa_T, respectively.

A common analytical representation of the shift factor for amorphous polymers is known as the WLF Equation, which is based on free volume considerations in the neighborhood of the glass transition temperature, T_g [21]:

$$\log a_T = \frac{-8.86(T-T_s)}{101.6 + T-T_s} \tag{26}$$

where T is measured in degrees Kelvin.

A somewhat better representation of the temperature shift factor for solid propellant is obtained using the modified power law representation [14]

$$a_T = \left(\frac{T_R - T_a}{T - T_a}\right)^m \tag{27}$$

where T_R is the reference temperature, and T_a is a characteristic temperature. The representation given by Equation (27) is more convenient for analyzing propellant test data than the WLF equation.

VI. ANALYSIS OF VARIANCE MODEL

The problem of variability in solid propellant mechanical properties has been known for a long time. Bills and Svob [22] discussed the "large statistical variation" in a composite propellant mechanical properties as i relates to establishment of mechanical properties criteria. Marti, Morill and Bersche [23] reported typical values of the standard deviation for various material properties studied during an aging program. Majerus [24] presented histograms of strain data from uniaxial and biaxial tests on propellant, and Wiegand [25] correlated maximum stress and modulus for uniaxial tensile samples tested under various conditions of humidity and temperature and found a strong positive linear correlation between stress and modulus when plotted on log-log paper. An application of statistics to failure criteria was given by Briar and Wiegand [26], and in another publication, Briar [27] presented application of Monte Carlo simulation in modeling constant strain failures in solid propellants. More recently statistical techniques have been applied to the structural analysis of a cast double-base solid propellant grain [28] and the interpretation of elevated temperature data in connection with propellant service life predictions [29].

Many sources of variation operate together to produce the final variability in solid propellant mechanical properties. Variability in propellant ingredients, curative ratio, temperature and duration of cure, test sample machining, storage, handling, testing and data reduction are

all responsible for the variability in the final propellant test data. This variability may be classified in two major components:

(1) variability due to inhomogeneities in the propellant (propellant variance).

(2) variability from all other sources including testing, machining, storage, handling, data reduction, etc. (sampling variance).

The first component, propellant variance, should be used in a statistical stress analysis since it represents the actual variability of the physical property of interest. The second component does not characterize the propellant, but occurs because the sampling procedure is imperfect.

The objective of the statistical analyses of the SRM propellant test data is to determine the form of the probability distributions, the applicable parameters of the probability distributions and the extent, if any, of correlations between parameters.

Previous experience with solid propellants indicates that most data is normally distributed and thus the distribution may be characterized by mean and variance. The applicability of a normal distribution may be investigated from cumulative frequency diagrams using the χ^2-goodness-of-fit test, and by investigating the asymmetry or skewness and the kurtosis of the assumed normal distribution [30]. If the form of the distribution is not normal, then other closed form probability distributions may be considered; e.g., log normal, exponential, gamma, etc. If an exact closed form probability distribution cannot be obtained, then an approximation to the distribution may be generated.

The following subsections present the analysis of variance for the two major components of propellant variability and a probabilistic analysis of the SRM propellant dynamic response model. These analyses are applied to the SRM shuttle propellant in the next section of this report.

6.1 ANALYSIS OF VARIANCE

An analysis of variance is a technique by which the variations associated with certain components of the variance may be isolated and estimated [30,31].

When two or more independent sources of variation operate, the resulting variance is the sum of the separate variances. The procedure followed here is for two independent variances:

(1) variance between castings denoted by σ_1^2

(2) variance within a given batch denoted by σ_0^2

The total variation is obtained by simple addition of the two independent components:

$$\sigma^2 = \sigma_1^2 + \sigma_0^2 \tag{28}$$

To determine the variance exactly requires an infinite number of observations; thus, in practice the variance may only be estimated.

If, in the statistical model, it is assumed that test samples from each batch can be regarded as random elements from a normally distributed population of test samples whose variation is completely specified by the variance σ_0^2, then each casting may be regarded as a random element

from a normally distributed population of batches whose variation is completely specified by the variance σ_1^2. The purpose in analyzing the data is to estimate σ_0^2 and σ_1^2.

Suppose that there are k batches and n propellant samples tested from each batch; then the total number of samples is N = kn. Denote the observations on the i^{th} batch by $(X_{i1}, X_{i2}, X_{i3} - - -, X_{in})$ with mean $\bar{X}_i$. An estimate of the within-batch variance is then given by:

$$\sigma_0^2 \rightarrow \frac{1}{n-1} \sum_{j=1}^{n} (X_{ij} - \bar{X}_i)^2 \tag{29}$$

where the arrow means "is estimated by". A similar expression can be obtained for each sample, and on the reasonable assumption that the variance does not vary from batch-to-batch, a better estimate of σ_0^2 may be obtained by averaging the variance estimated from each batch:

$$\sigma_0^2 \rightarrow \frac{1}{k} \sum_{i=1}^{k} \left(\frac{1}{n-1} \sum_{j=1}^{n} (X_{ij} - \bar{X}_i)^2 \right) \tag{30}$$

If the means of batches are denoted by $(X_1, X_2, - - -, \bar{X}_k)$ and the grand mean by $\bar{\ }$, then an estimate of the variance of the mean is

$$\frac{1}{k-1} \sum_{i=1}^{k} (\bar{X}_i - \bar{X})^2 \tag{31}$$

The variance of the mean of n tests on a given batch due to within-batch variation is σ_0^2. The k batch means will differ also because of the batch-to-batch component of variations σ_1^2, and since the within and

between sources of error are independent, their variances are additive and the variance of each sample mean is $\sigma_1^2 + \sigma_0^2/n$, or

$$\sigma_1^2 + \sigma_0^2/n \rightarrow \frac{1}{k-1} \sum_{i=1}^{k} (\bar{X}_i - \bar{\bar{X}})^2 \tag{32}$$

To facilitate the Analysis of Variance and to help organize the calculations, the format in Table XX is followed. Table XX indicates that the Sum of Squares and Degress of Freedom are additive so that $S_1 + S_0 = S$ and $(k-1) + k(n-1) = n(k-1)$. Solving the expressions given in Table XX results in estimates of σ_0^2 and σ_1^2.

$$\sigma_0^2 \rightarrow M_0 \tag{33}$$

$$\sigma_1^2 \rightarrow (M_1 - M_0)/n \tag{34}$$

TABLE XX

ANALYSIS OF VARIANCE TABLE FOR TWO SOURCES OF VARIATION

Source of Variation	Sum of Squares	Degrees of Freedom	Mean Square	Estimated by Mean Square
Between lots	$n \sum_{i=1}^{k} (\bar{X}_i - \bar{\bar{X}})^2 = S_1$	$k-1$	$M_1 = \frac{S_1}{k-1}$	$\sigma_0^2 + n\,\sigma_1^2$
Within lots	$\sum_{i=1}^{k} \sum_{j=1}^{n} (X_{ij} - X_i)^2 = S_0$	$k(n-1)$	$M_0 = \frac{S_0}{k(n-1)}$	σ_0^2
Total	$\sum_{i=1}^{k} \sum_{j=1}^{n} (X_{ij} - \bar{\bar{X}})^2 = S$	$nk-1$		

The previous procedure may be applied when there are more than two sources of variation. For example, it is possible to introduce variations in propellant ingredients such as oxidizer lot-to-lot variations, polymer lot-to-lot variability, curative lot-to-lot variability, etc. The analysis of variance is not difficult; however, a very substantial test program is required for such an analysis. Such data does not exist; therefore, we have chosen to investigate only the influence of batch-to-batch variability and within-batch variability on the SRM propellant dynamic response.

6.2 CORRELATION ANALYSIS

A correlation analysis of the relationship between two variables begins with an attempt to discover the approximate form of the relationship by graphing the data in a so-called "scatter diagram"; a plot of the points representing corresponding pairs of measurements of the two variables being studied. The most common relationship is a linear relationship where the data tend to form a straight line.

The usual measure of the degree to which the variables are linearly related is the correlation coefficient r. For two variables, X and Y, the correlation coefficient is defined by:

$$r = \frac{1}{n\sigma_X\sigma_Y} \sum_{i=1}^{n} (X_i - \bar{X})(Y_i - \bar{Y}) \qquad (35)$$

The absolute magnitude of r indicates the degree of correlation between the two variables. When all of the points lie on a straight line

(perfect linear correlation) the correlation coefficient is $\pm$ 1. The correlation coefficient is zero when there is no linear correlation between the two variables; however, there may be a nonlinear correlation. A positive correlation coefficient indicates that an increase in one variable tends to be accompanied by an increase in the second variable, and a negative correlation indicates an inverse relationship.

It is also useful to consider the correlation coefficient with regard to a linear regression model. In using a linear regression model with one dependent variable (X), it is assumed that the independent variable (Y) is normally distributed with constant variance σ^2_{XY} at each value of the dependent variable. Thus, σ^2_{YX} is an estimate of the variation of Y about the regression line Y on X. The square of the correlation coefficient indicates the relative portion of the variation in Y which can be explained by the dependence on X,

$$\sigma^2_{YX} = \left(\frac{n-2}{n-1}\right)\left(1-r^2\right)\sigma^2_Y \tag{36}$$

For a multivariate correlation analysis of several variables, such as the situation with the SRM propellant dynamic response model, the covariance, Equation (36) becomes a matrix of the form

$$\left[\sum_E\right] = \begin{bmatrix} \sigma^2_E & \sigma^2_{En} & \sigma^2_{ET_a} & \sigma^2_{Em} \\ \sigma^2_{Em} & \sigma^2_n & \sigma^2_{nT_a} & \sigma^2_{nm} \\ \sigma^2_{ET_a} & \sigma^2_{nT_a} & \sigma^2_{T_a} & \sigma^2_{T_am} \\ \sigma^2_{Em} & \sigma^2_{nm} & \sigma^2_{T_am} & \sigma^2_m \end{bmatrix} \tag{37}$$

Confidence limits for the estimates for the means, standard deviations and correlation coefficients can be estimated using the χ^2 goodness-of-fit test or the students t-distribution.

6.3 PROBABILITY ANALYSIS OF SRM PROPELLANT DYNAMIC RESPONSE MODEL

The SRM propellant dynamic response model is a power-law relationship of the form

$$E = E_o(\omega a_T)^n \tag{38}$$

for either the real (G' or E') or imaginary (G" or E") parts of the complex tensile (E*) or shear (G*) moduli, where ω is the circular frequency and a_T is the time-temperature shift factor defined by

$$a_T = \left(\frac{T_R - T_a}{T - T_a}\right)^m \tag{39}$$

and T_R is the reference temperature to which data at other temperatures are shifted and T_a and m are experimentally determined parameters. The constant E_o in Equation (38) represents the value of the dynamic modulus at a temperature-reduced frequency of $\omega a_T = 1$, and n is the slope of the curve on a log E versus log ωa_T plot.

A computer code, developed in [4] performs a least-squares curve-fit of the master dynamic modulus versus temperature-reduced frequency test data to determine the parameters E_o and n, or predicts dynamic modulus as a function of temperature and frequency, given E_o and n. The computer code is applicable to the real and imaginary parts of the tensile or shear modulus.

In order to account for propellant variability it is desirable to incorporate probability concepts into the SRM propellant dynamic response model. There are basically four approaches for accomplishing this objective [32]:

(1) Monte Carlo Simulation

(2) Maximum Likelihood Methods

(3) Moment Generating Functions

(4) First-Order, Second-Moment Theory

Monte Carlo simulation techniques consist of evaluating Eq. (38) using randomly selected values of the input parameters, E_o and n. In order to use the method and select representative values of E_o and n at random it is necessary to first have a statistical description of each parameter defining the manner in which the parameter can be expected to vary.

Maximum likelihood methods deal primarily with finding a point estimate of the variance based on multiple sets of values for a function of more than one variable. For functions of one variable, this method of estimation is efficient and with large sample sizes is very consistent. If the functional relationships are known, the likelihood methods may be extended to functional combinations.

The variance of a function $h(x_1, x_2 \cdots x_n)$ of n independent random variables may be computed by means of moment generating functions. Let

$$z = h(x_1, x_2 \cdots , x_n) \tag{40}$$

then the variance of z is given by the expected value of $(z-\bar{z})^2$, $E[(z-\bar{z})^2]$, where

$$E[(z-\bar{z})^2] = \int_{-\infty}^{\infty}(z-\bar{z})^2 f(z)dz \tag{41}$$

and f(z) is the probability density function of z.

Therefore,

$$E[(z-\bar{z})^2] = \int_{-\infty}^{\infty}\cdots\int_{-\infty}^{\infty}[h(x_1,x_2,\ldots,x_n)-\bar{z}]^2 * f(x_1,\ldots,x_n)dx_1\ldots dx_n \tag{42}$$

Now a moment generating function for z is given by

$$MGF(z-\bar{z}) = \int_{-\infty}^{\infty} e^{t(z-\bar{z})} f(z)dz \tag{43}$$

Differentiating twice with respect to t and setting t = 0, the variance of z is obtained:

$$var[z] = \left[\frac{d^2MFG(z-\bar{z})}{dt^2}\right]_{t=0} = \int_{-\infty}^{\infty}(z-\bar{z})^2 f(z)dz \tag{44}$$

Using suitable transformations one can then transform to integrals involving $x_1,x_2,\ldots,x_n$.

First-order, second-moment theory probably offers the most advantage because of its relative ease of application and accuracy. Cornell [33] in attempting to encourage wider usage of probability

concepts by non-specialists, proposed a so-called "first-order second-moment" reliability theory.

The term "first-order" indicates the linearization of nonlinear equations and the term "second-moment" refers to the fact that only the first two moments of the involved random variables are needed. For example, some random variables can be characterized by their mean $\bar{X}$ and variance σ_x^2 (or equivalently their standard deviation, σ_x, or coefficient of variation $V_x = \sigma_x/\bar{X}$). The stochastic dependence between a random variable X and a random variable Y is measured by their covariance Cov [X,Y] (or equivalently by their correlation coefficient, $r_{XY} = \text{Cov}[X,Y]/\sigma_x\sigma_y$).

The application of first-order, second moment theory is illustrated in the following example. Let Y be a continuous function of X, i.e., $Y = g(X)$, where X and Y are random variables. Denote the mean of X by $\bar{X}$ or E[X]. Taking a Taylor series expansion of g(X) about $\bar{X}$, g(X) may then be expressed as:

$$g(X) = g(\bar{X}) + (X-\bar{X}) \left.\frac{dg(X)}{dx}\right|_{X=\bar{X}} + \frac{(X-\bar{X})^2}{2!} \left.\frac{d^2g(X)}{dx^2}\right|_{X=\bar{X}} + \ldots \tag{45}$$

Keeping only the first two terms in the expansion and taking the expectation of both sides,

$$E[Y] = E[g(X)] \doteq g(E[X]) \tag{46}$$

since $E(X-\bar{X}) = 0$. Similarly, keeping the same terms and finding the variance of both sides yields the approximation

$$\mathrm{Var}[Y] = \mathrm{Var}[g(X)] \doteq \mathrm{Var}[X]\left[\left.\frac{dg(X)}{dx}\right|_{X=\bar{X}}\right]^2 \tag{47}$$

Since $g(\bar{X})$ is a constant,

$$\mathrm{Var}[g(\bar{X})] = 0 \tag{48}$$

and

$$\mathrm{Var}\left[\left[\left.\frac{dg(X)}{dx}\right|_{X=\bar{X}}\right](X-\bar{X})\right] = \left[\left.\frac{dg(X)}{dx}\right|_{X=\bar{X}}\right]^2 \mathrm{Var}[X] \tag{49}$$

Using this same principle for a variable, say Z, which is a continuous function of several variables, X_1, X_2, ..., X_n (whose means, variances, and covariances are known), the first order approximation of the mean and variance of Z can be obtained by expanding the function $g(X_1,X_2,\ldots,X_n)$ in a Taylor series about the mean of the X's. Keeping only the linear terms in the deviation from the means and applying the same linear transformation rules for the mean and variance, yields

$$Z \doteq g(\bar{X}_1,\bar{X}_2,\ldots,\bar{X}_n) \tag{50}$$

and

$$\mathrm{Var}[Z] = \sigma_Z^2 \doteq \sum_{i=1}^{n}\left(\left.\frac{\partial g}{\partial X_i}\right|_{X=\bar{X}}\right)^2 \sigma_{X_i}^2$$

$$+ \sum_{i=1}^{n}\sum_{\substack{j=1\\ j\neq i}}^{n}\left(\left.\frac{\partial g}{\partial X_i}\right|_{X=\bar{X}}\right)\left(\left.\frac{\partial g}{\partial X_j}\right|_{X=\bar{X}}\right) r_{ij}\,\sigma_{X_i}\,\sigma_{X_j} \tag{51}$$

in which the derivatives are evaluated at the mean values of X_i and X_j.

If the random variables X_i and X_j are independent, then Eq. (51) simplifies to

$$\text{Var}[Z] = \sigma_Z^2 \doteq \sum_{i=1}^{n} \left(\frac{\partial g}{\partial X_i} \bigg|_{X=\bar{X}} \right)^2 \sigma_{X_i}^2 \tag{52}$$

Treating E_o, n, T_a and m as random variables in Eqs. (38) and (39) and ω, T_R and T as deterministic, then

$$E = E(E_o, n, T_a, m) \tag{53}$$

and

$$\frac{\partial E}{\partial E_o} \bigg|_{E=\bar{E}} = (\omega \bar{a}_T)^{\bar{n}} = \frac{\bar{E}}{\bar{E}_o} \tag{54}$$

$$\frac{\partial E}{\partial n} \bigg|_{E=\bar{E}} = \frac{\bar{n}\,\bar{E}}{\omega \bar{a}_T} \tag{55}$$

$$\frac{\partial E}{\partial T_a} \bigg|_{E=\bar{E}} = \frac{\partial E}{\partial a_T} \frac{\partial a_T}{\partial T_a} \bigg|_{E=\bar{E}} = \bar{n}\,\bar{m}\,\bar{E}\,\frac{(T-T_R)}{(T_R-\bar{T}_a)^2} \tag{56}$$

$$\frac{\partial E}{\partial m} \bigg|_{E=\bar{E}} = \frac{\partial E}{\partial a_T} \frac{\partial a_T}{\partial m} \bigg|_{E=\bar{E}} = \bar{n}\,\bar{m}\,\bar{E} \left(\frac{T-\bar{T}_a}{T_R-\bar{T}_a} \right) \tag{57}$$

Applying the previous developments, i.e., Eqs. (50) and (51), it follows that

$$\bar{E} \doteq \bar{E}_o(\omega \bar{a}_T)^{\bar{n}} \tag{58}$$

$$\bar{a}_T \doteq \left(\frac{T_R - \bar{T}_a}{T - \bar{T}_a}\right)^{\bar{m}} \tag{59}$$

$$\begin{aligned}
\mathrm{Var}[E] = \sigma_E^2 \doteq (\bar{n}\,\bar{E})^2 \Bigg\{ & \frac{\sigma_{E_o}^2}{(n\,\bar{E}_o)^2} + \frac{\sigma_n^2}{(\omega \bar{a}_T)^2} \\
& + \bar{m}^2 \frac{(T-T_R)^2}{(T_R - \bar{T}_a)^4}\, \sigma_{T_a}^2 + \bar{m}^2 \left(\frac{T-\bar{T}_a}{T_R - \bar{T}_a}\right)^2 \sigma_m^2 \\
& + 2\, \frac{r_{E_o n}\, \sigma_{E_o}\, \sigma_n}{\bar{n}\bar{E}_o\, \omega \bar{a}_T} \Bigg\} \\
+ \frac{2\,\bar{m}\,\bar{E}\,\bar{a}_T}{(T_R - \bar{T}_a)} \Bigg\{ & \left(\frac{T-T_R}{T_R - \bar{T}_a}\right) \frac{r_{E_o T_a}\, \sigma_{E_o}\, \sigma_{T_a}}{\bar{E}_o} \\
& + \left(\frac{T-\bar{T}_a}{\bar{E}_o}\right) r_{E_o m}\, \sigma_{E_o}\, \sigma_m + \frac{\bar{n}}{\bar{a}_T} \left(\frac{T-T_R}{T_R - \bar{T}_a}\right) r_{n T_a}\, \sigma_n\, \sigma_{T_a} \\
& + \frac{\bar{n}}{\omega \bar{a}_T} (T - \bar{T}_a)\, r_{nm}\, \sigma_n\, \sigma_m + \frac{\bar{m}\bar{n}}{\omega \bar{a}_T} \frac{(T-T_R)(T-\bar{T}_a)}{(T_R - \bar{T}_a)^2}\, r_{m T_a}\, \sigma_m\, \sigma_{T_a} \Bigg\}
\end{aligned} \tag{60}$$

If the random variables E_o, n, T_a and m are not correlated then Eq. (60) reduces to

$$\text{Var}[E] = \sigma_E^2 \doteq (\bar{n}\bar{E})^2 \left\{ \frac{\sigma_{E_o}^2}{(\bar{n}\bar{E}_o)^2} + \frac{\sigma_n^2}{(\bar{a}_T)^2} + \bar{m}^2 \frac{(T-T_R)^2}{(T_R-\bar{T}_a)^4} \sigma_{T_a}^2 + \bar{m}^2 \left(\frac{T-\bar{T}_a}{(T_R-\bar{T}_a)} \right)^2 \sigma_m^2 \right\} \qquad (61)$$

A distinct advantage of this approximate closed form probabilistic approach is that the results are independent of any assumptions regarding the form of the underlying probability distributions.

VII. ANALYSIS OF SRM AND RELATED PROPELLANT DATA

Statistical analyses of UTI-610 inert propellant test data and SRM propellant test data generated by Thiokol and CSD have been analyzed according to the statistical models of Section VI in order to estimate the expected variance of propellant dynamic response properties in the Shuttle SRM. In addition, the influences of dynamic and static strain levels are considered and incorporated as necessary into the SRM propellant dynamic response model. Based on accelerated aging test data of Thiokol [10] an estimate of aging behavior is also made.

7.1 STATISTICAL ANALYSIS OF PROPELLANT DATA

The probabilistic analysis developed in Section 6.3 has been applied to the University of Utah test data on UTI-610 inert propellant in an attempt to estimate the influence of model parameters on dynamic response. An analysis of variance was conducted on the Thiokol and CSD test data to determine expected within-batch and batch-to-batch visibility.

The results of statistical analysis of UTI-610 propellant are presented in Tables XXI through XXVI. Tables XXI and XXII present the model parameters at -18°C, 4°C, 24°C and 49°C and static strain levels of 0.1, 0.5, 1.0, 2.5, and 5.0 percent. The temperature shifted model parameters are presented in Tables XXIII and XXIV. Substantial dependence on static strain level is noted; however, the coefficients

TABLE XXI - MODEL PARAMETERS, REAL PART OF DYNAMIC TENSILE MODULUS AS A FUNCTION OF TEMPERATURE AND STRAIN

Temp. (°C)	Strain (%)	E''_o (MN/m^2)	σ_{E_o} (MN/m^2)	n	σ_n	r	log a_T	$\sigma_{\log a_T}$
-18°C	0.1	243	31.6	0.13	0.04	0.42	22.6	1.58
	0.5	134	9.8	0.17	0.022	0.80	5.1	0.26
	1.0	129	10.8	0.19	0.026	0.79	4.58	0.26
	2.5	122	13.9	0.2	0.035	0.69	5.09	0.32
	5.0	88.1	21.7	0.24	0.075	0.42	3.54	0.53
4°C	0.1	52.0	12.0	0.07	0.07	0.06	10.1	2.54
	0.5	29.5	3.9	0.22	0.04	0.68	2.40	0.39
	1.0	27.6	3.7	0.24	0.04	0.70	1.98	0.71
	2.5	24.9	4.4	0.27	0.054	0.64	1.97	0.42
	5.0	18.3	58	0.34	0.077	0.60	2.84	1.06
24°C	0.1	13.0	4.0	0.06	0.07	0.04	0.14	3.21
	0.5	8.7	0.73	0.22	0.025	0.84	- .03	0.25
	1.0	7.71	0.744	0.25	0.030	0.83	0	0.26
	2.5	6.76	1.01	0.28	0.046	0.73	0.02	0.35
	5.0	5.13	1.73	0.32	0.102	0.41	0	0.69
49°C	0.1	3.02	0.7	0.22	0.07	0.55	-7.18	2.66
	0.5	3.9	0.38	0.20	0.03	0.76	-1.69	0.30
	1.0	3.67	0.31	0.22	0.026	0.84	-1.46	0.23
	2.5	3.06	0.40	0.27	0.040	0.77	-1.28	0.30
	5.0	2.22	0.54	0.33	0.074	0.59	-1.10	0.51

TABLE XXII - MODEL PARAMETERS, IMAGINARY PART OF DYNAMIC TENSILE MODULUS AS A FUNCTION OF TEMPERATURE AND STRAIN

Temp. (°C)	Strain (%)	E''_o (MN/m^2)	σ_E (MN/m^2)	n	σ_n	r	log a_T	$\sigma_{log\ a_T}$
-18°C	0.1	74	5.39	0.18	0.022	0.83	2.94	0.315
	0.5	47	2.47	0.11	0.016	0.78	2.53	0.399
	1.0	48	2.87	0.11	0.018	0.73	2.36	0.420
	2.5	46.8	2.97	0.10	0.020	0.67	2.28	0.436
	5.0	33.6	4.76	0.16	0.044	0.50	2.17	0.421
4°C	0.1	17	3.04	0.29	0.055	0.66	1.54	0.345
	0.5	12.6	1.26	0.28	0.031	0.85	1.47	0.222
	1.0	11.8	1.18	0.30	0.031	0.87	1.38	0.214
	2.5	10.7	1.37	0.31	0.039	0.82	1.34	0.245
	5.0	7.7	1.74	0.38	0.070	0.69	1.34	0.350
25°C	0.1	3.81	0.92	0.36	0.056	0.67	0.02	0.432
	0.5	3.3	0.34	0.34	0.032	0.88	-0.01	0.212
	1.0	2.74	0.32	0.38	0.036	0.89	0.01	0.207
	2.5	2.57	0.32	0.39	0.038	0.88	0.02	0.211
	5.0	1.63	0.49	0.44	0.091	0.62	-0.003	0.446
49°C	0.1	0.69	0.088	0.54	0.039	0.96	-1.40	0.378
	0.5	1.04	0.12	0.36	0.034	0.89	-1.40	0.220
	1.0	0.9	0.094	0.39	0.032	0.91	-1.24	0.184
	2.5	0.75	0.12	0.44	0.049	0.85	-1.22	0.280
	5.0	0.48	0.15	0.52	0.090	0.70	-0.98	0.452

TABLE XXIII - TEMPERATURE-SHIFTED MODEL PARAMETERS, REAL PART OF DYNAMIC TENSILE MODULUS AS A FUNCTION OF STRAIN

Strain (%)	E'_o (MN/m^2)	σ_{E_o} (MN/m^2)	n	σ_n	r
0.1	16.8	1.41	0.056	0.0025	0.88
0.5	8.76	0.24	0.22	0.0032	0.99
1.0	8.20	0.26	0.25	0.0040	0.94
2.5	6.83	0.31	0.28	0.0058	0.97
5.0	5.56	0.58	0.28	0.014	0.88

TABLE XXIV - TEMPERATURE-SHIFTED MODEL PARAMETERS, IMAGINARY PART OF DYNAMIC TENSILE MODULUS AS A FUNCTION OF STRAIN

Strain (%)	E'_o (MN/m^2)	σ_{E_o} (MN/m^2)	n	σ_n	r
0.1	3.88	0.26	0.36	0.01	0.96
0.5	3.43	0.14	0.33	0.0072	0.97
1.0	2.89	0.13	0.37	0.0075	0.97
2.5	2.67	0.15	0.38	0.010	0.96
5.0	1.72	0.16	0.43	0.017	0.91

TABLE XXV - MEAN AND STANDARD DEVIATION, REAL PART OF DYNAMIC TENSILE MODULUS

Temperature-Reduced Frequency (ωa_T)	STRAIN 0.5% $\bar{E}$ (MN/m^2)	0.5% σ_{E_o} (MN/m^2)	1% $\bar{E}$ (MN/m^2)	1% σ_{E_o} (MN/m^2)	2.5% $\bar{E}$ (MN/m^2)	2.5% σ_{E_o} (NM/m^2)	5% $\bar{E}$ (NM/m^2)	5% σ_{E_o} (NM/m^2)
0.01	3.13	1.34	2.59	1.21	1.91	1.19	1.35	1.10
0.1	5.20	2.18	4.61	2.10	3.63	2.18	2.96	1.80
1.0	8.63	3.62	8.20	3.74	6.92	4.15	5.63	3.42
3.5	11.4	4.77	11.2	5.11	9.83	5.90	8.0	4.86
10.0	14.3	6.02	14.6	6.65	13.2	7.91	10.7	6.52
11.0	14.6	6.14	14.9	6.81	13.5	8.13	11.0	6.70
35.0	18.9	7.92	19.9	9.1	18 7	11.2	15.2	9.26
100.0	23.8	9.98	25.9	11.8	25.1	15.1	20.5	12.4
110.0	24.3	10.2	26.6	12.1	25.8	15.5	21.0	12.8
350.0	31.3	13.2	35.5	16.2	35.7	21.4	29.0	17.6
700.0	36.5	15.3	42.2	19.2	43.3	26.0	35.3	21.4
1000.0	39.4	16.5	46.1	19.2	47.9	28.7	39.0	23.7

TABLE XXVI - MEAN AND STANDARD DEVIATION, IMAGINARY PART OF DYNAMIC TENSILE MODULUS

STRAIN

Temperature-Reduced Frequency (ωa_T)	0.5%		1%		2.5%		5%	
	$\bar{E}$ (MN/m^2)	σ_E (MN/m^2)	$\bar{E}$ (MN/m^2)	σ_E (MN/m^2)	$\bar{E}$ (MN/m^2)	σ_E (MN/m^2)	$\bar{E}$ (MN/m^2)	σ_E (MN/m^2)
0.01	0.74	0.41	0.55	0.34	0.47	0.33	0.24	0.34
0.1	1.59	0.88	1.24	0.73	1.13	0.67	0.64	0.77
1.0	3.40	1.88	3.91	1.70	2.72	1.61	1.71	2.10
3.5	5.15	2.84	4.63	2.71	4.37	2.59	2.94	3.56
10.0	7.28	4.02	6.83	3.99	6.52	3.86	4.62	5.60
11.0	7.51	4.14	7.08	4.13	6.76	4.00	4.81	5.83
35.0	11.0	6.07	10.9	6.34	10.5	6.20	7.91	9.59
100.0	15.6	8.58	16.0	9.36	15.6	9.30	12.4	25.1
110.0	16.1	8.86	16.6	9.69	16.2	9.61	12.9	15.7
350.0	23.5	13.0	25.5	14.9	25.2	14.9	21.3	25.8
700.0	29.6	16.3	32.9	19.2	32.8	19.4	28.1	34.8
1000.0	33.3	18.4	37.6	21.9	37.5	22.2	33.4	40.6

of variation associated with the coefficient of the power law, E_o, and the slope, n, of the dynamic moduli curves are generally considerably less than 10 percent, and the coefficients of correlation are generally good. Even though the individual variances in the model parameters is small, the overall effect on the propellant dynamic response, as shown in Tables XXV and XXVI, is to produce expected variances of $\pm$ 50 percent.

An analysis of variance of variance was conducted on the Thiokol test data of TP-H1148 presented in Tables X through XV in Section 3.2. The analyses were carried out at frequencies of 10 and 50 Hz, and the results are summarized in Tables XXVII through XXXVIII. The value F given in the tables is determined by the ratio of the mean squares of the batch-to-batch variations and represents the F-distribution. At a significance level of 1 percent for the specified degrees of freedom, $F^{0.01}$ (5,12) = 5.06, indicating that there is no significant difference among the means of the batches tested.

The total standard deviations are summarized in Table XXXIX. In the case of the loss modulus, G", it can only be concluded that the total variation due to batch-to-batch variation and within batch variation increase with testing frequency. In the case of G', the deviation is approximately the same at 90 and 70°F with an increase at 40°F. The deviation also increases with increasing test frequency.

The test data obtained by CSD on batches TP-H1148-6, -7, -8, -9, 9997-0096 and 9991-0115 and summarized in Tables XVIII and XIX were also analyzed. The ANOVA tables are presented in Tables XL through XLV.

TABLE XXVII. ANOVA Table G' at 90°F and 10 Hz

Source of Variation	Sum of Squares	Degrees of Freedom	Mean Square	Standard Deviation	F
Batch-to Batch	19111	5	3822	11.8	1.12
Within-Batch	40851	12	3404	58.3	
Total	59962	17		59.5	

TABLE XXVIII. ANOVA Table G' at 90°F and 50 Hz

Source of Variation	Sum of Squares	Degrees of Freedom	Mean Square	Standard Deviation	F
Batch-to-Batch	115178	5	23036	56.0	1.69
Within-Batch	163600	12	13633	117	
Total	278778	17		130	

TABLE XXIX. ANOVA Table G' at 70°F and 10 Hz

Source of Variation	Sum of Squares	Degrees of Freedom	Mean Square	Standard Deviation	F
Batch-to-Batch	11859	5	2372	48.7	0.47
Within-Batch	60887	12	5074	30.0	
Total	72746	17		57.2	

TABLE XXX. ANOVA Table G' at 70°F and 50 Hz

Source of Variation	Sum of Squares	Degrees of Freedom	Mean Square	Standard Deviation	F
Batch-to Batch	75730	5	15150	123	0.78
Within-Batch	231867	12	19320	373	
Total	307600			129	

TABLE XXXI. ANOVA Table G' at 40°F and 10 Hz

Source of Variation	Sum of Squares	Degrees of Freedom	Mean Square	Standard Deviation	F
Batch-to-Batch	55933	5	11190	106	0.84
Within-Batch	160067	12	13339	26.8	
Total	21600	17		109	

TABLE XXXII. ANOVA Table G' at 40°F and 50 Hz

Source of Variation	Sum of Squares	Degrees of Freedom	Mean Squares	Standard Deviation	F
Batch-to-Batch	240361	5	48072	94.0	2.23
Within-Batch	259000	12	21583	147	
Total	499361	17		174	

TABLE XXXIII. ANOVA Table G" at 90°F and 10 Hz

Source of Variation	Sum of Squares	Degrees of Freedom	Mean Square	Standard Deviation	F
Batch-to Batch	7764	5	1553	6.6	1.09
Within-Batch	17055	12	1422	37.7	
Total	24819	17		38.3	

TABLE XXXIV. ANOVA Table G" at 90°F and 50 Hz

Source of Variation	Sum of Squares	Degrees of Freedom	Mean Square	Standard Deviation	F
Batch-to-Batch	59395	5	11879	43.8	1.84
Within-Batch	73567	12	6131	78.3	
Total	132962	17		89.7	

TABLE XXXV. ANOVA Table G" at 70°F and 10 Hz

Source or Variation	Sum of Squares	Degrees of Freedom	Mean Square	Standard Deviation	F
Batch-to-Batch	33802	5	6760	40.4	3.64
Within-Batch	22314	12	1860	43.1	
Ttoal	56116	17		59.1	

TABLE XXXVI. ANOVA Table G" at 70°F and 50 Hz

Source of Variation	Sum of Squares	Degrees of Freedom	Mean Square	Standard Deviation	F
Batch-to-Batch	17317	5	3463	58.9	0.36
Within-Batch	115733	12	9644	45.4	
Total	133050	17		74.3	

TABLE XXXVII. ANOVA Table G" at 40°F and 10 Hz

Source of Variation	Sum of Squares	Degrees of Freedom	Mean Square	Standard Deviation	F
Batch-to-Batch	4333	5	867	29.4	0.28
Within-Batch	37377	12	3115	27.4	
Total	41710	17		40.2	

TABLE XXXVIII. ANOVA Table G" at 40°F and 50 Hz

Source of Variation	Sum of Squares	Degrees of Freedom	Mean Square	Standard Deviation	F
Batch-to-Batch	109427	5	21886	67.1	2.61
Within-Batch	100533	12	8378	91.5	
Total	209961	17		113	

TABLE XXXIX. Summary of Total Standard Deviations

	G'		G"	
Temperature (°F)	10 Hz	50 Hz	10 Hz	50 Hz
90°F	59.5	130	38.3	89.7
70°F	57.2	129	59.1	74.3
40°F	109	174	40.2	113

TABLE XL. ANOVA Table G' at 90°F, 2.9% Static Strain, 0.001% to Dynamic Strain and 50 Hz

Source of Variation	Sum of Squares	Degrees of Freedom	Mean Square	Standard Deviation	F
Batch-to-Batch	2360544	5	472109	93.1	112
Within-Batch	202390	48	4216	64.9	
Total	2562934	53		113	

TABLE XLI. ANOVA Table G' at 70°F, 2.9% Static Strain, 0.001% Dynamic Strain and 50 Hz

Source of Variation	Sum of Squares	Degrees of Freedom	Mean Square	Standard Deviation	F
Batch-to-Batch	7803855	5	1560771	161	178.5
Within-Batch	472152	54	8744	93.5	
Total	8276006	59		186	

TABLE XLII. ANOVA Table G' at 40°F, 2.9% Static Strain, 0.001% Dynamic Strain and 50 Hz

Source of Variation	Sum of Squares	Degrees of Freedom	Mean Square	Standard Deviation	F
Batch-to-Batch	233157028	5	46631406	929	840
Within-Batch	2664118	48	55502	236	
Total	235821146	53		958	

TABLE XLIII. ANOVA Table G" at 90°F, 2.9% Static Strain, 0.001% Dynamic Strain and 50 Hz

Source of Variation	Sum of Squares	Degrees of Freedom	Mean Square	Standard Deviation	F
Batch-to-Batch	1591385	5	318277	76.5	119
Within-Batch	128037	48	2667	51.6	
Total	1719423	53		92.3	

TABLE XLIV. ANOVA Table G" at 70°F, 2.9% Static Strain, 0.001% Dynamic Strain and 50 Hz

Source of Variation	Sum of Squares	Degrees of Freedom	Mean Square	Standard Deviation	F
Batch-to-Batch	2387931	5	443272	85.6	140
Within-Batch	171510	54	3177	56.4	
Total	2387931	59		102	

TABLE XLV. ANOVA Table G" at 40°F, 2.9% Static Strain, 0.001% Dynamic Strain and 50 Hz

Source of Variation	Sum of Squares	Degrees of Freedom	Mean Square	Standard Deviation	F
Batch-to-Batch	22672440	5	4534488	289	282
Within-Batch	771010	48	16063	127	
Total	23443449	53		316	

Additional test data at 70°F (Tables XLVI and XLVII) were also analyzed in order to investigate variance as a function of static and dynamic strain level and frequency. The ANOVA tables for the test data in Tables XLVI and XLVII are presented in Tables XLVIII through L. For the CSD test data we cannot conclude that the batch-to-batch means are the same.

A summary of the total standard deviations is presented in Table LI. These data indicate a slight increase in the total variation between 90 and 70°F and a significant increase between 70°F and 40°F. The data presented in Tables XXVIII and XLVI indicate no significant dependence on dynamic strain level between 0.001% and 0.01% dynamic strain. A decrease in dynamic modulus is noted at a dynamic strain of 0.12%.

7.2 INFLUENCE OF STATIC STRAIN LEVEL ON PROPELLANT RESPONSE

The test data previously presented indicate considerable stiffening with increasing compressive strain between 3% and 12% static strains. At 70°F the real part of the modulus approximately doubles between 3% and 6% and doubles again between 6% and 12%. Thus it is possible to construct a static strain shift factor analogous to the time-temperature shift factor by the relation

$$a_\varepsilon = 0.65\, e^{0.15\varepsilon_s} \qquad (62)$$

where $a_\varepsilon = 1$ at 3% strain. Equation (62) applies to the real part of the dynamic modulus, G'. A similar analysis for the loss modulus, G", yields

$$a_\varepsilon = 0.74\, e^{0.10\varepsilon_s} \qquad (63)$$

where $a_\varepsilon = 1$ at 3% strain and ε_s is again expressed in percent strain.

ORIGINAL PAGE IS
OF POOR QUALITY

TABLE XLVI.

STATISTICAL DATA FOR TP-H1148 - 9 AT A NOMINAL 70°F

Sample No.	Static Strain 2.9% Dynamic Strain									Static Strain 5.8% Dynamic Strain					
	.001%			.01%			.12%			.001%			.01%		
	G' 10 Hz	G' 100 Hz	G" 10 Hz	G' 10 Hz	G' 100 Hz	G" 10 Hz	G' 10 Hz	G' 100 Hz	G" 10 Hz	G' 10 Hz	G' 100 Hz	G" 10 Hz	G' 10 Hz	G' 100 Hz	G" 10 Hz
1	908	2043	524	840	2020	485	591	1622	532	1408	3019	813	1597	3067	519
2	793	1881	456	748	1844	432	578	1537	520	1068	2492	616	1547	3009	503
3	1046	2229	604	807	1971	466	584	1608	526	1208	2740	697	1472	2876	478
4	932	2183	538	950	2126	548	519	1449	468	1531	3158	682	1196	2716	609
5	838	1994	484	652	1687	377	503	1467	453	1341	2873	597	1493	3089	573
6	995	2148	574	967	2135	581	699	1804	629	1317	2873	586	1346	2850	517
7	789	1757	455	885	2043	511	601	1609	541	1222	2732	544	1321	2850	507
8	832	1931	500	818	1954	472	617	1627	556	1490	3077	664	1438	3044	640
9	809	1908	486	813	1952	528	536	1486	483	1202	2692	535	1198	2660	534
10	764	1863	459	1041	2196	626	902	1981	655	1298	[illegible]2	578	1270	2780	566
Mean	871	1994	508	852	1993	503	613	1619	536	1308	[illegible]47	631	1388	2894	545
Std. Dev.	95.3	154	51.4	113	150	72.6	116	164	64.9	142	199	84.4	142	152	51.2

TABLE XLVII.

STATISTICAL DATA FOR TP-H1148 AT 2.9% STATIC AND 0.01% DYNAMIC STRAIN

BATCH NUMBER

Sample No.	-9 G' 10 Hz	-9 G' 100 Hz	-9 G'' 10 Hz	-8 G' 10 Hz	-8 G' 100 Hz	-8 G'' 10 Hz	-7 G' 10 Hz	-7 G' 100 Hz	-7 G'' 10Hz	-6 G' 10 Hz	-6 G' 100 Hz	-6 G'' 10 Hz
1	840	2020	485	833	1896	371	693	1767	400	635	1582	367
2	748	1844	432	905	1986	403	949	2126	548	770	1799	444
3	807	1971	466	833	1896	371	769	1900	444	655	1663	378
4	950	2126	548	930	2058	414	950	2171	548	610	1576	352
5	652	1687	377	883	1968	393	746	1900	431	610	1576	352
6	967	2135	581	803	2051	522	820	1964	474	692	1685	399
7	885	2043	511	794	2051	516	782	1938	452	633	1620	365
8	818	1954	472	706	1891	459	796	1982	460	588	1532	339
9	813	1952	528	652	1819	423	841	2026	486	520	1401	300
10	1041	2196	626	661	1819	429	864	2026	499	475	1313	274
Mean	852	1993	503	800	1944	430	821	1980	474	619	1575	357
Std. Dev.	113	150	72.6	98.4	92.4	58.3	83.1	117	47.9	82.7	139	47.7

TABLE XLVIII. ANOVA Table G' at 70°F, 2.9% Static Strain, 0.01% Dynamic Strain and 10 Hz

Source of Variation	Sum of Squares	Degrees of Freedom	Mean Square	Standard Deviation	F
Batch-to-Batch	330675	3	110225	50.3	12.2
Within-Batch	326070	36	9058	95.2	
Total	656745	39		108	

TABLE XLIX. ANOVA Table G' at 70°F, 2.9% Static Strain, 0.01% Dynamic Strain and 100 Hz

Source of Variation	Sum of Squares	Degrees of Freedom	Mean Square	Standard Deviation	F
Batch-to-Batch	1191539	3	399180	97.9	25.0
Within-Batch	573798	36	15939	126	
Total	1771338	39		160	

TABLE L. ANOVA Table G" at 70°F, 2.9% Static Strain, 0.01% Dynamic Strain and 10 Hz

Source of Variation	Sum of Squares	Degrees of Freedom	Mean Square	Standard Deviation	F
Batch-to-Batch	90491	3	30164	24.6	5.97
Within-Batch	217599	36	6044	77.7	
Total	308090	39		81.5	

TABLE LI. SUMMARY OF TOTAL STANDARD DEVIATIONS AT 2.9% STATIC STRAIN

Temperature (°F)	Dynamic Strain (%)	G'			G"	
		10 Hz	50 Hz	100 Hz	10 Hz	50 Hz
90°F	0.001		113			92.3
70°F	0.001		186			102
	0.001	108		160	81.5	
40°F	0.001		958			316

7.3 INFLUENCE OF AGING ON PROPELLANT RESPONSE

Solid propellants typically experience changes in chemical and physical properties due to normal aging during long term storage and thus the SRM propellant may be expected to undergo aging. Thiokol [10] has conducted preliminary accelerated aging tests on TP-H1148 propellant at 75, 110, 135 and 150°F, and interpreted the data according to a previously developed aging model [34,35]. Thiokol has shown that the reaction responsible for the propellant cure is essentially complete in one week and contributes little to the mechanical property changes with age. The aging rate is determined by following the change in gel formation in the binder, which follows an Arrehenius rate equation. The initial aging data obtained on TP-H1148 obtained by Thiokol, although difficult to interpret quantitatively due to initial softening of the propellant rather than the more typical continued post curing, qualitatively suggests that the propellant may be expected to show about a five percent increase in modulus per year. Thus, for a maximum storage of 5 years the dynamic modulus may be expected to increase on the order of 25 percent.

7.4 LIMITS OF PROPELLANT VARIABILITY

The limits of expected propellant variability are established based on the analysis of the previous subsections. The master dynamic data for the 6 batches of propellant tested by CDS have been curve fit to the SRM propellant dynamic response model developed in [4] over the frequency range of 10 to 100 Hz with the results

$$G'(\omega a_T) = 253\ (\omega a_T)^{0.50}\ (r^2 = 0.999) \tag{64}$$

$$G''(\omega a_T) = 200\ (\omega a_T)^{0.38}\ (r^2 = 0.97) \tag{65}$$

and

$$\tan\delta = \frac{G''}{G'} = 0.79\ (\omega a_T)^{-0.12} \tag{66}$$

Figures 30 through 32 present the mean and $\pm$ 3σ standard deviation curves for G', G" and the loss tangent G"/G', based on the analysis of variance results summarized in Table LI.

Table LII summarizes the anticipated limits of the dynamic response of the SRM propellant at several frequencies. The $\pm$ 3σ limits estimated for tanδ are based on the $\pm$ 3σ curves for G' and G", since experience indicates that G" increases as G' does and vice versa. From Figures 30 and 31, and Table LII, it may be seen that G' may vary by as much as a factor of two and G" may vary by a factor of three. G' and G" may be expected to each increase approximately 25% with aging, but tanδ should remain approximately unchanged with aging.

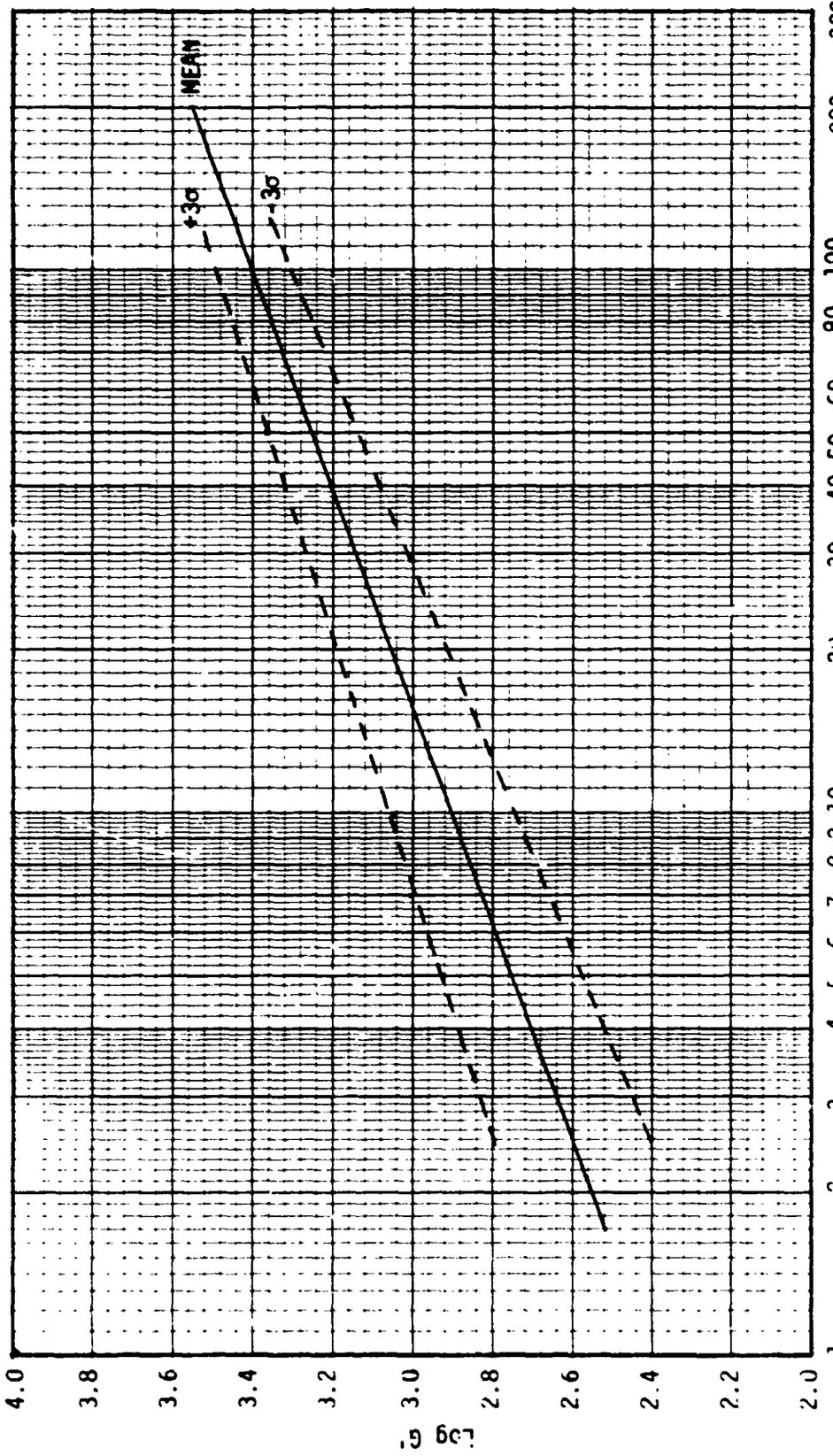

FIGURE 30. Master Dynamic Modulus, G', Versus Temperature Reduced Frequency Mean and 3 Sigma Deviations.

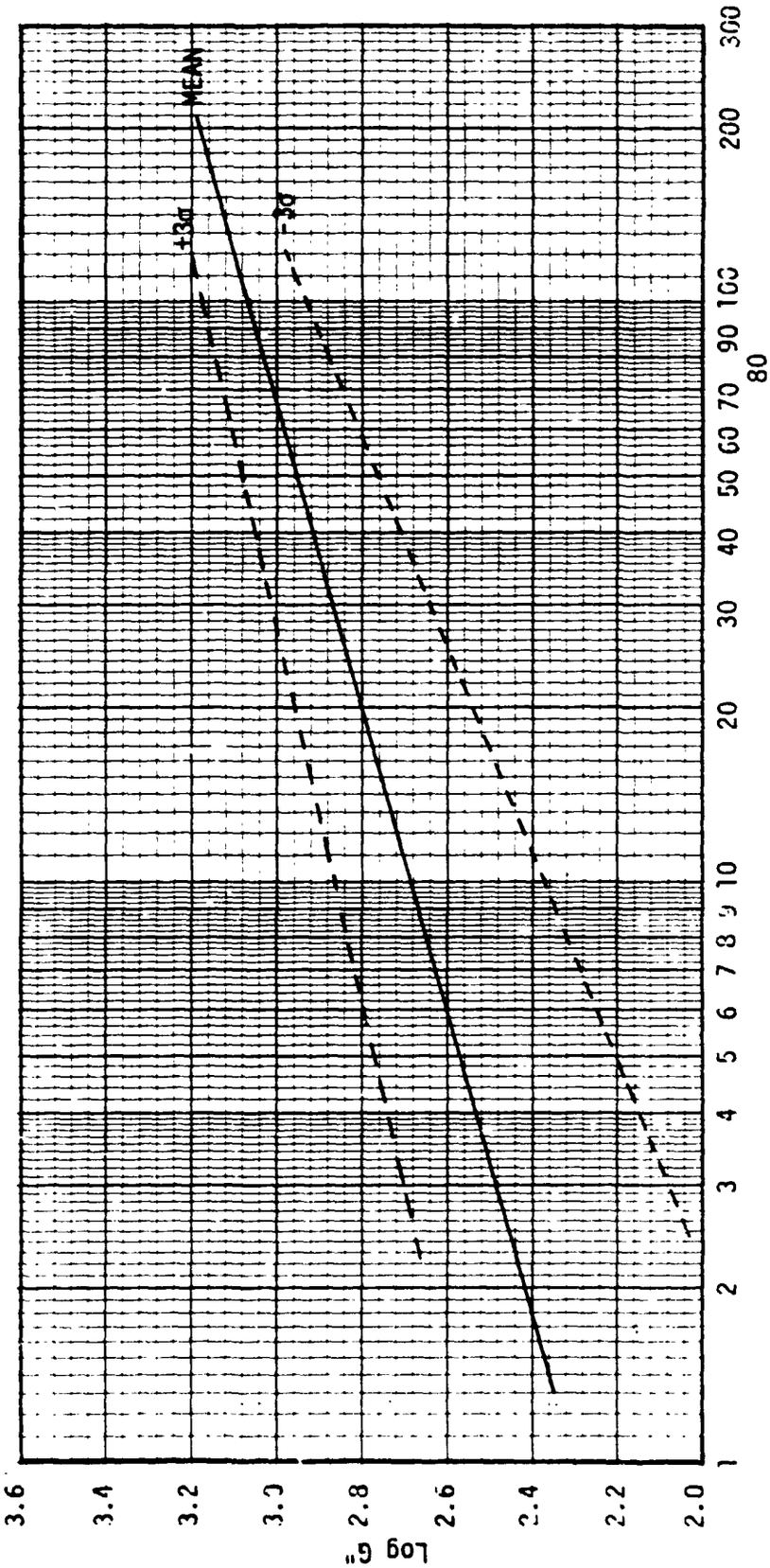

FIGURE 31. Master Dynamic Modulus, G", Versus Temperature Reduced Frequency, Mean and 3 Sigma Deviations.

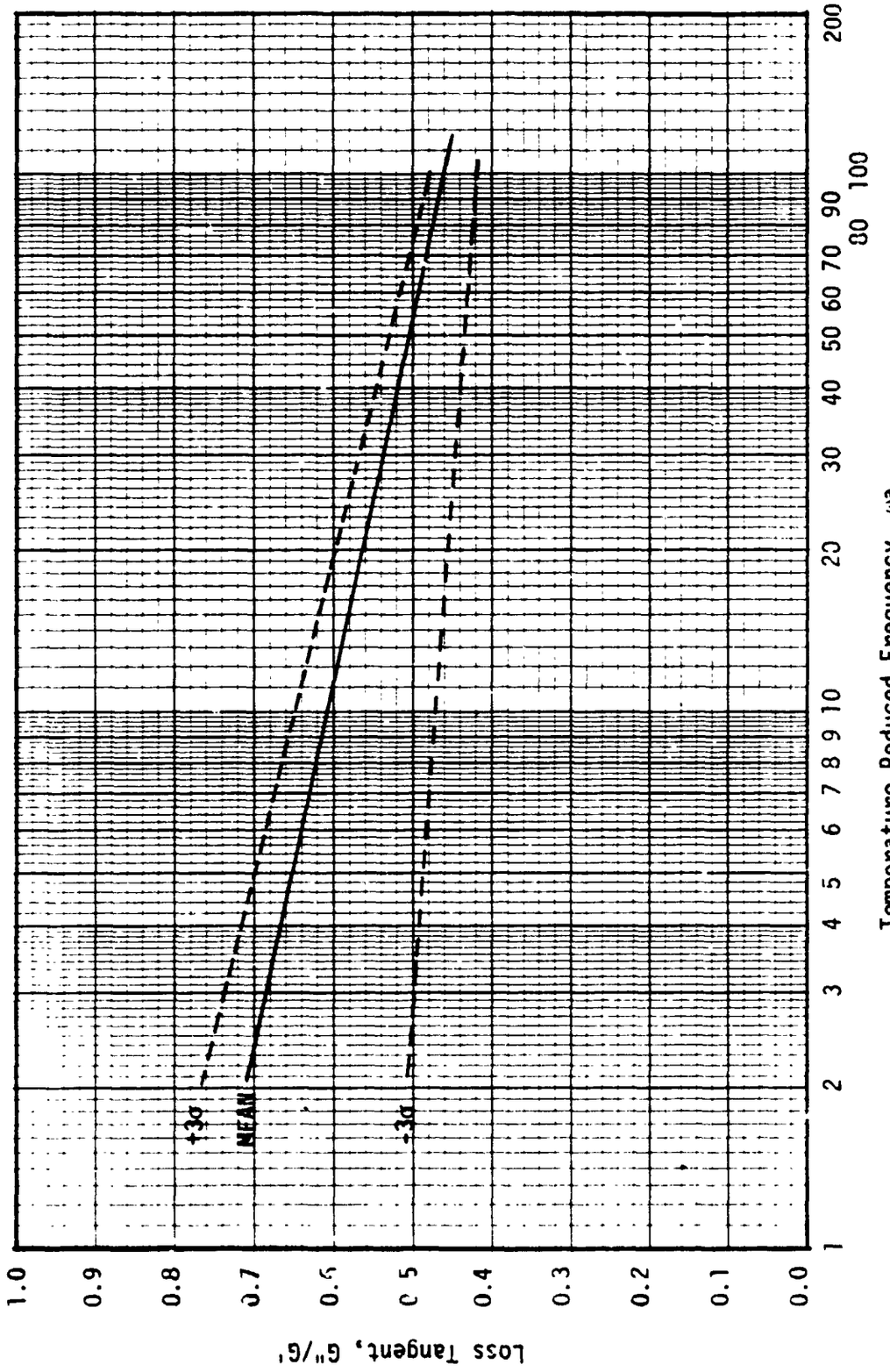

FIGURE 32. Loss Tangent, G"/G' Versus Temperature Reduced Frequency, Mean and Standard Deviations.

TABLE LII. SUMMARY OF SRM PROPELLANT DYNAMIC RESPONSE VERSUS FREQUENCY

	G'			G"			tanδ = G"/G'		
Frequency ωa_T (Hz)	-3σ (psi)	Mean (psi)	+3σ (psi)	-3σ (psi)	Mean (psi)	+3σ (psi)	-3σ	Mean	+3σ
4	331	506	759	141	339	550	0.49	0.67	0.72
7	457	669	1000	195	419	661	0.48	0.63	0.68
10	562	800	1150	234	480	724	0.47	0.61	0.65
15	692	980	1380	302	560	832	0.46	0.58	0.62
20	813	1130	1550	347	624	912	0.45	0.56	0.60
40	1200	1600	2090	517	812	1120	0.44	0.52	0.55
70	1660	2120	2690	708	1005	1350	0.43	0.48	0.51
100	2040	2530	3090	851	1150	1510	0.42	0.46	0.48

VIII. ANALYSIS OF SRM DYNAMIC RESPONSE

Dynamic response analyses of the Shuttle SRM have been conducted to investigate the sensitivity of the SRM frequency response to propellant variability. In addition, a heat conduction analysis has been conducted to determine if significant temperature gradients may exist in the SRM at launch time.

8.1 GENERAL DISCUSSION OF VIBRATION ANALYSES OF SOLID ROCKET MOTORS

General surveys of vibration effects on solid rocket motors have been presented by IBM [1,3], Hufferd and Fitzgerald [14], Fitzgerald and Hufferd [13], Achenbach [36], and Baltrukonis [37]. An extensive bibliography, including abstracts, is presented in [4].

Compared to other structures, solid propellant rocket motors possess rather unique structural features. Whereas the mass of the propellant is very large compared to the mass of the thin-walled case, the propellant is generally compliant and contributes little to the stiffness of the composite structure, affecting the gross dynamic behavior of the motor mainly through its mass. Furthermore, since propellants are viscoelastic materials, the propellant provides considerable damping to the system. Consequently, transient effects attenuate very quickly and steady-state oscillations require a high energy input since a large amount of energy is dissipated.

In recent years finite element models have been developed for the steady state vibration of solid propellant rocket motors [38-42].

The finite element models lead to definition of a stiffness matrix, a mass matrix and a damping coefficient matrix for the discretized system. Lumped-mass and consistent-mass methods are used for defining the mass distribution. The lumped-mass method concentrates the element masses in a manner that maintains the location of the center of mass of the structure, whereas, in the consistent-mass approach the mass is represented as it is actually distributed in the structure. In practice, better agreement has been obtained using the lumped-mass approach. This approach requires a large number of coordinate points for accurate analysis of systems with primarily distributed masses; however, the mass matrix for the entire structural assemblage is diagonal and positive definite, thereby reducing computation times. On the other hand, the consistent-mass approach requires excessive computational effort to obtain a desired degree of accuracy.

Damping matrices can be derived analogous to those used for the mass and stiffness matrices of appropriate internal damping characteristics. Propellant damping is accounted for using the dynamic complex representation of material properties.

In dynamic problems, Hamilton's variational principle is frequently used to derive Lagrange's equations of motion for the discrete system. In the absence of damping the system of equations to be solved has the form

$$[M]\{\ddot{r}(t)\} + [K]\{r(t)\} = \{R(t)\} \qquad (67)$$

where the mass matrix [M] is composed of the element masses, {R(t)} represents the vector of nodal point forces at time t, and {r(t)}

represents the vector of nodal point displacements at time t. The natural frequencies of the system are obtained by taking the nodal point force vector R(t) to be the null-vector.

For damped systems it is necessary to employ nodal damping to obtain solutions for the damped structure. Several methods are available for introducing damping for a propellant grain. An effective damping coefficient, $[C_{eff}]$ may be defined by

$$[C_{eff}] = \frac{[K"]}{\omega} \tag{68}$$

where [K"] represents the imaginary part of the complex stiffness matrix. Some structural codes, such as NASTRAN, employ a structural damping coefficient, ζ, defined by

$$\zeta = \frac{G"}{2G'} = \frac{1}{2} \tan \delta \tag{69}$$

where G" and G' are, respectively, the imaginary and real part of the complex shear modulus.

More directly, steady state dynamic viscoelastic analysis may be obtained from the corresponding elastic counterpart, employing the viscoelastic-elastic correspondence principle, in which all elastic material constants are replaced by their corresponding viscoelastic counterpart expressed as frequency dependent complex numbers, i.e.,

$$E \rightarrow E^*(i\omega) = E'(\omega) + iE"(\omega)$$

$$G \rightarrow G^*(i\omega) = G^*(\omega) + iG"(\omega)$$

$$K \rightarrow K^*(i\omega) = K'(\omega) + iK"(\omega)$$

$$\nu \rightarrow \nu^*(i\omega) = \nu'(\omega) + i\nu"(\omega)$$

where K denotes the bulk modulus and ν represents Poisson's ratio. Lamés relations still hold among the complex moduli in the frequency plane so that

$$\nu^*(i\omega) = \frac{1}{2} - \frac{E^*(i\omega)}{6K^*(i\omega)} \tag{70}$$

An elastic material is represented in this notation by a complex modulus with a real part which is constant with frequency and imaginary part which is zero for all frequencies. The common assumption of a constant, elastic bulk modulus implies that the dynamic Poisson's ratio will contain a nonzero imaginary part. Equation (67), for the natural frequencies of vibration, then takes the form

$$[-\omega^2 M + K' + iK''] \{r^*\} = 0 \tag{71}$$

or

$$\begin{bmatrix} -\omega^2 M + K' & K'' \\ K'' & \omega^2 M - K' \end{bmatrix} \begin{Bmatrix} r' \\ r'' \end{Bmatrix} = \begin{Bmatrix} 0 \end{Bmatrix} \tag{72}$$

The above replacement leads to a system of equations with twice as many unknowns as the corresponding elastic problem; however, the solutions may be obtained in a manner analogous to the static case. Obvious simplifications are noted if the problem is handled throughout in complex arithmetic.

Two general techniques are employed for solving the equations of motion for vibration loading. The first consists of direct step-by-step integration of the simultaneous differential equations. The response history is divided into a sequence of time increments of equal length and the equations of motion are formulated on an incremental basis. The motion computed during each time increment is added to the conditi s at the beginning of the increment to obtain the conditions at the end. Thus, the response is evaluated step-by-step through the desired time range, starting with any given initial condition. The acceleration is assumed to vary linearly during the time increment, which leads to expressions for the change in acceleration (and velocity) in terms of the initial conditions and the change of displacement.

The incremental equations of motion are solved by standard static analysis methods; for example, Gauss elimination.

In the second method of solving the equations of motion, the equations are first decoupled by transforming to normal (mode shape) coordinates which are solved independently mode by mode, and the modal results superposed to obtain the total response. In this method, known as mode superposition, the displacement vector is expressed as a linear combination of mode shapes. Substitution of this expression into the equations of motion results in a single uncoupled equation for the n^{th} mode of the system. The solutions of each modal response equation are obtained by any convenient procedure.

8.2 PREVIOUS VIBRATION ANALYSES OF THE SHUTTLE SRM

Several vibration analyses of the space shuttle SRM have been conducted by IBM [1,3] and Thiokol/Wasatch Division [6]. Additional one-eighth scale dynamic model tests have been conducted by the NASA/ Langley facility [5]. Analyses of the one-eighth scale models has been carried out by Grumman Aerospace Corporation [2]. The results indicate that reasonably good agreement is obtained from simplified analyses of dynamic response with more sophisticated NASTRAN analyses and experimental results.

IBM [1] conducted simplified and NASTRAN analysis for, among other things, longitudinal through-the-thickness shear vibrations. They also investigated the effects of moduli and grain length. The properties shown below, representative of the shuttle SRM, were used in their analysis for longitudinal shear vibrations:

$$a = 20 \text{ inches}$$

$$b = 70 \text{ inches}$$

$$\rho_p = 0.064 \text{ lb/in}^3$$

$$\nu_p = 0.495$$

They assumed the outer boundary to be rigidly clamped. In addition, based on information received from CSD, two different expressions were used for representation of the dynamic complex shear modulus, depending upon strain level. For low strains the representation

$$G' = 2800\ \omega^{.220}$$

was used in their simplified analysis, and

$$G^* = 6244\ (1 + 0.384i)$$

was used in their NASTRAN complex eigenvalue analysis. A value of $G' = 6244$ was used in a NASTRAN real eigenvalue analysis.

At high strains, the corresponding representations were

$$G' = 900\ \omega^{.145}$$

and

$$G^* = 1365\ (1 + .245i)$$

The simplified analyses were carried out using the expression

$$\omega_n = \frac{\Omega_n}{2}\sqrt{\frac{G'}{\rho b^2}\ g} \qquad (73)$$

where Ω_n is a circular frequency coefficient which depends on the ratio a/b. Table LIII presents the results for the first natural frequency using Equation (73) and a NASTRAN real and complex eigenvalue analysis, including the effects of length as determined from the NASTRAN analysis.

IBM subsequently conducted a more complete NASTRAN analysis of longitudinal shear vibration including coupling with the case [3] and forced vibrations. These analyses treated several geometries which included more realistic representations of propellant grain configuration with forward and aft skirts, nose cone and nozzle attached. A constant shear modulus of 1333 psi and a loss tangent of 0.246 were used in all analyses. The results indicated several longitudinal modes below 50 Hz with the first in the neighborhood of 15 Hz with a maximum shear strain of 0.95%.

TABLE LIII. RESULTS FOR THE FIRST NATIONAL FREQUENCY OF SHUTTLE SRM [3]

	Low Strains	High Strains
Equation (73)	38.1 Hz	17.9 Hz
Real Modulus	38.2 Hz	17.9 Hz
Complex Modulus	38.8 Hz	18.0 Hz
L = 100 inches	37.0 Hz	17.3 Hz
L = 150 inches	37.7 Hz	17.6 Hz
L = 300 inches	38.2 Hz	17.9 Hz

The NASA/Langley Research Center has conducted dynamic tests of one-eighth scale models of the shuttle SRM and mated external tank model. Three propellant grain configurations were manufactured by CSD using inert UTI-610 propellant which has the same binder-fuel-curative components as UTP-3001 propellant used in the TITAN III-C with inert sodium chloride and inert ammonium sulphate substituted for the live oxidizer, ammonium perchlorate. All had 0.1875 inch thick aluminum shells and were 19.5 inches in diameter and 147.32 inches long. The propellant length was approximately 145.4 inches. The propellant grain inner diameters were varied to represent lift-off, mid-burn and end-of-burn configurations.

The model test at NASA/Langley [5] for the lift-off configuration indicated the first bending mode at 54.1 Hz, the first torsional mode at 135.3 Hz and the first longitudinal mode at 149.7 Hz.

Grumman [2] has also conducted dynamic analysis of the SRM models tested at the NASA/Langley facility using NASTRAN. They used a constant modulus of elasticity of E = 25,000 psi (G = 8333 psi) and a loss tangent of 0.52 based on material property data supplied by CSD.

The results of Grumman's NASTRAN analysis for the lift-off configuration gave the first bending mode at 56.2 Hz (compared to 58.4 Hz for simple beam theory), 168.3 Hz for the first torsional mode (compared to 161 for simple beam theory) and 196 Hz for the first longitudinal mode (compared to 180 for simple beam theory).

Part of the reason for the discrepancy between Grumman's analyses and the experimental results of NASA/Langley may be attributed to the fact that the material properties used by Grumman are probably unrealistic for the actual test conditions.

The final set of analyses conducted on the shuttle SRM, to be discussed herein, were conducted by Thiokol/Wasatch Division [6] on a model 312 inches long, a grain O,D, of 146 inches and an inner port diameter of 67 inches using properties of TP-H1123 and H-13 (inert TR-H1123) propellant, which are similar to the shuttle SRM propellant. Their results indicated a first longitudinal thickness shear mode at 14.6 Hz with G' = 650 psi for TP-H123 propellant and 11.4 Hz with G' = 380 psi for H-13 inert propellant at 70°F. The natural frequencies varied from 8.6 Hz at 40°F to 26 Hz at 90°F for the first longitudinal shear mode.

8.3 SHUTTLE SRM HEAT CONDUCTION ANALYSIS

Biot's approximation method [43] has been applied to cooldown of the Shuttle SRM in order to estimate the temperature distribution that would exist in the SRM at launch time. The analysis is axisymmetric so that the temperature, T, must satisfy the one-dimensional (radial) heat conduction equation:

$$k \frac{\partial^2 T}{\partial r^2} = \rho c \frac{\partial T}{\partial t} \tag{74}$$

where

T = temperature

r = direction of heat flux

t = time

c = specific heat capacity

ρ = density

k = coefficient of thermal conductivity

Defining a heat flow vector H by

$$k \frac{\partial^2 T}{\partial r^2} = \rho c \frac{\partial T}{\partial t} = - \frac{\partial^2 H}{\partial r \partial t} \tag{75}$$

it follows that

$$\rho c T = - \frac{\partial H}{\partial t}$$

or

$$H = - \int_{q'}^{t} \rho c T \, dr \tag{76}$$

and

$$k \frac{\partial T}{\partial t} = - \frac{\partial H}{\partial t} \tag{77}$$

where q_1 is the depth to which heat has penetrated at time, t. Employing variational techniques, one can define functions

$$V = \frac{1}{2} \rho c \int_0^r T^2 \, dr$$

$$D = \frac{1}{2k} \int_0^{q_1} \left(\frac{\partial H}{\partial t}\right)^2 dr \tag{78}$$

and

$$Q = T(t) \left. \frac{\partial H}{\partial q_1} \right|_{r=o}$$

where V is the thermal potential, D is the dissipation, and Q is the thermal force which satisfy Lagranges equation

$$\frac{\partial V}{\partial q_1} + \frac{\partial D}{\partial \dot{q}_1} = Q \tag{79}$$

Solution of Equation (79) yields the penetration depth, q_1, as a function of time, and hence the temperature spatial distribution as a function of time.

The solution to Equation (79) is obtained for a circular port grain with inner radius a and outer radius b. The inner port is assumed insulated and a step temperature change is applied to the outer boundary. Two time regimes are considered:

(1) $0 \leq t \leq t_a$

(2) $t_a \leq t \leq \infty$

where the time t_a is the time for the heat front, defined as the distance q_1 from the outside, to reach the inner port. The input temperature is written as

$$T(b,t) = T_1 \, u(t) \tag{80}$$

where u(t) is the Heaviside unit step function. The spatial temperature distribution, based on experimental evidence and the form of the exact solution, is represented by

$$T(r,t) = \begin{cases} T_o \left(1 - \frac{b-r}{q_1}\right) & \text{for } b-r \leq q_1 \text{ and } 0 \leq t \leq t_a \\ \cdot & \\ 0 & \text{for } b-r \geq q_1 \text{ and } t_a \leq t < 0 \end{cases} \tag{81}$$

Substituting into Equations (75) through (78), Equation (79) becomes

$$q_1^2 \, \dot{q}_1 - 2b \, q_1 \, \dot{q}_1 = - 10 \, \kappa b \tag{82}$$

for the penetration depth, q_1, where $\kappa = k/\rho c$ is the thermal diffusivity. Equation (82) may be integrated directly to yield the cubic relation

$$\frac{q_1^3}{3} - b \, q_1^2 = - 10 \, \kappa b t \tag{83}$$

Equation (83) has only one real root

$$q_1 = b\left[2\cos\left(\frac{\theta+4\pi}{3}\right) + 1\right] \tag{84}$$

where

$$\cos\theta = 1 - 15\,\frac{\kappa t}{b^2} \tag{85}$$

Defining the thermal diffusion parameter, η^2 by

$$\eta^2 = \frac{\kappa t}{b^2}$$

Equation (84) may be written

$$q_1 \cong b\sqrt{11.03\,\eta^2} = \frac{10}{3}\,\eta b = \frac{10}{3}\sqrt{\kappa t} \tag{86}$$

Setting $q_1 = b - a$ and defining $\lambda = b/a$, Equation (86) may be solved for the time t_a for the heat to reach the inner port,

$$t_a = \frac{9}{100}\,\frac{b^2}{\kappa}\,\left(\frac{\lambda-1}{\lambda}\right)^2 \tag{87}$$

or somewhat more accurately

$$t_a = \frac{b^2}{30\kappa}\left(\frac{2\lambda^3 - 3\lambda^2 + 1}{\lambda^3}\right) \tag{88}$$

In the limit as $a \to 0$, $\lambda \to \infty$ for a solid cylinder and $t_a \to \frac{2b^2}{30}$.

For a thin cylinder, as $a \to b$, $\lambda \to 1$ and $t_a \to 0$.

In terms of the thermal diffusion parameter, η^2, Equation (88) may be written

$$\eta_a^2 = \frac{1 - 3\lambda^2 + 2\lambda^3}{3C\,\lambda^3} \tag{89}$$

Once the temperature field reaches the inner port a new function must be defined in lieu of Equation (81) since the temperature at the inner port, T_a, must gradually increase. Since the inner port was assumed insulated, the derivative of the temperature with respect to r must be zero at r = a. Thus, for $t \geq t_a$, or $\eta^2 \geq \eta_a^2$, the following temperature field is appropriate

$$T = T_o \left(1 - \frac{T_a}{T_o}\right) \left(1 - \left(\frac{b-r}{b-a}\right)^2\right) + T_a \tag{90}$$

Equation (90) may be solved in the same fashion as that used to determine q_1, yielding

$$T_a = T_o \left[1 - e^{-0.214(\bar{\eta}^2 - 1)}\right] \tag{91}$$

where

$$\bar{\eta}^2 = \frac{\kappa t}{b^2 \eta_a^2} = \frac{\eta^2}{\eta_a^2} = t/t_a \tag{92}$$

An inspection of Equation (91) reveals that it solves the appropriate boundary conditions; that is, for $\eta^2 = \eta_a^2$, $\bar{\eta}^2 = 1$ and $T_a = 0$, and for $\bar{\eta}^2 \to \infty$, $T_a \to T_o$.

The nominal properties of the center segments of the shuttle SRM are:

$$b = 72 \text{ in.}$$

$$a = 30 \text{ in.}$$

$$\lambda = b/a = 2.4$$

$$\kappa \cong 1 \text{ in}^2/\text{hr}$$

Thus, assuming a step input temperature from cure at a nominal 140°F to 70°F at the case with the inner port insulated, the time for the temperature change to be felt at the inner bore is, from Equation (88), t_a = 6 days. From Equations (91) and (92), the ratio t/t_a is given by

$$t/t_a = 1 - 4.67 \log_e \left(1 - \frac{T_a}{T_o}\right)$$

Thus, the time for the inner port to reach the near equilibrium condition of 95 percent of the temperature change at the outside (i.e., T_a = 74°F), is

$$t_{95} = 15\ t_a = 90 \text{ days.}$$

Thus, since the shuttle is not scheduled to be launched within 90 days of the manufacture of the SRM, it may be safely assumed that the SRM will be at a nearly equilibrium temperature equal to the local ambient temperature with only slight gradients through the propellant grain. These conditions represent the maximum cooling time, since internal and external cooling would achieve equilibrium more rapidly.

8.4 SRM DYNAMIC ANALYSIS

Nine dynamic analyses were conducted following the procedures outlined in Section 8.1. Since temperature gradients of any consequence are not expected in the SRM, analyses were conducted at 60, 70, and 80°F for the mean and $\pm 3\sigma$ variations in dynamic modulus. The pertinent analysis variables are shown in Table LIV.

The analysis results and the corresponding propellant dynamic moduli are presented in Table LV. The results substantiate that the propellant contributes to the overall mass of the system, but does not

TABLE LIV. DYNAMIC ANALYSIS VARIABLES

a	=	30 in.
b	=	72 in.
t_c	=	0.5 in.
L	=	320 in.
ρ_c	=	0.28 lb/in^3
ρ_p	=	0.064 lb/in^3
E_c	=	29 x 10^6 psi

TABLE LV. DYNAMIC ANALYSIS RESULTS, FIRST RESONANT FREQUENCY

	-3σ			Mean			+3σ		
Temperature (°F)	G' (psi)	tanδ	ω (Hz)	G' (psi)	tanδ	ω (Hz)	G" (psi)	tanδ	ω (Hz)
60°F	1683	0.424	19.04	2128	0.48	19.05	2667	0.50	19.07
70°F	881	0.455	19.06	1193	0.56	19 08	1622	0.591	19.10
80°F	472	0.480	19.10	684	0.628	19.13	1005	0.672	19.15

effect the overall stiffness. For moduli varying between 472 psi and 2667 psi and structure damping coefficient, $\zeta = \frac{G''}{G'}$ varying between 0.21 and 0.34, the differences in the resonant frequency are indistinguishable.

As a point of comparison, the simplified approximate analyses outlined in [4] were also conducted yielding resonant frequencies varying between 10 Hz at 60°F and 26 Hz at 80°F. These values are in agreement with those obtained by Thiokol [6], but show more variation since a rigid casing is assumed in their determination.

IX. CONCLUSIONS AND RECOMMENDATIONS

Six batches of TP-H1148 propellant have been characterized for dynamic shear modulus and the influence of expected propellant variability on the dynamic response of the Space Shuttle SRM has been examined.

Static and dynamic physical property characterization tests were conducted by the Chemical Systems Division of United Technologies Corporation on six batches of TP-H1148 propellant (TP-H1148-6,-7,-8, -9,9970096 and 9970115) furnished by Thiokol/Wasatch Division. The static tests consisted of constant elongation rate tests to failure and stress relaxation modulus tests at 40, 70 and 90°F. These tests were conducted to establish that the propellant batches tested were representative of propellant tested by Thiokol and to be used in the Shuttle SRM. Although more variation was evident than in similar test results obtained by Thiokol, nominal results are the same and typical of PBAN propellants.

Dynamic shear modulus tests were conducted at various superimposed static (compressive) strain levels and several dynamic strain amplitudes. Typical of other solid propellants material nonlinearities were observed. The test data show stiffening of the dynamic modulus with increasing compressive static strain due to the reinforcing effect of the Ammonium Perchlorate and aluminum particles, and a softening with increasing dynamic shear strain level due to inherent nonlinearities and debonding between the filler particles and the propellant binder.

The dynamic tests were conducted at static strain levels approximating those expected in the SRM due to cure shrinkage, thermal cooldown grain slump, and ignition in pressurization.

The test data generated by CSD and previously obtained data at Thiokol and the University of Utah on TP-H1148 and related PBAN propellants were analyzed in order to estimate expected batch-to-batch and within-batch propellant variability. Analyses of variance and a probabilistic analysis of the SRM propellant dynamic response indicate an expected one-sigma coefficient of variation of approximately 10 to 15 percent. This variation yields a possible six- ld variation in dynamic modulus, however, from the dynamic response analysis of the SRM it is noted that the propellant provides so little stiffness to the overall structure that even a ten-fold change in dynamic properties has no effect on the first resonance frequency.

Since the space shuttle could be launched between 90 days and 5 years following manufacture of the SRM, a heat conduction analysis of the SRM was conducted to determine the length of time required for the SRM to reach equilibrium ambient temperatures following cure. We also wanted to determine the effect a temperature gradient through the grain, if one existed at the time of launch, would have on propellant variability and the SRM dynamic response. Based on the heat conduction analysis conducted it is estimated that the SRM will reach thermal equilibrium approximately 90 days after the completion of cure. Therefore, it is anticipated the temperature through the grain will be near equilibrium, perhaps oscillating slightly about the ambient temperature.

Based on the results of the thermal analysis, dynamic response analyses of the Shuttle SRM were conducted at 60, 70 and 80°F using the expected $\pm$ 3 and mean dynamic modulus values determined from the analysis of variance. These properties encompass a six-fold increase in dynamic modulus from low to high and a 50 percent change in the structural damping coefficient; but absolutely no difference in resonant frequency could be detected. Thus, in agreement with other studies, it is recommended that future dynamic analyses of the SRM consider only the stiffness of the case, but include the mass of the propellant.

The results of the SRM dynamic analysis indicate that it is not necessary that any dynamic testing be performed for batch acceptance. The normal static physical property and burn rate testing for quality control are sufficient to assure batch-to-batch reproducibility. It is thus recommended that dynamic testing not be conducted on a routine basis.

The only dynamic loading environment not considered in this program or in previous programs is that arising from combustion instabilities. The most common instability in large solid rocket motors such as the Shuttle SRM is acoustic instability. The prevailing frequency modes are determined by the geometry and properties of the gas-and solid-filled rocket chamber. Acoustic mode vibrations in the gas and normal pressure fluctuations in the chamber cause a dynamic loading to the propellant. If the oscillations interact so as to cause resonance conditions in the propellant more pronounced pressure oscillations result, leading to an instability in burning and potential

over pressurization of the motor case. Since combustion instability is predominant in large motors under steady-state thrust conditions it is recommended that a study be undertaken to determine if combustion instability represents a potential mode of structural failure for the SRM.

REFERENCES

1. Anon.; "Dynamic Characterization of Solid Rockets," Report No. 13W-00241, IBM Federal Systems Division, Electronics System Center, Huntsville, Alabama, September 1973.

2. Levy, H., Zalesak, J., Bernstein, M. and Mason, P. W.; "Development of Technology for Modeling of 1/8-Scale Dynamic Model of the Shuttle Solid Rocket Booster (SRB)," NASA CR-132492, Grumman Aerospace Corporation, July 1974.

3. Anon.; "Dynamic Analysis of the Solid Rocket Motor for the Space Shuttle," Report No. 75W-00144, IBM Federal Systems Division, Huntsville, Alabama, July 1975.

4. Hufferd, W. L. and Fizgerald, J. E.; "Development of A Solid Propellant Viscoelastic Dynamic Model," Final Report, Contract NAS-8-31342, J. E. Fitgerald & Associates, April 1976.

5. Leadbetter, S. A., Stephens, W. B., Sewall, J. L., Majka, J. W. and Barrett, J. R.; "Vibration Characteristics of 1/8-Scale Dynamic Models of the Space-Shuttle Solid Rocket Booster," NASA Tn D-8158, Langley Research Center, May 1976.

6. Stoker, J. H. and Mason, D. R.; "Space Shuttle SRM Propellant Dynamic Properties," TWR-10543, Thiokol/Wasatch Division, June 1975.

7. Hufferd, W. L.; "Measured Properties of Propellant for Solid Rocket Booster of One-Eighth Scale Dynamic Shuttle Model," NASA CR 144938, University of Utah, November 1975.

8. Yorgiadis, A. J.; "Dynamic Properties of Inert Propellant for Quarter Scale SRM," Rockwell International, March 1977.

9. Wood, W. R.; "Vibration Tests on SRM Propellant Samples in Support of QS GVT," LTR 2205-3401, Rockwell International, April 1977.

10. Hammond, W. E.; "TP-H1148 Propellant Mechanical Properties Determination," TWR-11501, Thiokol/Wasatch Division, May 1977.

11. Hammond, W. E.; "Space Shuttle SRM Propellant Dynamic Properties," TWR-11779, Thiokol/Wasatch Division, March 1978.

12. ICRPG Solid Propellant Mechanical Behavior Manual, CPIA Publication No. 21, The Johns Hopkins University, 1963.

13. Fitzgerald, J. E. and Hufferd, W. L.; Handbook for the Engineering Structural Analysis of Solid Propellants, CPIA Publication No. 214, The Johns Hopkins University, May 1971.

14. JANNAF Solid Propellant Structural Integrity Handbook, edited by W. L. Hufferd and J. E. Fitzgerald, CPIA Publication No. 230, The Johns Hopkins University, September 1972.

15. Hufferd, W. L.; "Creep and Stress Relaxation of Polymers," Proceedings of the Polymer Conference Series on Mechanical Behavior, University of Utah, UTEC CE 72-096, June 1972.

16. Francis, E. G., Peeters, R. L. and Hufferd, W. L.; "Considerations in the Applications of Nonlinear Structural Materials," Proceedings of the Second International Conference on Mechanical Behavior of Materials, pp. .

17. Francis, E. C., Peeters, R. L. and Murch S. A.; "Nonlinear Effects in Thermal Stress Analysis of A Solid Rocket Motor," Proceedings of the 13th Annual Society of Engineering Science Meeting,

18. Francis, E. C. and Carlton, C. H.; "Research Study of TP-H1148 and Other Similar Solid Propellants," CSD 2608-FR, Chemical Systems Division, April 1978.

19. Miles, D. O.; "Sinusoidal Shear Generator for Study of Viscoelasticity," J. Appl. Physics, Vol. 33, p. 1422, 1962.

20. Miles, D. O., Knollman, G. C., and Hamamoto, A. S.; "Technique for Calibration of A Dynamic Rheological Shear Apparatus," The Review of Scientific Instruments, Vol. 36, pp. 158-161, 1965.

21. Williams, M. L., Landel, R. F., and Ferry, J. D.; "The Temperature Dependence of Relaxation Mechanisms in Amorphous Polymers and Other Glass-Forming Liquids," J. Amer. Chemical Soc., Vol. 77, p. 3701, 1955.

22. Bills, K. W., Jr., and Svob, G. J.; "Establishing Mechanical Properties Criteria," Bulletin of the 4th Meeting, Interagency Chemical Rocket Propulsion Group (ICRPG), Working Group on Mechanical Behavior, CPIA Publ. No. 94U, The Johns Hopkins University, pp. 269-286, October 1975.

23. Marti, L. A., Morrill, L. G., and Bersche, C. V.; "Predicting Propellant Storage Life by Superposition," Bulletin of the 5th Meeting, Interagency Chemical Rocket Propulsion Group (ICRPG), Working Group on Mechanical Behavior, CPIA Publ. No. 119, Vol. I, The Johns Hopkins University, pp. 39-64, October 1966.

24. Majerus, J. N.; "A Unified Approach to Failure and Its Application to Solid Propellant Materials," Bulletin of the 3rd Meeting, Interagency Chemical Rocket Propulsion Group (ICRPG), Working Group on Mechanical Behavior, CPIA Publ. No. 610, The Johns Hopkins University, pp. 395-420, October 1964.

25. Weigand, J. H.; "The Interrelation of Modulus and Nominal Maximum Stress," Bulletin of the 4th Meeting, Interagency Chemical Rocket Propulsion Group (ICRPG), Working Group on Mechanical Behavior, CPIA Publ. No. 94U, The Johns Hopkins University, pp. 235-242, October 1965.

26. Briar, H. P. and Weigand, J. H.; "A Statistical Approach to Failure Criteria," Bulletin of the 3rd Meeting, Interagency Chemical Rocket Propulsion Group (ICRPG), Working Group on Mechanical Behavior, CPIA Publ. No. 61U, The Johns Hopkins University, pp. 455-468, October 1964.

27. Briar, H. P.; "A Statistical Model for Constant Strain Failures in Solid Rocket Propellants," Bulletin of the 4th Meeting, Interagency Chemical Rocket Propulsion Group (ICRPG), Working Group on Mechanical Behavior, CPIA Publ. No. 94U, Vol. I, pp. 321-332, October 1965.

28. Jensen, F. R.; "An Application of Statistical Techniques to the Structural Analysis of a Solid Propellant Rocket Motor Grain," M.S. Thesis, University of Utah, August 1968.

29. Nichols, P. L.; "The Use of Elevated Temperature Aging to Predict Propellant Service Life," Bulletin of the JANNAF Operational Serviceability and Structures and Mechanical Behavior Working Groups Combined Annual Meeting, CPIA Publ. No. 264, The Johns Hopkins University, pp. 19-62, May 19.

30. Hicks, C. R.; Fundamental Concepts in the Design of Experiments, 2nd Edition, Holt, Rinehart and Winston, 1973.

31. Brandt, S.; Statistical and Computational Methods in Data Analysis, North Holland/American Elsevier, New York, 1970.

32. Mann, N. R., Schafer, R. E., and Singpurwalla, N.D.; Methods for Statistical Analysis of Reliability and Life Data, John Wiley & Sons, Inc., 1974.

33. Cornell, C. A.; "A Probability-based Structural Code," Am. Conc. Inst. J., Vol. 66, No. 12, 1969.

34. Layton, L. H., Bennett, S. J. and Stoker, J. H.; "Chemical Structural Aging Effects, "Proceedings of the JANNAF Combined OSWG and S&MBWG Annual Meeting, CPIA Publication No. 253, The Johns Hopkins University, pp. 99-116, July 1974.

35. Layton, L. H. and Bennett, S. J.; "Application of Aging Models to Predictions of Propellant Long Term Aging Characteristics," Proceedings of the Combined Annual OSWG and S&MBWG Meeting, CPIA Publication No. 264, The Johns Hopkins University, pp. 1-18, May 1975.

36. Achenbach, J. D.; "Dynamic Response Problems of Solid Propellant Rockets," Feature Article, Solid Rocket Structural Integrity Abstracts, The University of Utah, Vol. 5, No. 1, pp. 1-34, January 1968.

37. Baltrukonis, J. H.; "The Dynamics of Solid Propellant Rocket Motors," in Mechanics and Chemistry of Solid Propellants, edited by A. C. Eringen, H. Liebowitz, S. L. Koh, and J. M. Crowley, Pergamon Press, pp. 297-332, 1967 (also published as NASA CR-658, December 1966).

38. Anderson, J. M.; "Adaptation of the Finite-Element Stiffness Method to Viscoelastic Steady-State Vibration Solutions," Proceedings of the 5th ICRPG Mechanical Behavior Working Group Meeting, CPIA Publication No. 119, Vol. 1, The Johns Hopkins University, pp. 297-318, October 1966.

39. Baker, W. E. and Daly, J. M.; "Dynamic Analysis of Solid Propellant Grains Using the Finite Element Method (Direct Stiffness Method)," Proceedings of the 5th ICRPG Mechanical Behavior Working Group Meeting, CPIA Publication No. 119, Vol. 1, The Johns Hopkins University, pp. 319, 338, October 1966.

40. Leeming, H., et al.; "Solid Propellant Structural Test Vehicle, Systems Analysis and Cumulative Damage Program," Appendix A, AFRPL-TR-130, Lockheed Propulsion Company, October 1968.

41. Ghosh, S. and Wilson, E.; "Dynamic Stress Analysis of Axisymmetric Structures Under Arbitrary Loading," Report No. EERG 69-10, University of California, Berkeley, September 1969.

42. Goudreau, G. L.; "Evaluation of Discrete Methods for the Linear Dynamic Response of Elastic and Viscoelastic Solids," Report No. 69-15, University of California, Berkeley, June 1970.

43. Boley, B. A. and Weiner, J. H.; "Theory of Thermal Stresses," John Wiley & Sons, Inc., 1960.

APPENDIX

CHEMICAL SYSTEMS DIVISION

FINAL REPORT

CSD 2608-TR

"RESEARCH STUDY OF TP-H1148 AND OTHER SIMILAR PROPELLANTS"

CSD 2608-FR

RESEARCH STUDY OF TP-H1148 AND OTHER SIMILAR SOLID PROPELLANTS

Final Report for Period
17 September 1976 — 30 April 1978

April 1978

by

E. C. Francis and C. H. Carlton

Contract No. 76-001

Prepared for

National Aeronautics & Space Administration
George C. Marshall Space Flight Center
Marshall Space Flight Center, AL 35812

and

W. L. Hufferd & Associates
Consulting Engineers
2826 Devereaux Way
Salt Lake City, UT 84109

by

CHEMICAL SYSTEMS DIVISION

UNITED TECHNOLOGIES

CONTENTS

ILLUSTRATIONS

ILLUSTRATIONS (Continued)

TABLES

ABBREVIATIONS

CSD	Chemical Systems Division
ICRPG	Interagency Chemical Rocket Propulsion Group
JANNAF	Joint-Army-Navy-NASA-Air Force Interagency Propulsion Committee
PBAN	poly(butadiene-acrylic acid-acrylonitrile)
SRM	solid rocket motor
WLF	Williams, Landel, and Ferry

1.0 INTRODUCTION

Under contractual agreement No. 76-001 CSD undertook the task of evaluating the dynamic shear, constant rate to failure, and stress relaxation response for six batches of Space Shuttle SRM solid propellant (TP-H1148). These data are intended to be used to assess the effects of propellant variability on the dynamic response of the Space Shuttle SRM and to determine the accuracy with which the dynamic response properties may be known.

The propellant was furnished to CSD in two shipments totalling 234 lb. The first shipment was received 15 July 1977 on bill of lading No. B09063; the balance was received on 17 November 1977 on bill of lading No. B11968.

2.0 WORK TO BE ACCOMPLISHED

The specific work to be accomplished by CSD consisted of the following:

A. Dynamic Shear Response

Measure the dynamic shear modulus of six SRM solid propellant batches at various static and dynamic strain conditions.

B. Constant Rate Failure Properties

Measure constant rate properties of six SRM solid propellant batches at 2 in./min at 0^{o}, 40^{o}, 70^{o}, 90^{o}, and 120^{o}F.

C. Viscoelastic Relaxation Modulus

Measure viscoelastic modulus of six SRM solid propellant batches at 40^{o}, 70^{o}, and 90^{o}F.

All dynamic shear, constant rate, and stress relaxation tests have been completed and the test data are presented and analyzed in this final report.

3.0 TECHNICAL DATA

The propellant evaluated during this contract consisted of material from one 600-gal batch (TP-H1148-9) and five other batches. Their batch identifications were -6, -7, -8, -9, -9970096, and -9970115. Procedures used for the evaluation are presented with data for each test mode.

3.1 CONSTANT RATE DATA

Constant displacement rate uniaxial tests were conducted using ICRPG class B samples[1] with plastic extensometers as shown in figure 3-1. The tests were conducted using an Instron, with the standard strip chart recorder (figure 3-2) modified for automatic data reduction. The computerized output is presented as E_o, σ_m, ϵ_m, σ^c_m, ϵ^c_m, and ϵ_r where

E_o = initial modulus

$\sigma_m = \frac{F}{A_o}$ (engineering stress)

ϵ_m = strain at σ_m

σ^c_m = true stress (corrected, $\frac{F}{A_o}(1 + \epsilon^c_m)$

ϵ^c_m = strain at σ^c_m

ϵ_r = strain at rupture

The results for individual samples as well as mean and standard deviations of a group are listed on the computer printout. Additional details of the automated data acquisition system are presented in appendix A.

ICRPG constant rate tests were conducted at 2 in./min at 0°, 40°, 70°, 90°, and 120°F on all six batches identified above. The failure properties are shown in figures 3-3 through 3-8. Five replicate samples tested per test condition showed good reproducibility within batches and reasonable batch-to-batch

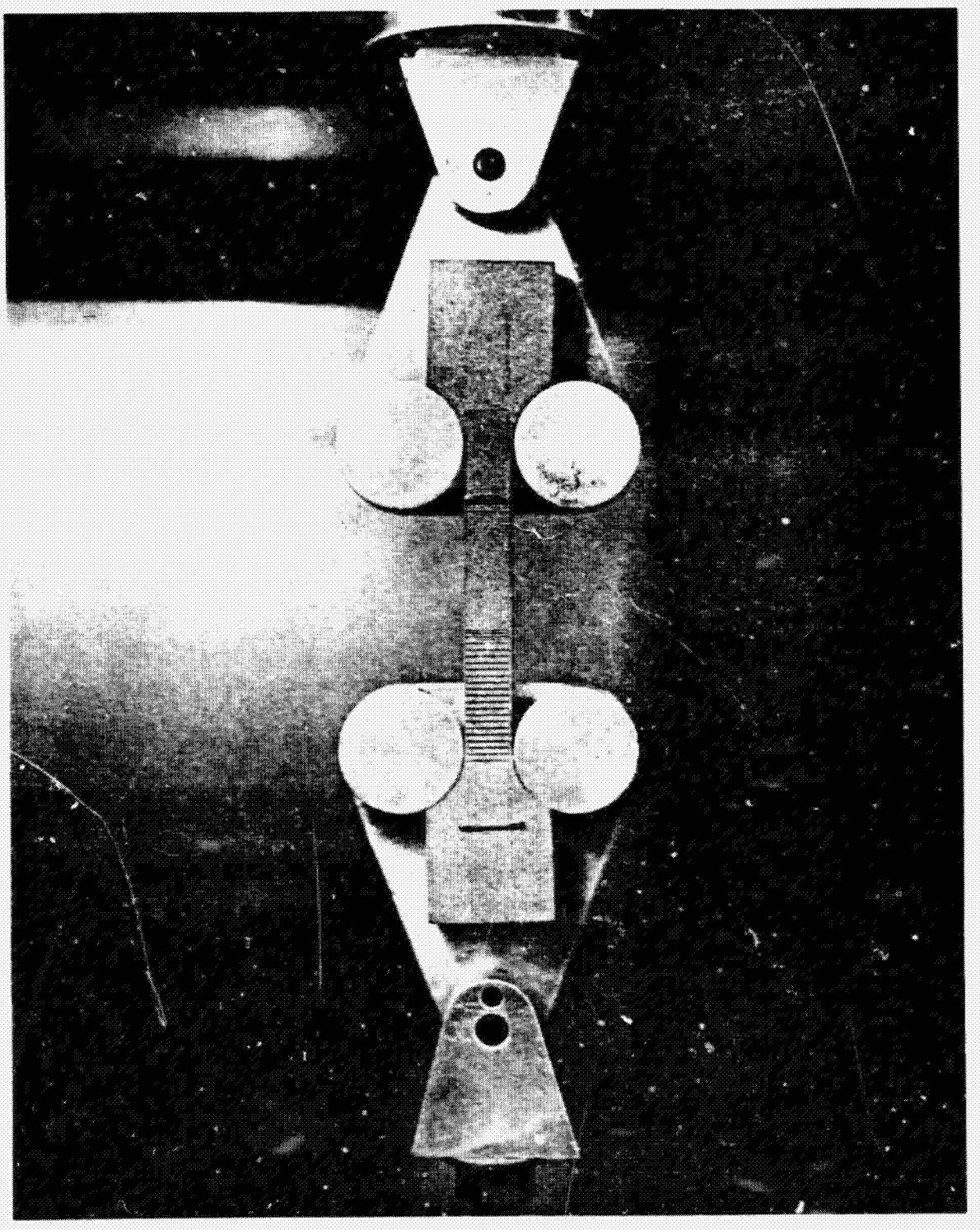

Figure 3-1. ICRPG Class B Tensile Specimen

3941-13

ORIGINAL PAGE IS OF POOR QUALITY

14328

Figure 3-2. Large Instron Tester with Wang Data Acquisition System

11055-11 14889

variability. Nominal values of rupture strain, maximum stress, and initial modulus at 70°F are presented in table 3-1 for all six batches.

3.2 STRESS RELAXATION

Stress relaxation tests were conducted at 40°, 70° and 90°F using 1/2- by 1/2-in. bonded-end tensile specimens (figure 3-9) with a nominal 6-in. gage length. The test method described in section 2.2 of the ICRPG Solid Propellant Mechanical Behavior Manual[2] was used for these tests. A strain of approximately 3% was applied and stress decay with time was measured. The test strain levels were determined from the gage length between the wood end-tabs; the increase in length was determined by optical cathetometer measurements (see figure 3-10).

$$\epsilon_o = \frac{\Delta L}{L_o} \qquad (1)$$

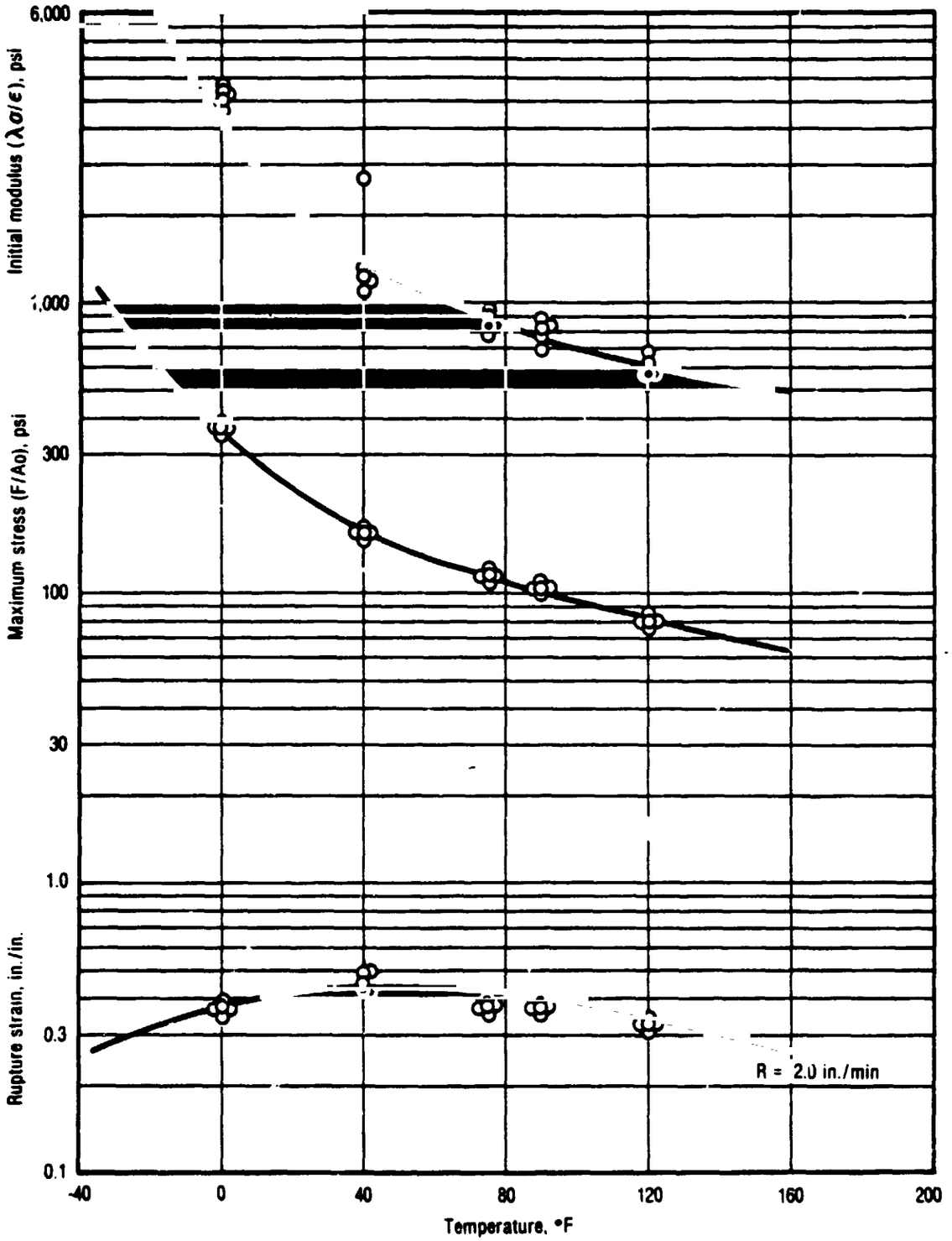

Figure 3-3. ICRPG Class B Data for Batch No. TP-H1148-6

14327

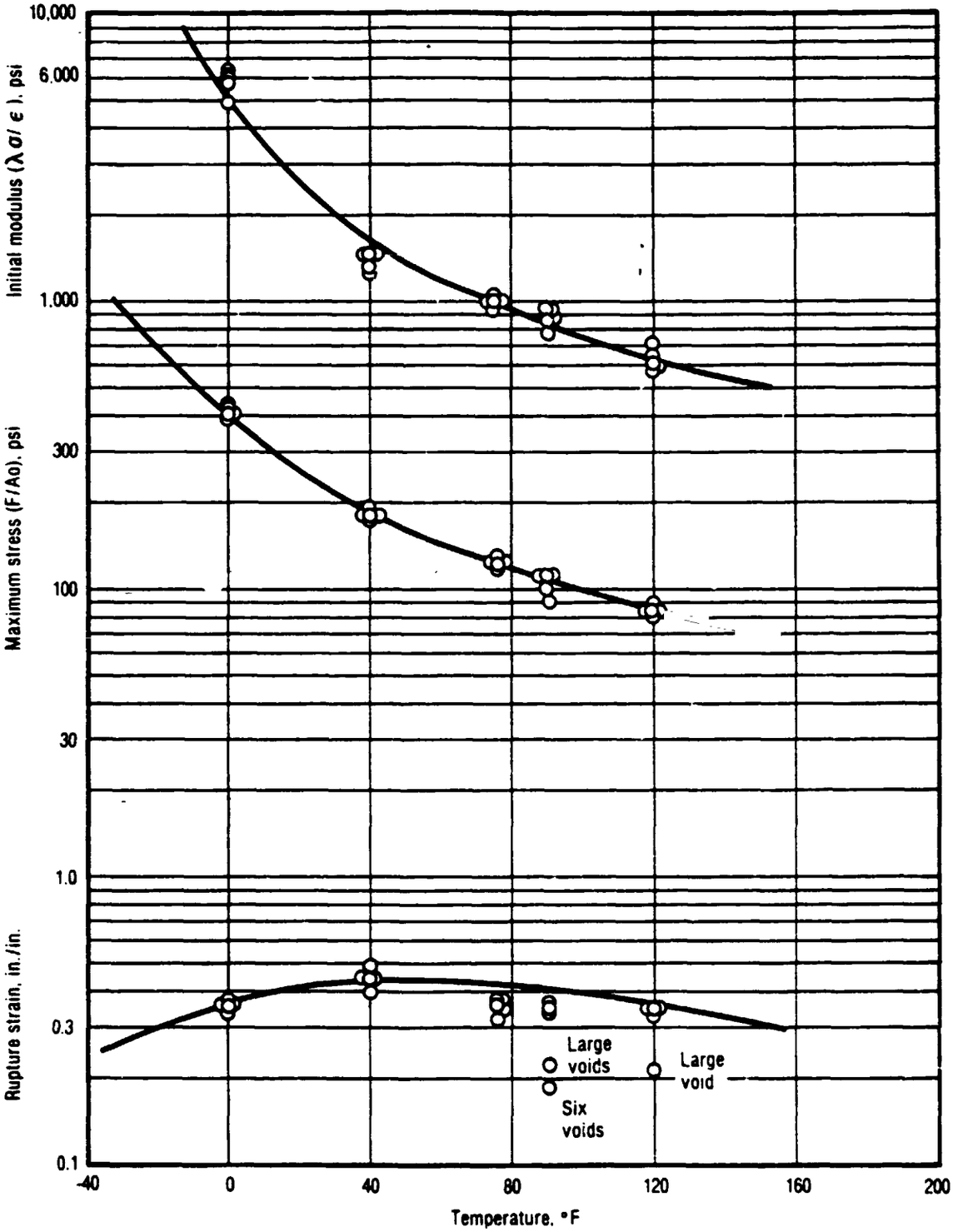

Figure 3-4. ICRPG Class B Data for Batch No. TP-H1148-7

14326

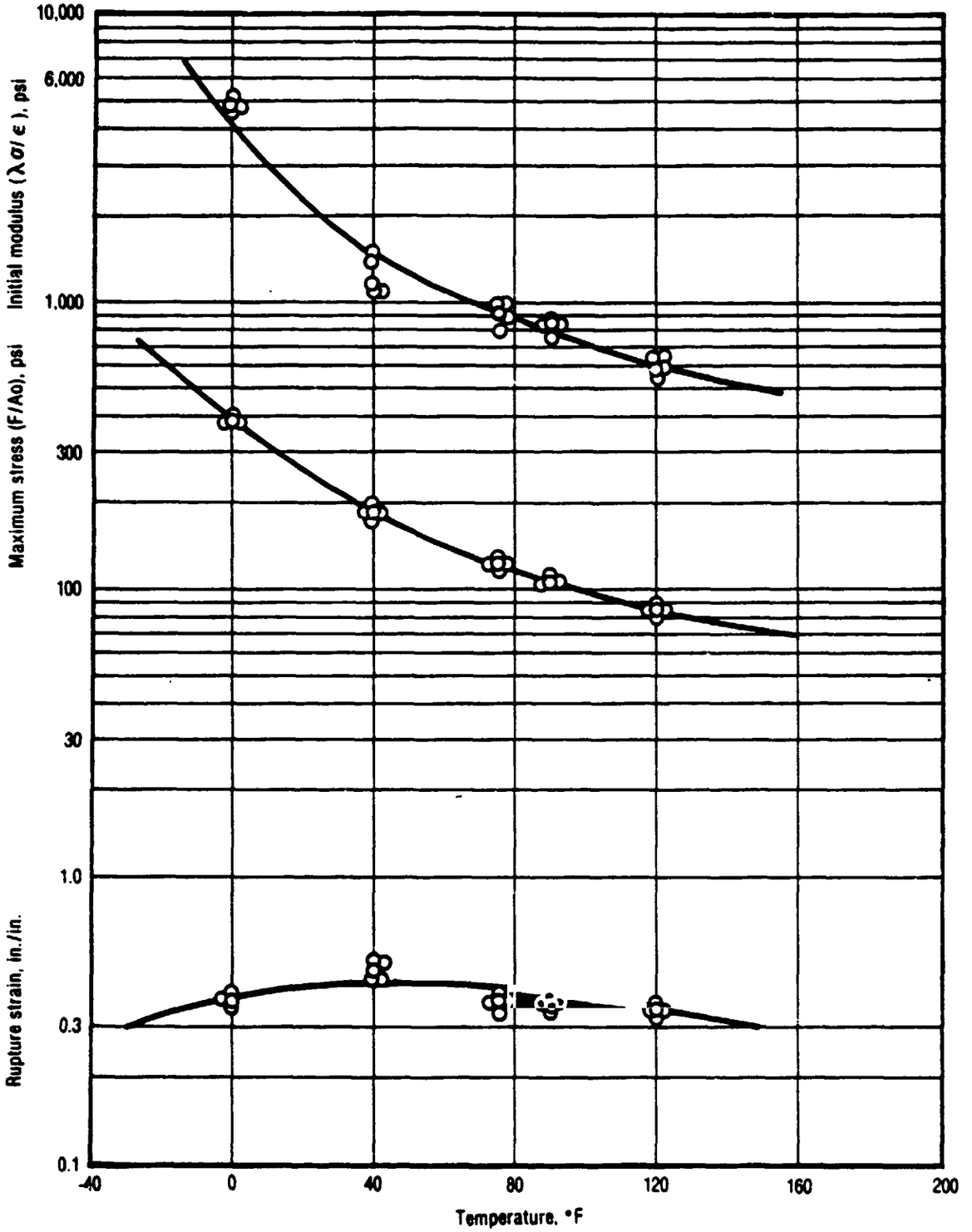

Figure 3-5. ICRPG Class B Data for Batch No. TP-H1148-8

14325

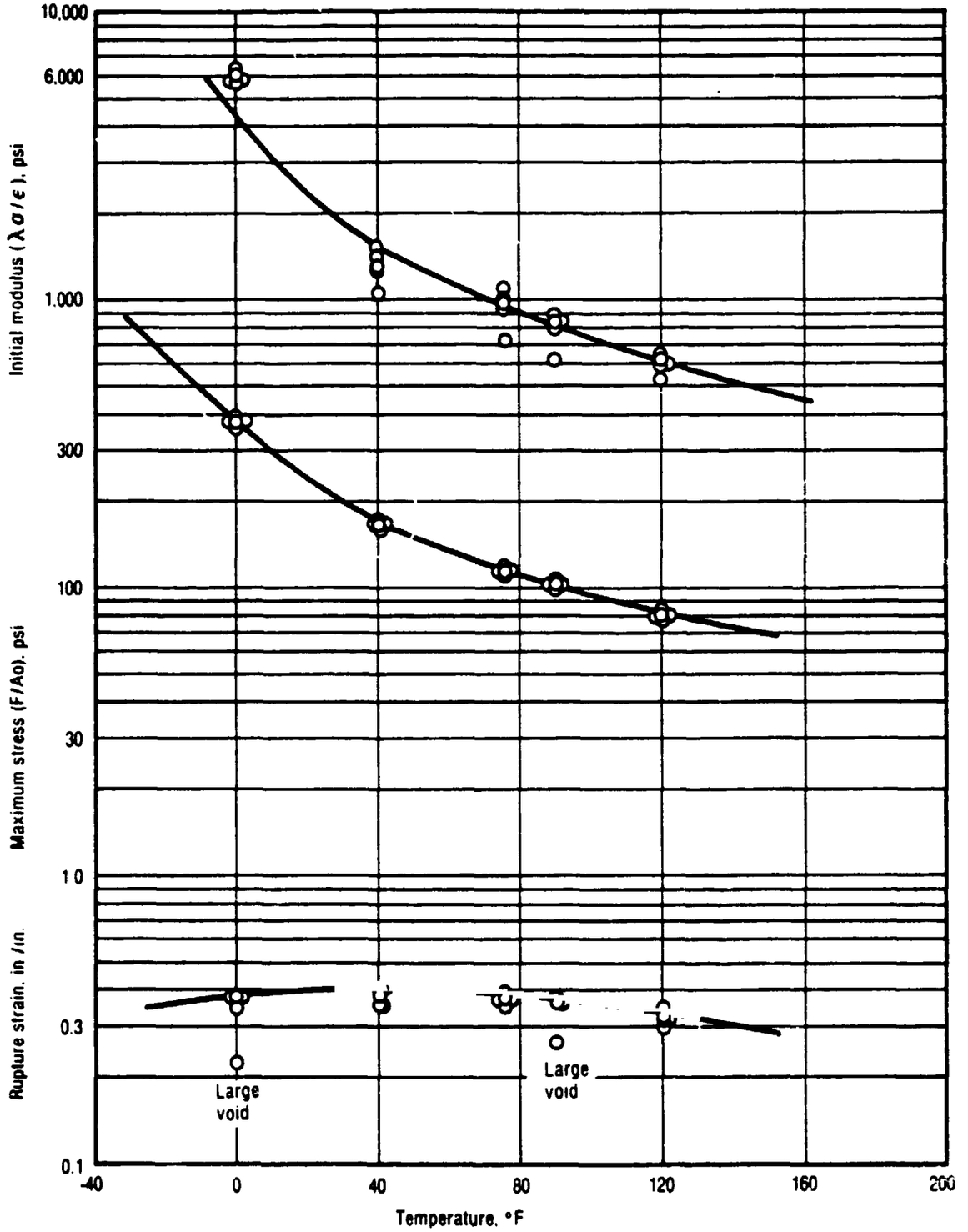

Figure 3-6. ICRPG Class B Data for Batch No. TP-H1148-9

14324

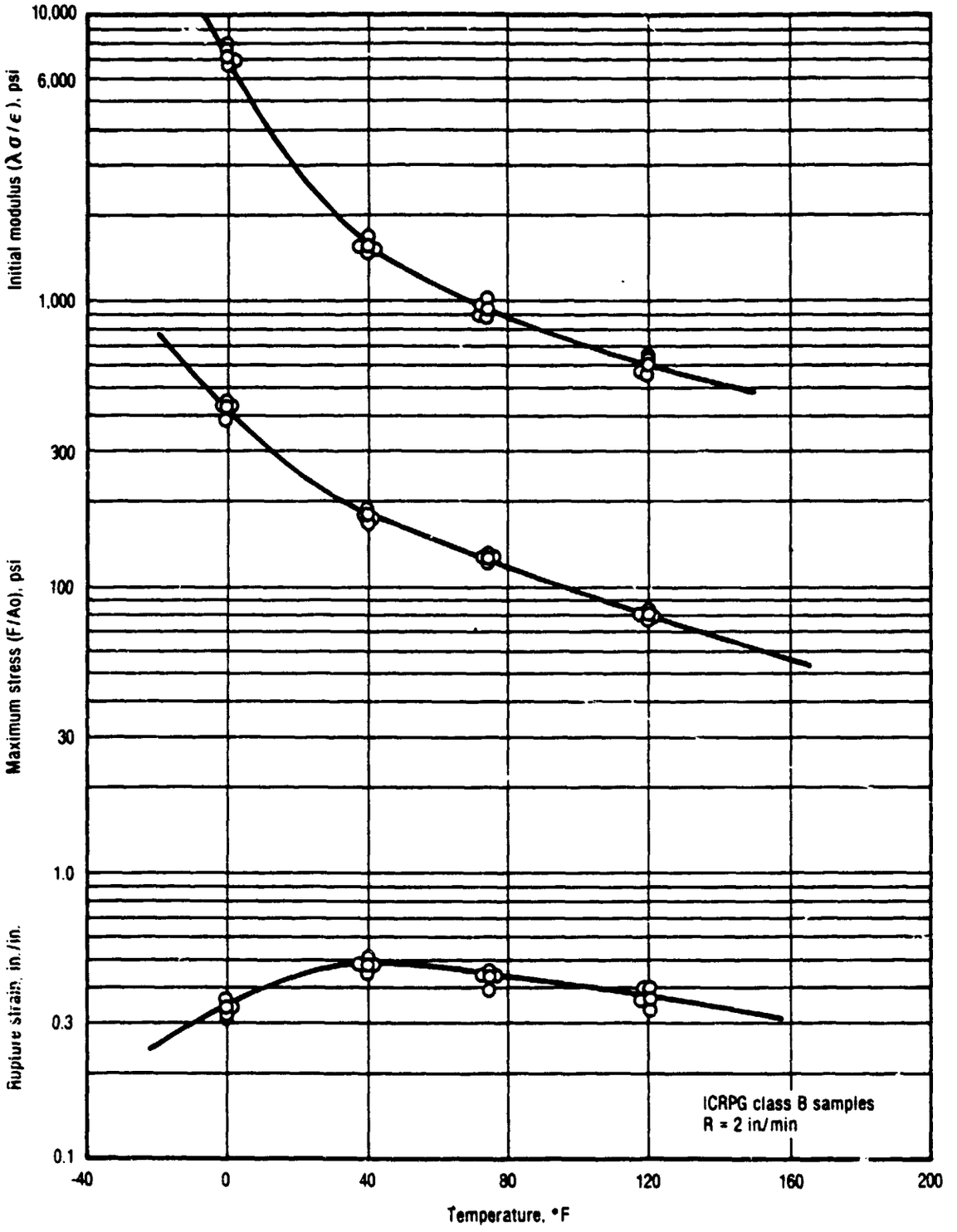

Figure 3-7. ICRPG Class B Data for Batch No. TP-H1148-9970096

14323

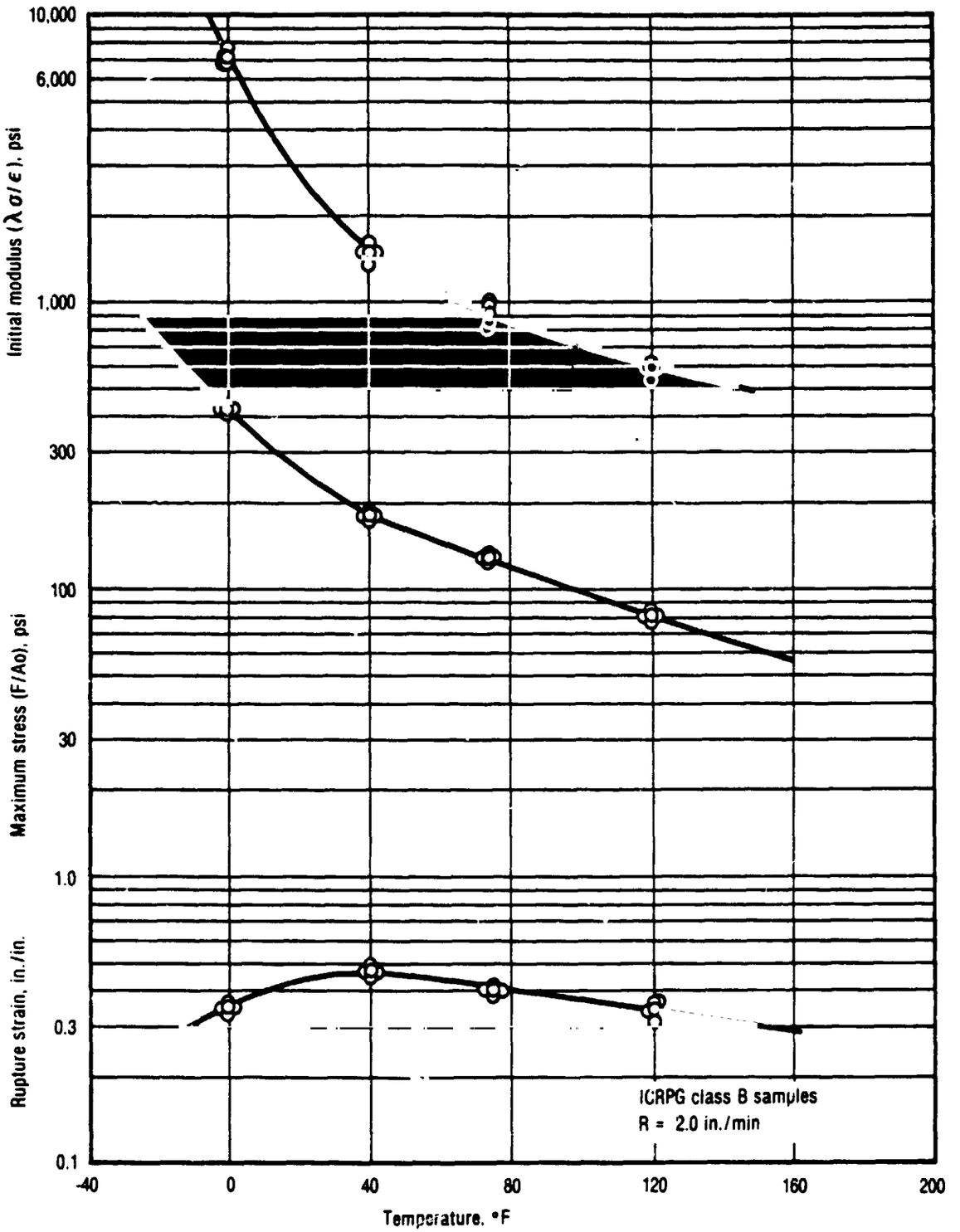

Figure 3-8. ICRPG Class B Data for Batch No. TP-H1148-9970115

14322

TABLE 3-1. UNIAXIAL CONSTANT RATE DATA FOR TP-H1148 PROPELLANT AT 70°F

T3177

TP-H1148 Batch No.	Rupture Strain at 70°F, %	Maximum Stress (F/A_o) at 70°F, psi	Initial Modulus ($\lambda\sigma/\varepsilon$) at 70°F. psi
6	42	120	940
7	44	130	1,050
8	42	127	960
9	38	120	1,010
9970096	44	130	1,000
9970115	42	131	960

ORIGINAL PAGE
BLACK AND WHITE PHOTOGRAPH

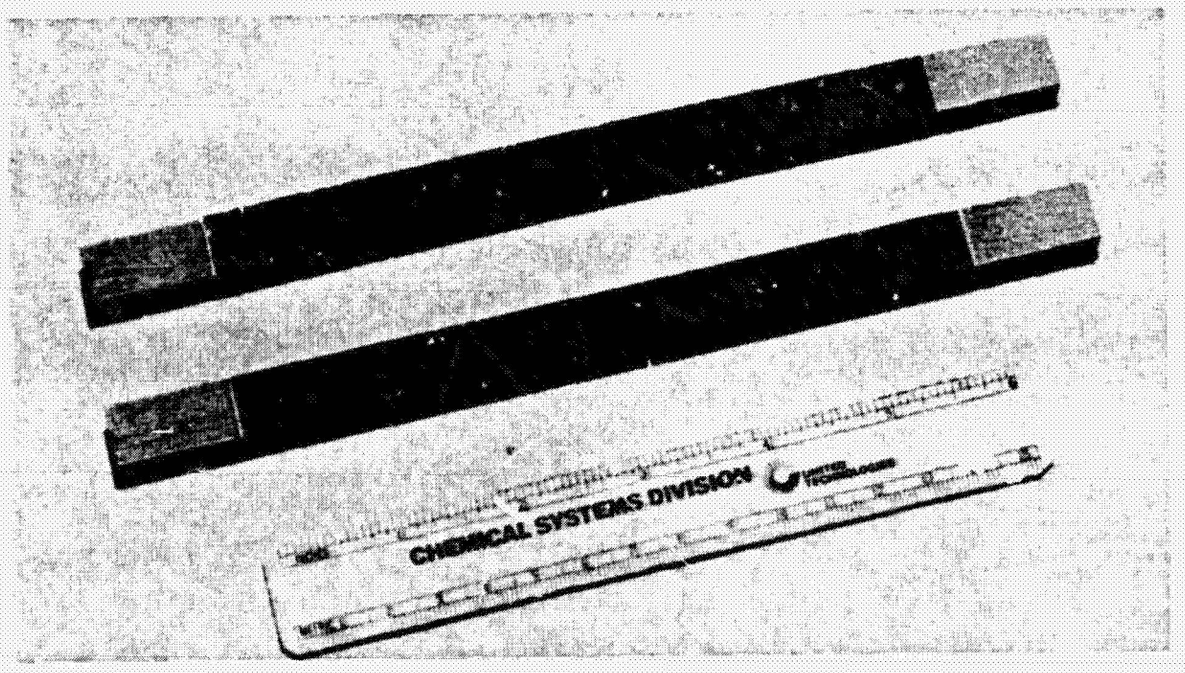

Figure 3-9. Bonded-End Tensile Specimen

11055-3

14881

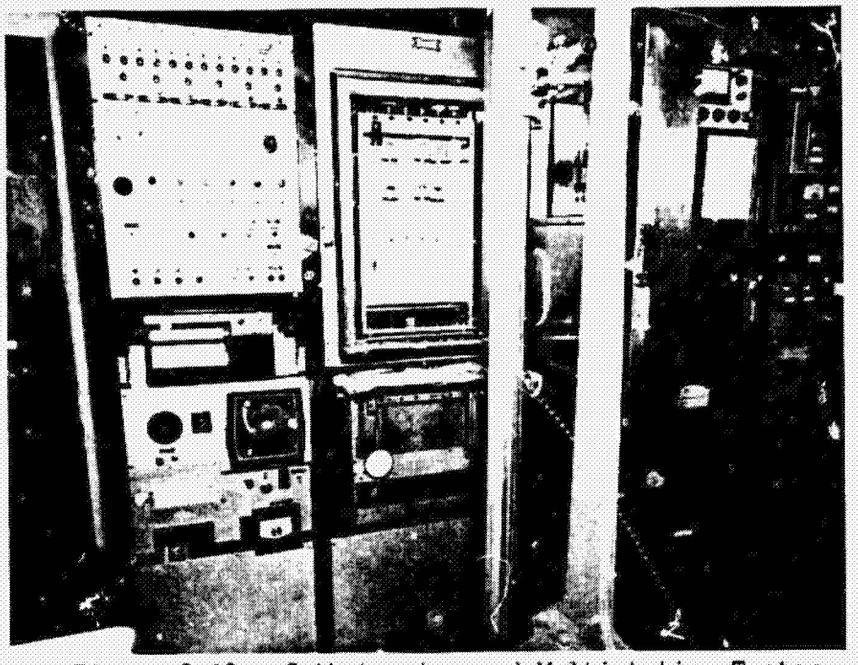

Figure 3-10. Cathetometer and Multistation Tester

11055-10 14882

where ϵ_o = initial strain

L_o = initial length

ΔL = change in length

ORIGINAL PAGE IS OF POOR QUALITY

The viscoelastic relaxation modulus was calculated by

$$E(t) = \frac{\lambda\sigma(t)}{\epsilon_o}$$

ere $E(t)$ = viscoelastic relaxation modulus at time t

$\sigma(t)$ = (load/area at time t)/area

$\lambda = 1 + \epsilon_o$

Strain levels for the individual samples and the relaxation modulus at or 4 min are given in table 3-2. The reduced stress relaxation modulus curves are shown in figures 3-11 through 3-16 for the individual batches along with the WLF temperature shift factors[3] (PBAN $T_g \approx -70^{o}C$). The theoretical WLF time temperature shift factors were used for initial data reduction, but where

TABLE 3-2. STRESS RELAXATION TEST VALUES FOR INDIVIDUAL SAMPLES OF TP-H1148 PROPELLANT

T3178

	Temperature					
	40°F		70°F		90°F	
TP-H1148 Batch No.	Strain, %	E at 1 min, psi	Strain, %	E at 4 min, psi	Strain, %	E at 1 min, psi
6	2.88	453	3.03	318	2.97	274
	2.03	401	2.47	345	2.76	334
	3.04	396	2.58	322	2.99	255
	2.85	546	2.59	285	2.80	280
	3.02	512	2.75	285	2.63	274
Average	2.96	462	2.68	311	2.83	283
7	2.81	634	3.06	374	2.90	444
	2.76	605	2.81	422	2.96	475
	2.69	642	3.12	370	2.87	377
	2.59	446	2.81	392	3.06	332
	2.61	[illegible]	3.04	382	2.78	456
Average	2.69	615	2.97	388	2.91	417
8	2.56	462	2.87	375	2.78	282
	2.94	400	3.06	313	2.88	265
	2.88	420	2.98	323	2.80	335
	2.91	493	2.99	278	2.54	340
	2.71	504	2.94	312	3.44	228
Average	2.80	456	2.97	320	2.89	290
9	2.94	563	2.92	404	3.00	323
	3.11	404	2.93	338	3.09	299
	2.88	409	2.96	419	2.91	323
	2.78	624	3.16	283	2.59	297
	2.38	524	2.96	346	3.06	325
Average	2.82	505	2.99	358	2.93	313
9970096	3.09	476	3.04	330	3.16	305
	2.89	509	3.02	333	2.74	317
	2.62	633	3.00	314	2.84	412
	-	-	-	-	3.07	304
Average	2.86	539	3.02	326	2.95	334
9970115	3.05	563	3.12	379	2.91	362
	2.98	552	3.19	360	2.91	345
	2.95	631	3.02	349	2.94	351
	-	-	-	-	2.78	415
Average	2.99	581	3.11	363	2.88	368

Note: E = stress relaxation modulus

ORIGINAL PAGE IS
OF POOR QUALITY

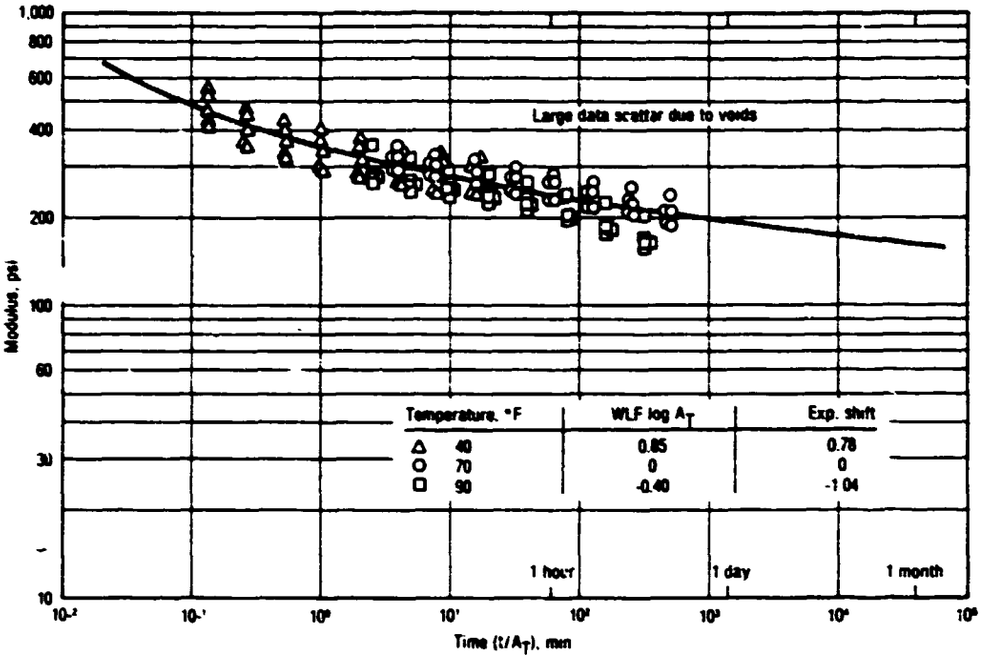

Figure 3-11. Stress Relaxation Modulus at 3% Strain for Batch No. TP-H1148-6

14321

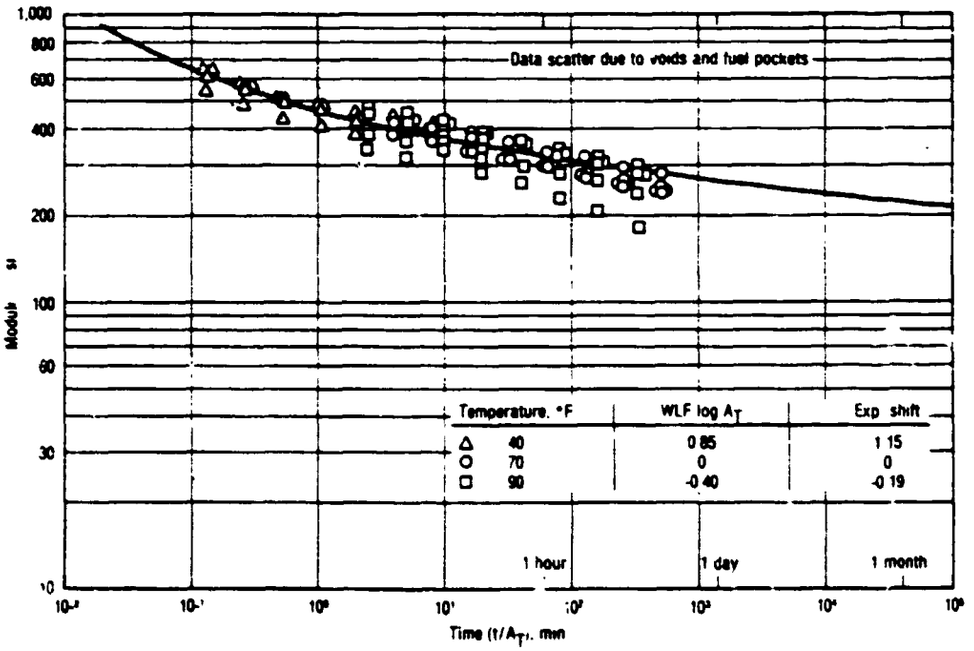

Figure 3-12. Stress Relaxation Modulus at 3% Strain for Batch No. TP-H1148-7

14320

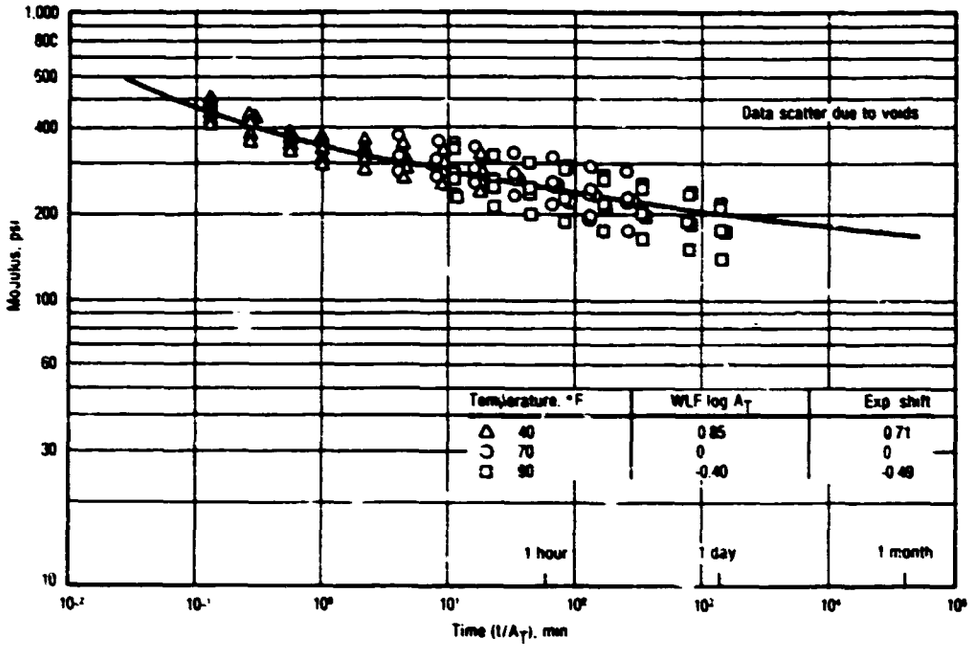

Figure 3-13. Stress Relaxation Modulus at 3% Strain for Batch No. TP-H1148-8

14319

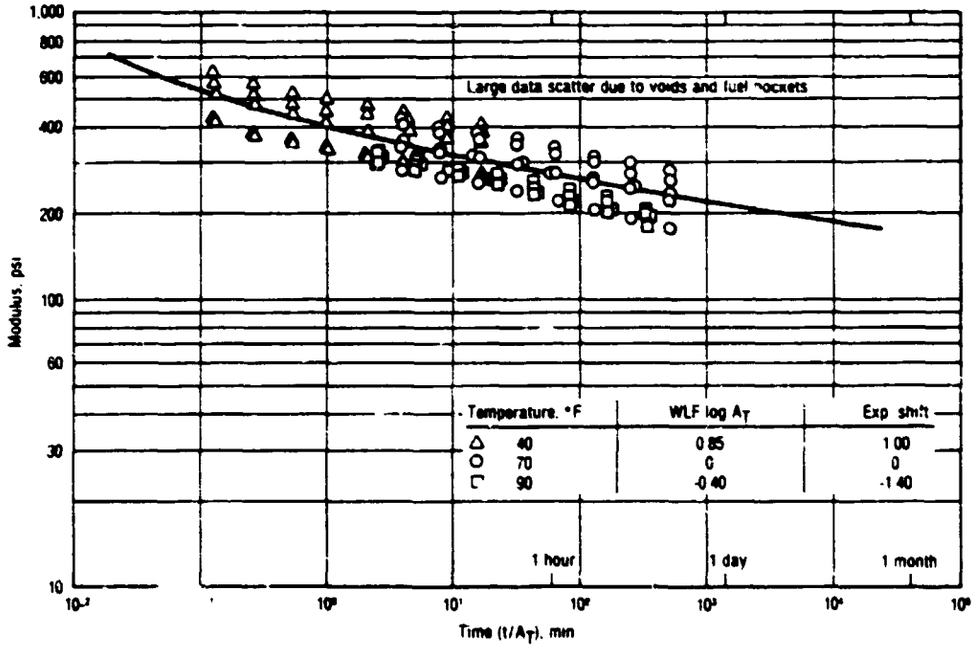

Figure 3-14. Stress Relaxation Modulus at 3% Strain for Batch No. TP-H1148-9

14318

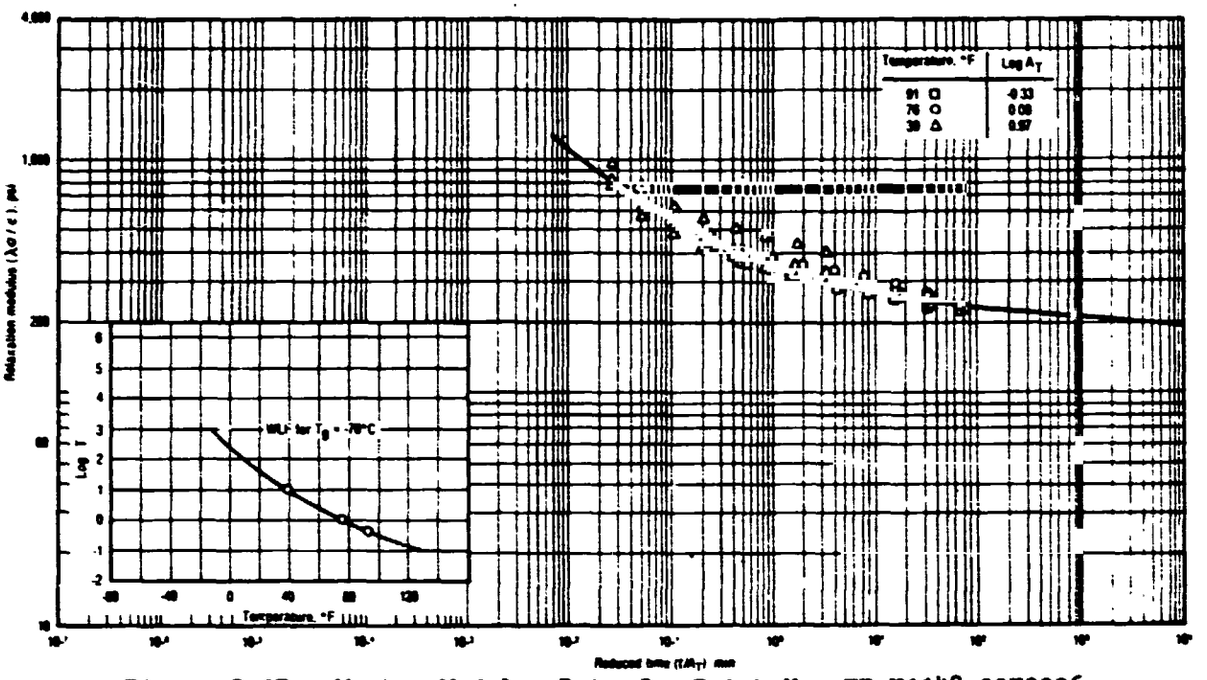

Figure 3-15. Master Modulus Data for Batch No. TP-H1148-9970096

14317

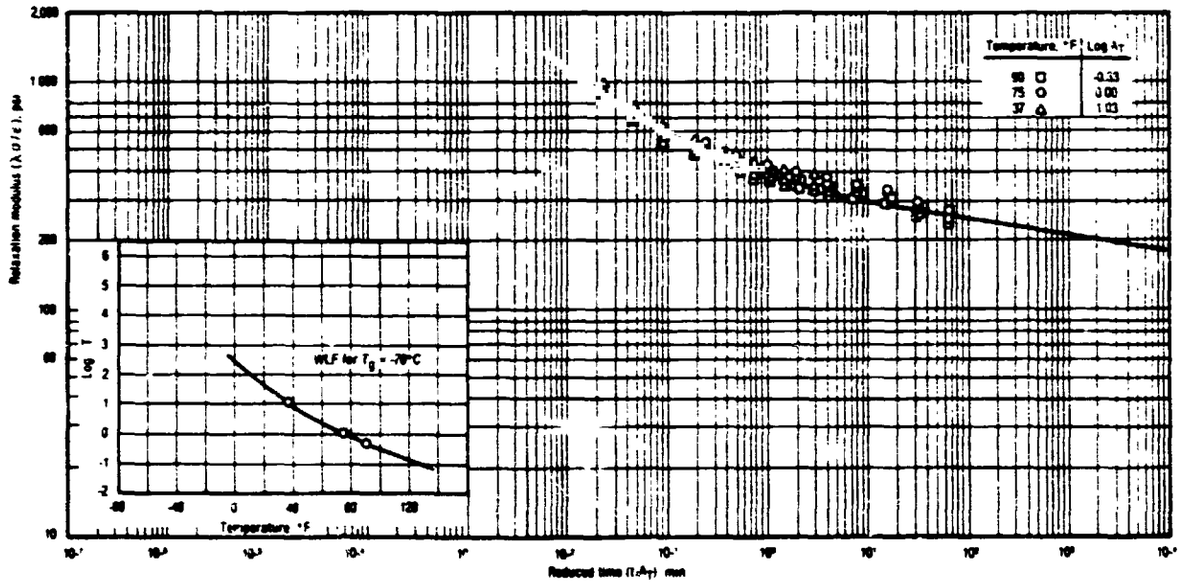

Figure 3-16. Master Modulus Data for Batch No. TP-H1148-9970115

14316

this shift did not adequately superimpose the data the shift factors were adjusted imperically. Both the WLF and imperical shifts are shown where applicable. The mean curves from the six batches are compared in figure 3-17 and the nominal 1-min moduli are given below:

TP-H1148 Batch No.	Stress Relaxation Modulus at 1 min, psi
6	345
7	460
8	350
9	395
9970096	360
9970115	385

Sample-sample variance noted on the stress relaxation graphs reflects the within-carton gradient, potential sample machining and handling damage, and experimental test uncertainties. A 6-in. gage length bonded-end sample was used to minimize the experimental errors caused by JANNAF dogbone flow through jaws and gage length errors. Actual strain measurements were obtained to 0.001-in. accuracy using the optical cathetometer. Load calibrations were conducted using dead weight tests on each test channel.

3.3 DYNAMIC SHEAR RESPONSE

Small strain dynamic shear properties of solid propellants and other low modulus materials are routinely measured at CSD using a piezoelectric transducer device. Illustrations of the dynamic test device and the associated electrical equipment are presented in figures 3-18 through 3-20. The device employs a stack of piezoelectric crystals as the dynamic driver source. This dynamic strain is transmitted through the solid propellant sample as shear and the output load is measured using a single piezoelectric crystal which functions as a load cell.

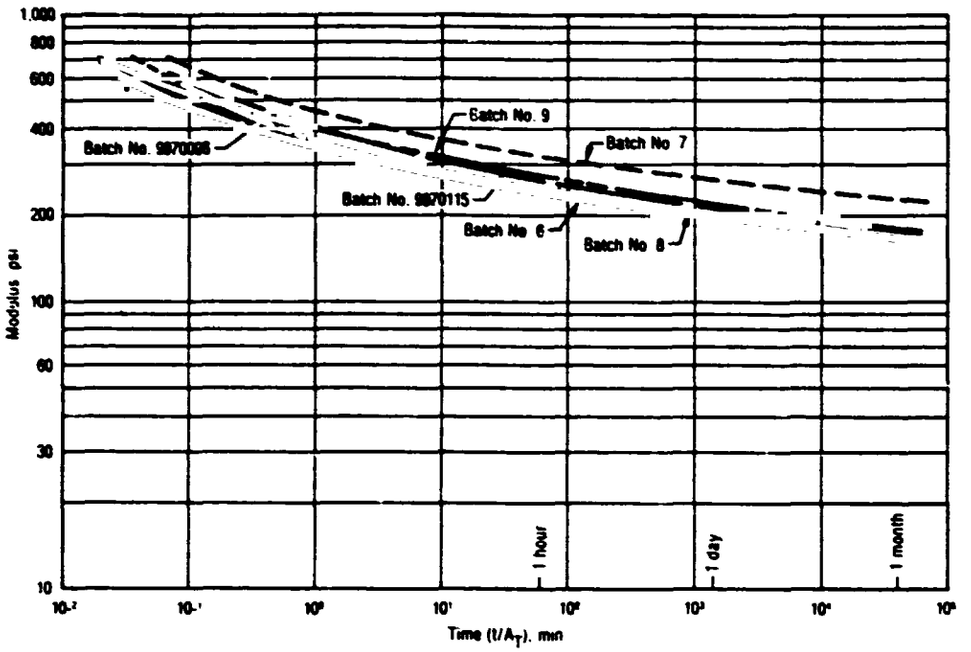

Figure 3-17. Comparison of Stress Relaxation Modulus Curves for TP-H1148 Propellant

14315

The complex modulus of the test material can be represented for shear as either

$$E^* = E' + i\,E'' \qquad (3)$$

or $G^* = G' + i\,G''$

In equation 3, E' is the real part and E" is the imaginary part of the complex modulus. The complex modulus E* is given by the ratio of the maximum stress to the maximum strain. For low or medium damping materials E' is nearly equal to the elastic tensile modulus. The imaginary part of the modulus E" is a damping term known as the loss modulus. The phase angle between the output force and driver crystal displacement is δ and the loss tangent is defined by

$$\tan \delta = \frac{E''}{E'} \quad \text{or} \quad \frac{G''}{G'} \qquad (4)$$

ORIGINAL PAGE
BLACK AND WHITE PHOTOGRAPH

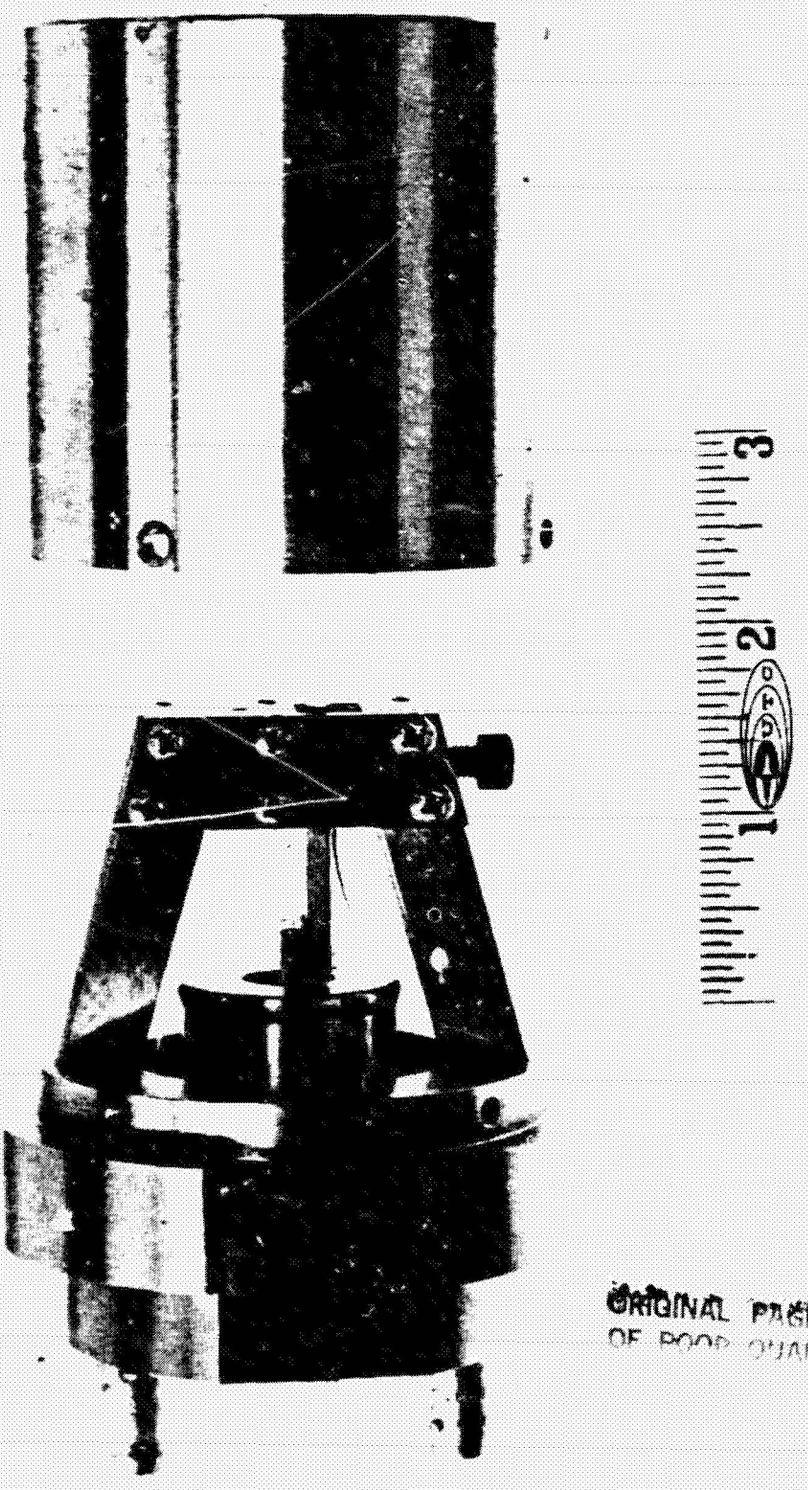

ORIGINAL PAGE IS
OF POOR QUALITY

Figure 3-18. Dynamic Shear Test Apparatus and Isolation Cover

14329

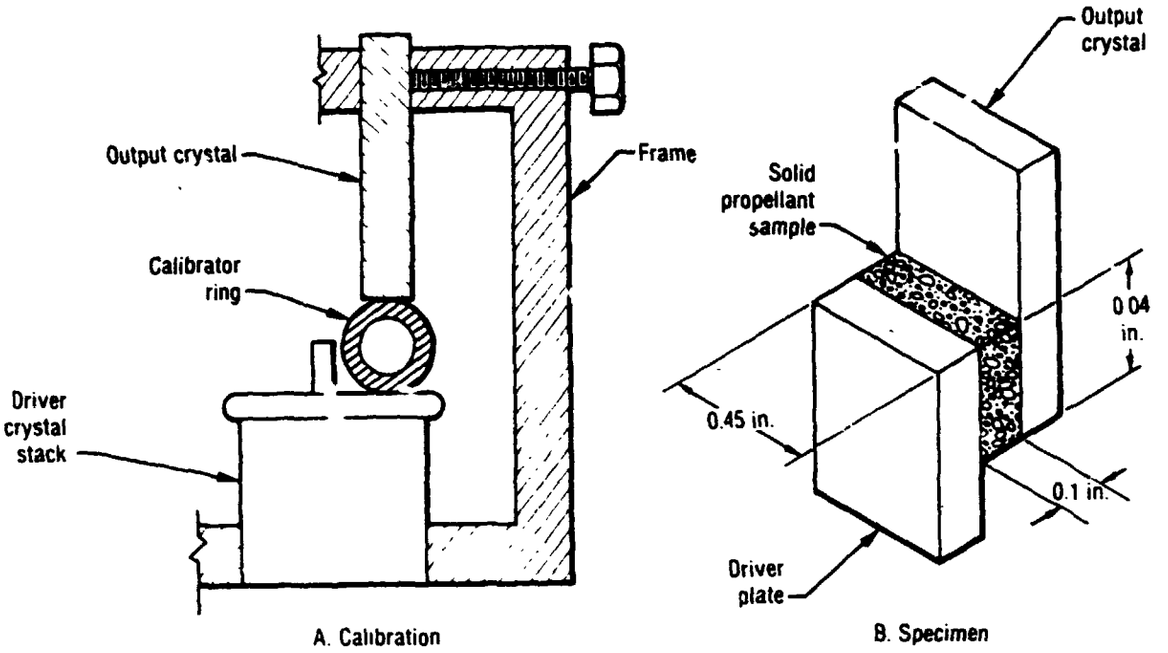

Figure 3-19. Schematic of Calibration Setup and Specimen

14314

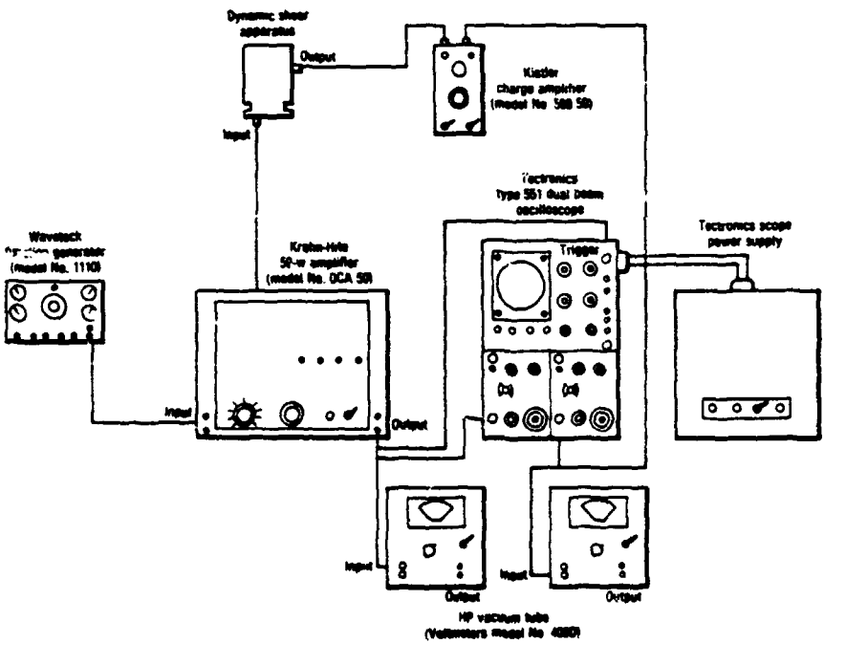

Figure 3-20. Electrical Equipment for Dynamic Shear Test

14313

For composite propellants the viscoelastic modulus is generally represented by a Prony series

$$E(t) = A_o + \sum_{i=1}^{n} A_i e^{-\alpha_i t} \qquad (5)$$

$$\text{or } G(t) = B_o + \sum_{i} = B_i e^{-\alpha_i t} \text{ (for shear)}$$

where the A's and B's are the Prony series coefficients and the α's are the time constants.

The real and imaginary parts of the complex modulus for a linear viscoelastic material can be calculated from the Prony series using

$$E'(w) = \sum_{i=0}^{n} \frac{A_i w^2}{w^2+\alpha_i^2}$$

$$E''(w) = \sum_{i=0}^{n} \frac{A_i w\alpha_i}{w^2+\alpha_i^2}$$

However, this conversion does not work well for propellants which usually exhibit nonlinear modulus variations [4,5].

The dynamics shear test device provides a direct measurement dynamic properties as a function of frequency and test temperature. The equipment is calibrated using stainless steel rings inserted between the piezoelectric driver stack (figure 3-19) and the readout crystal which are excited over a wide frequency range. During propellant tests the output signal and the phase angle are measured to determine the dynamic properties of the propellant over the desired frequency and test temperature ranges.

The dynamic strain amplitude and the static compressive strain levels can be varied to determine the modulus sensitivity to various loading conditions.

3.3.1 Dynamic Shear Propellant Data

The dynamics shear modulus behavior was measured for each of the six batches of Shuttle SRM propellant. Production batch No. TP-H1148-9 was

evaluated at three static and three dynamic strain levels. Test data at one strain level were obtained for each of the other batches of propellant at 90°, 72° and 40°F.

3.3.2 Batch No. TP-H1148-9

Dynamic modulus curves are presented in figures 3-21, 3-22, and 3-23 for batch No. TP-H1148-9 at 0.001% dynamic strain and static strain levels of 3%, 6% and 12%. A comparison of G' curves for each of these tests is presented in figure 3-24. Static strain sensitivity of batch No. TP-H1148-9 at 100 Hz and 72°F illustrates the dynamic modulus increase with compressive static strain levels:

Compressive Strain, %	G', psi
3	2,070
5.8	2,950
12	6,250

where temperature = 72°F, and dynamic strain = 0.001%.

Test data in figures 3-21, 3-22, and 3-23 shows that G' actually drops lower than G" at the 90°F test temperature for the 3% and 6% static strains. The soft propellant at 90°F is absorbing a larger percentage of the energy input to the sample or the sample may not be transmitting the load because of slippage.

Empirical shift factors at the three temperatures are independent of strain levels (figure 3-25). The WLF equation is also the same since strain dependence is not considered in its derivation.

Dynamic shear moduli as a function of dynamic strain level are presented in figures 3-26 through 3-29. The real part of the dynamic modulus did increase with decreasing strain level but the total change in modulus is less than 50%. This is a much smaller amplitude change than experienced with compressive static strain variations.

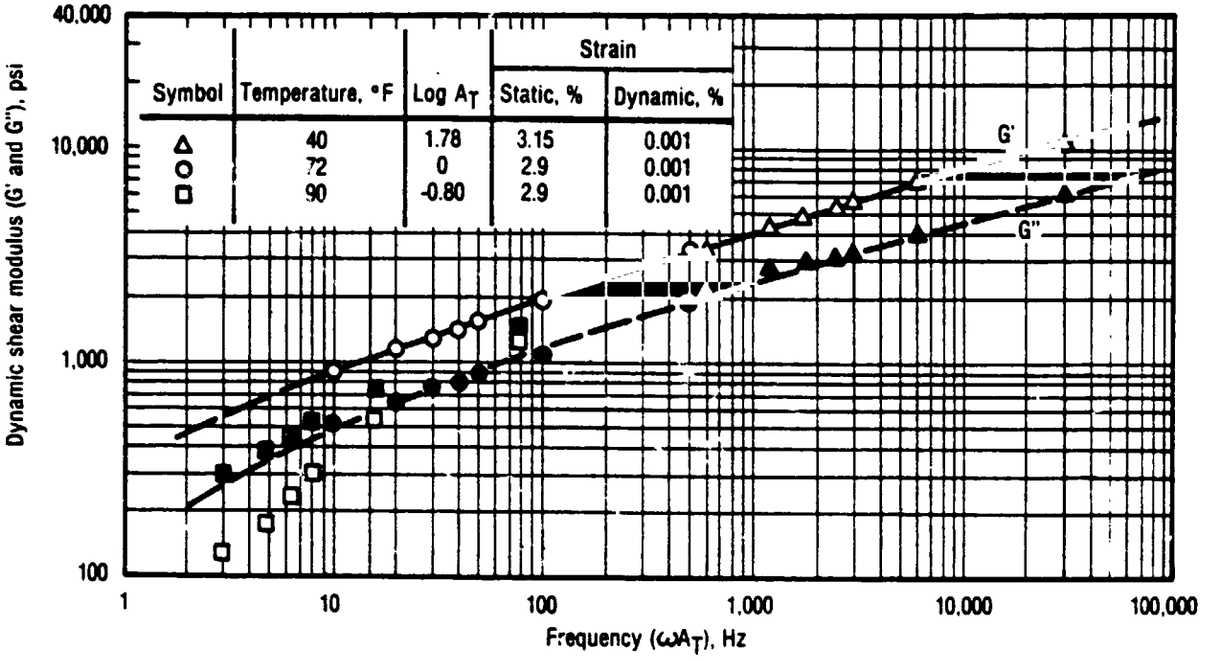

Figure 3-21. Master Dynamic Shear Modulus for Batch No. TP-H1148-9 at 3% Static and 0.001 Dynamic Strains

14312

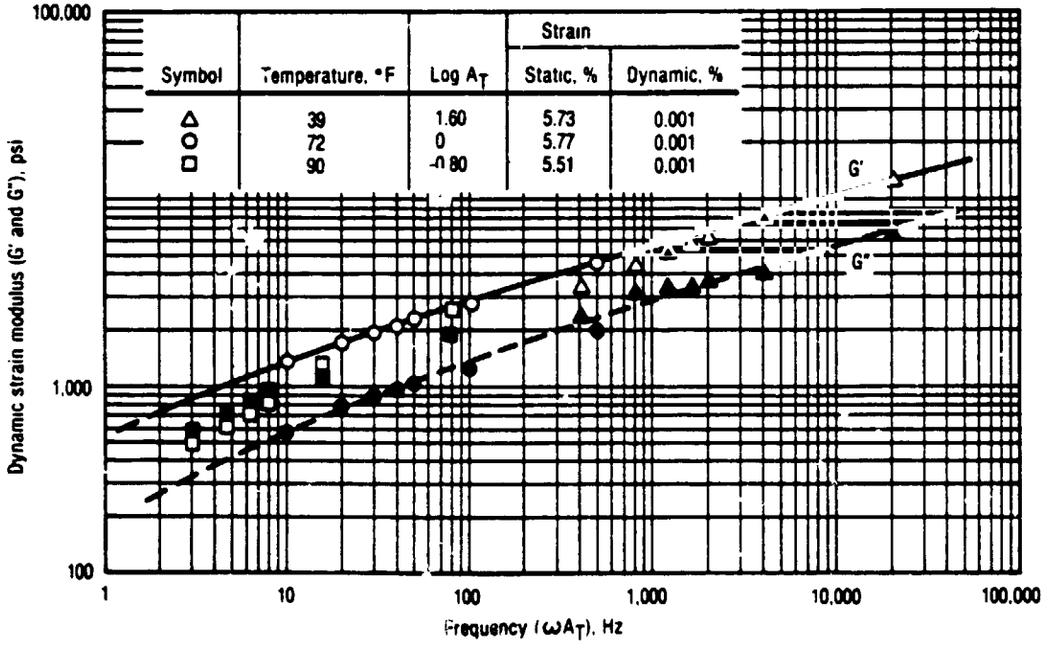

Figure 3-22. Master Dynamic Shear Modulus for Batch No. TP-H1148-9 at 6% Static and 0.001% Dynamic Strains

14311

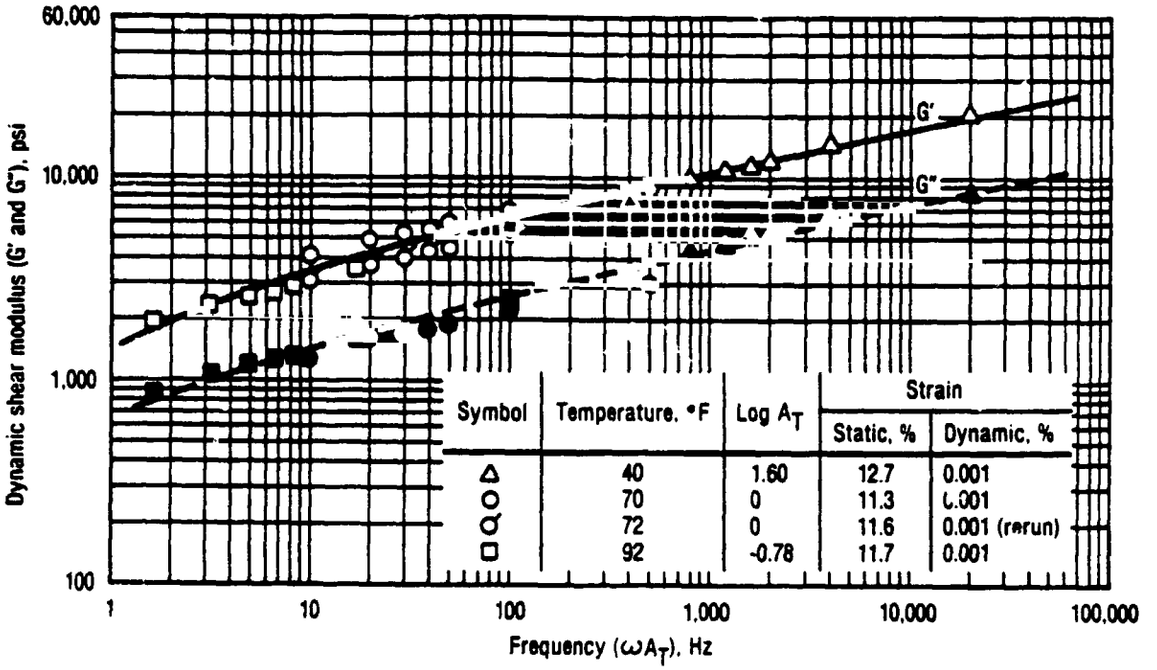

Figure 3-23. Master Dynamic Shear Modulus for Batch No. TP-H1148-9 at 12% Static and 0.001% Dynamic Strains

14310

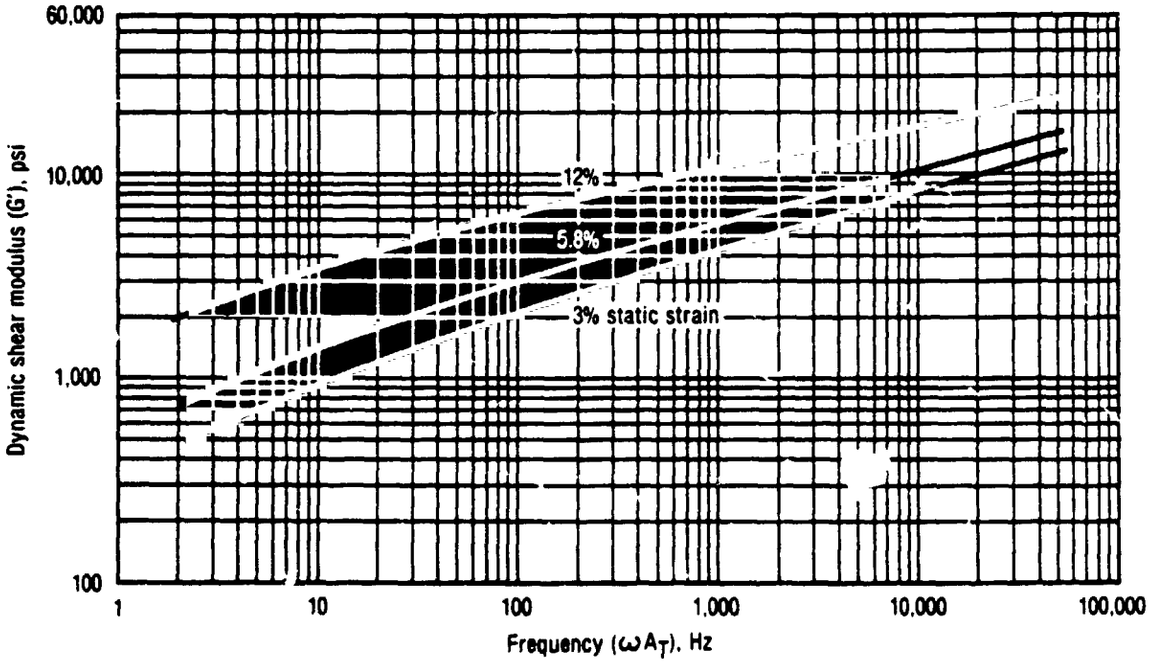

Figure 3-24. Comparison of Static Strain Levels for Batch No. TP-H1148-9

14309

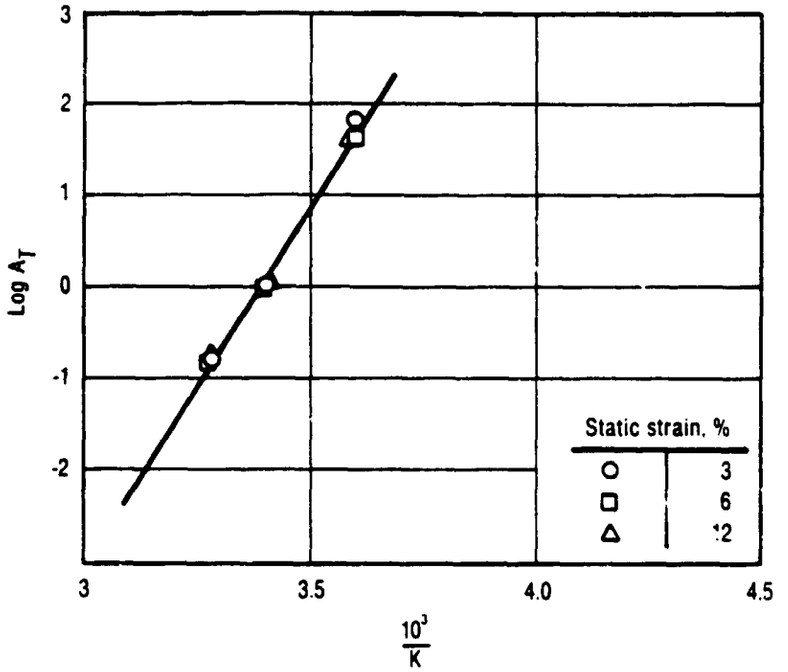

Figure 3-25. Shift Factors for Batch No. TP-H1148-9 at 0.001% Dynamic and 3% Static Strain Levels

14308

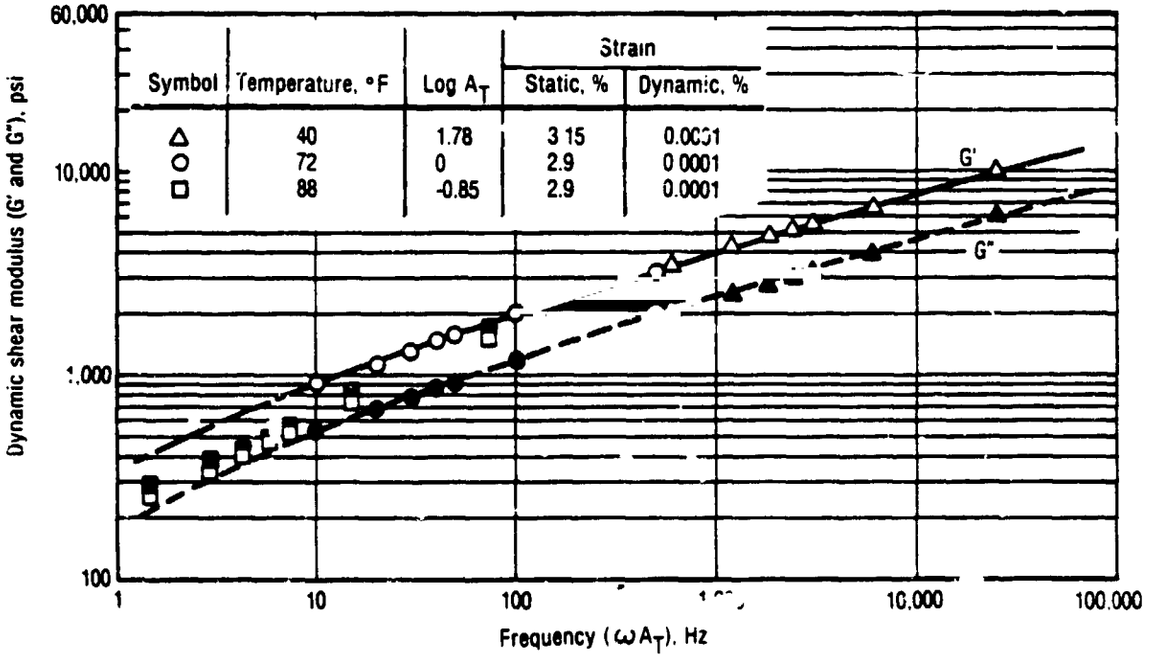

Figure 3-26. Master Dynamic Shear Modulus for Batch No. TP-H1148-9 at 3% Static and 0.0001% Dynamic Strain

14307

REPORT DISTRIBUTION

National Aeronautics & Space Administration
George C. Marshall Space Flight Center
Marshall Space Flight Center, Alabama 35812

Code	Number of Copies
ED23	10
EM34-01	1
AT01	1
As21D	5
AP13-K	1

Chief, DCASD Salt Lake City
1745 West 1700 South
Salt Lake City, Utah 84104

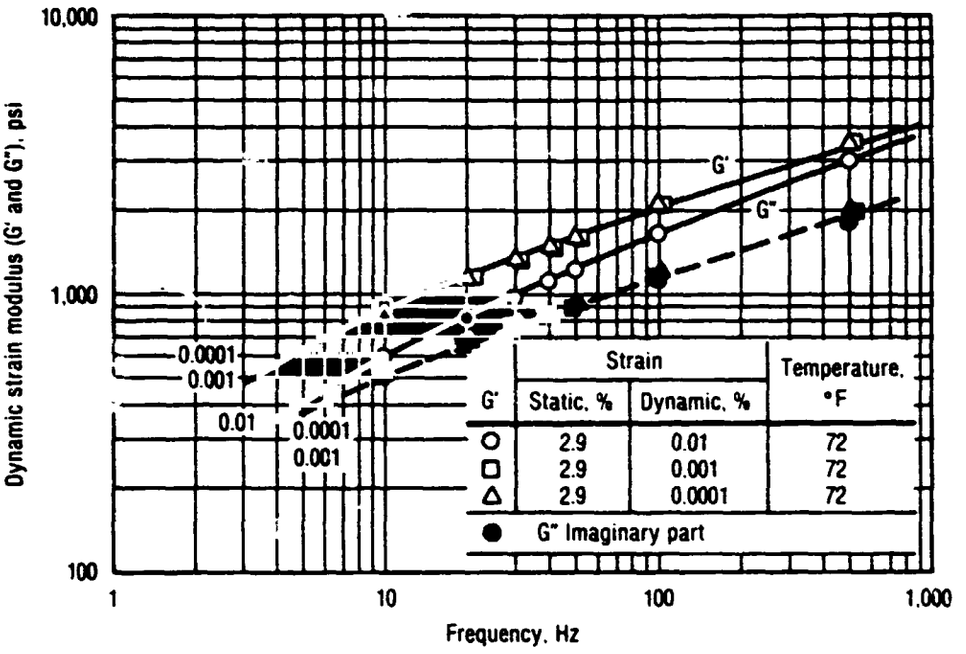

Figure 3-27. Comparison of Shear Modulus for Batch No. TP-H1148-9 at 2.9% Static and Different Dynamic Strain Levels

14306

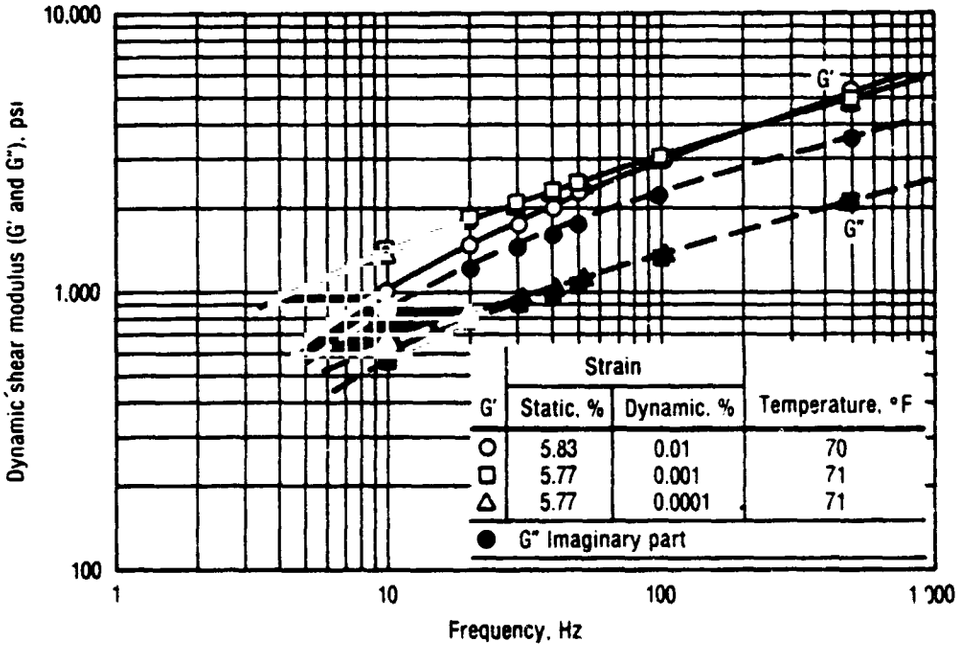

Figure 3-28. Comparison of Shear Modulus for Batch No. TP-H1148-9 at 5.8% Static and Different Dynamic Strain Levels

14305

C-3

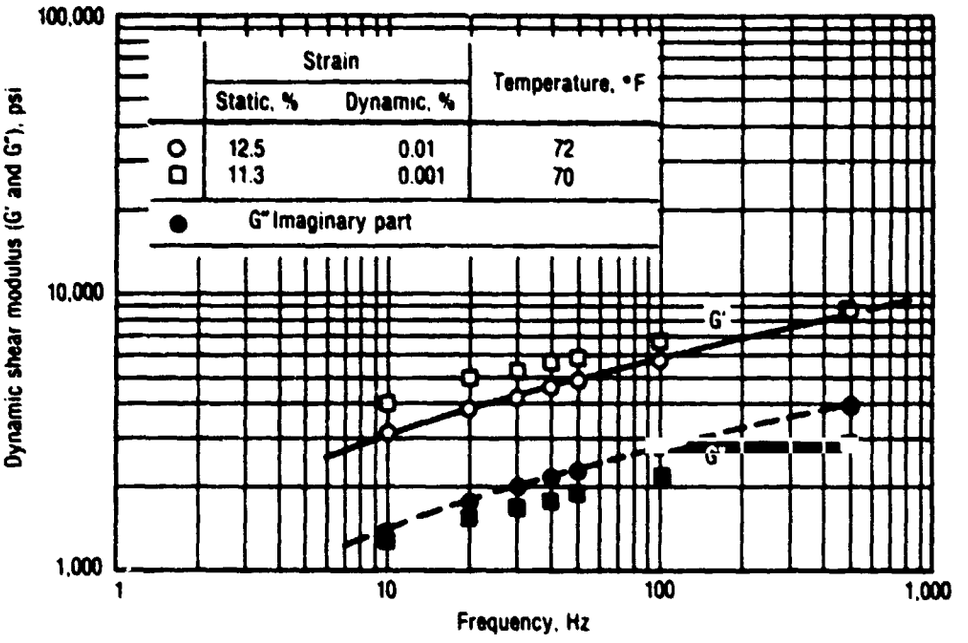

Figure 3-29. Comparison of Shear Modulus for Batch No. TP-H1148-9 at 12% Static and Different Dynamic Strain Levels

14304

Dynamic test results for the other batches of propellant are pre sented in figures 3-30 through 3-34. These batches are very similar to the major batch (-9). The real part of the dynamic modulus for each of the six batches is presented in figure 3-35.

The real part of the dynamic modulus at 100 Hz is given below:

Batch No.	G', psi at 100 Hz
9970115	3,100
-9	2,120
-7	2,120
-8	2,100
9970096	1,900
-6	1,800

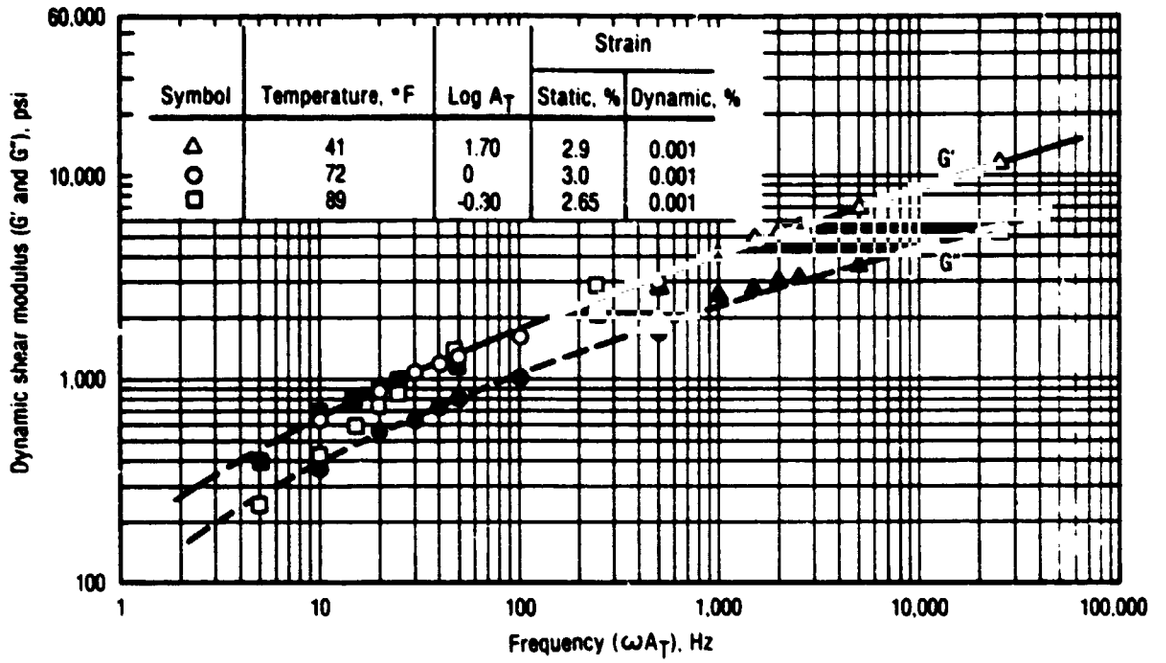

Figure 3-30. Master Dynamic Shear Modulus for Batch No. TP-H1148-6 at 3% Static and 0.001% Dynamic Strains

14303

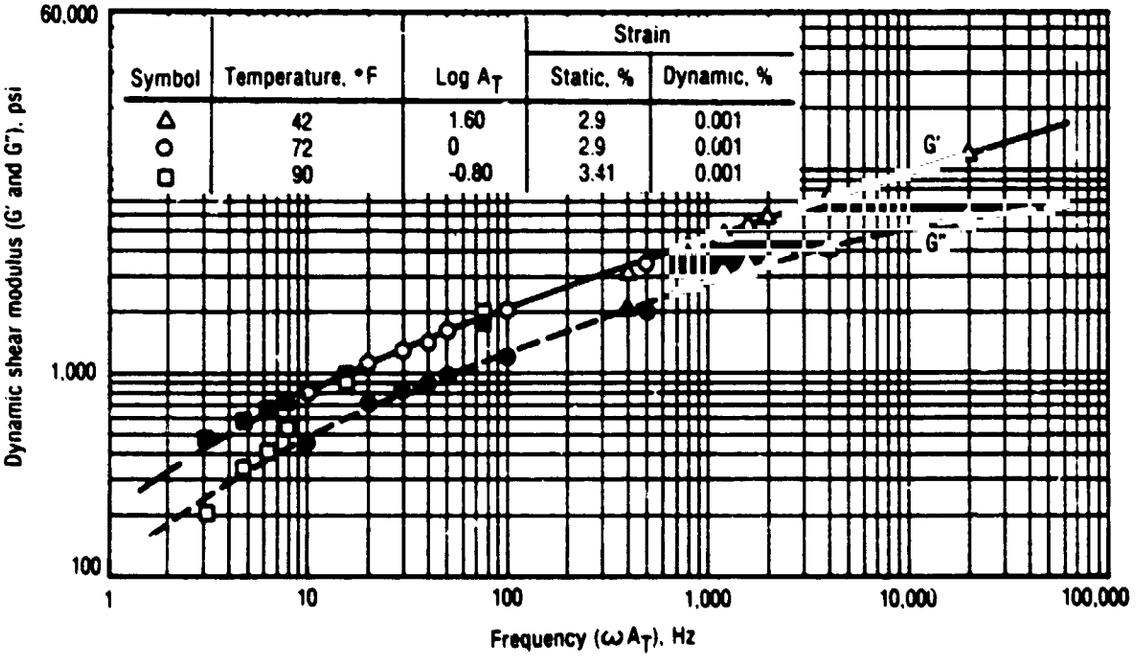

Figure 3-31. Master Dynamic Shear Modulus for Batch No. TP-H1148-7 at 3% Static and 0.001% Dynamic Strains

14302

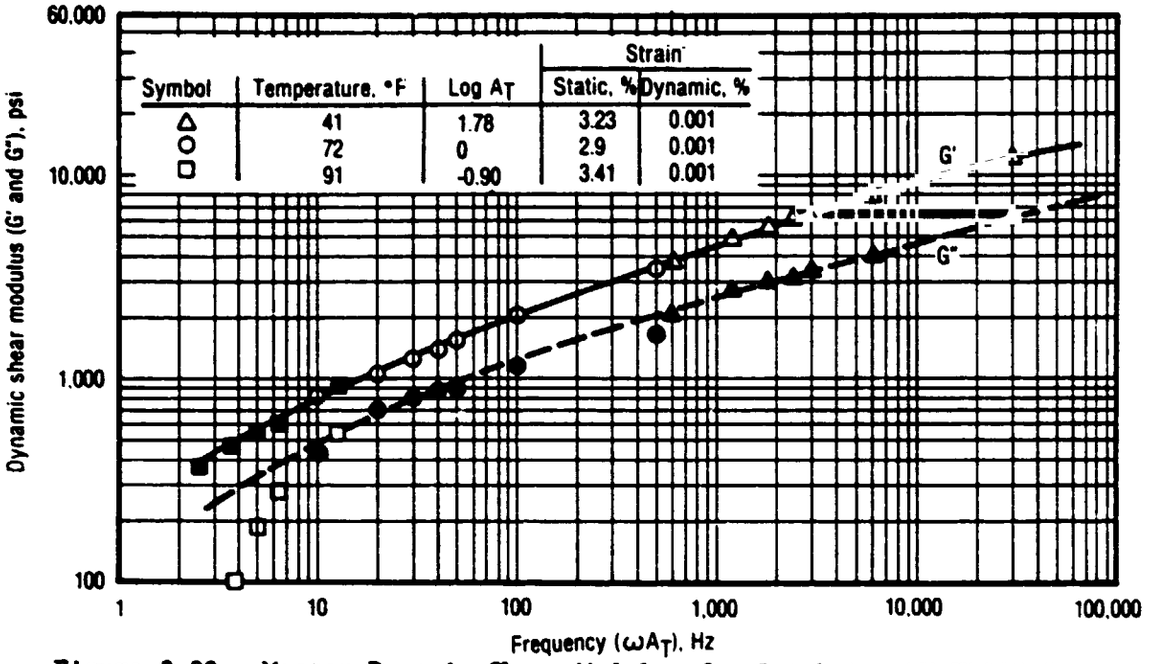

Figure 3-32. Master Dynamic Shear Modulus for Batch No. TP-H1148-8 at 3% Static and 0.001% Dynamic Strains

14301

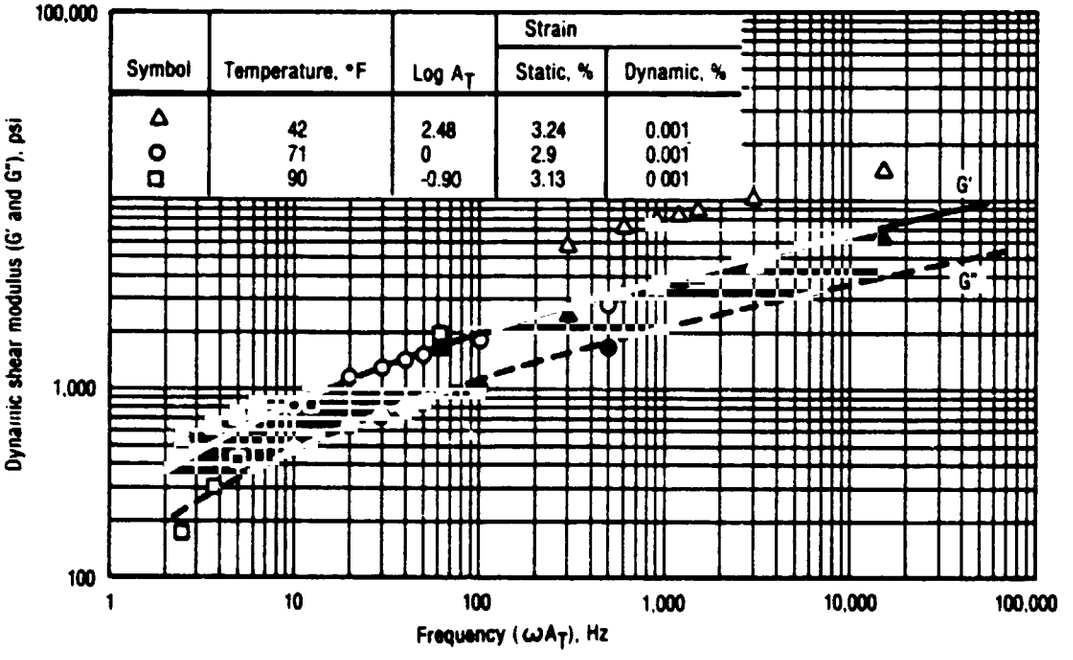

Figure 3-33. Master Dynamic Shear Modulus for Batch No. TP-H1148-9970096 at 3% Static and 0.001% Dynamic Strains

14300

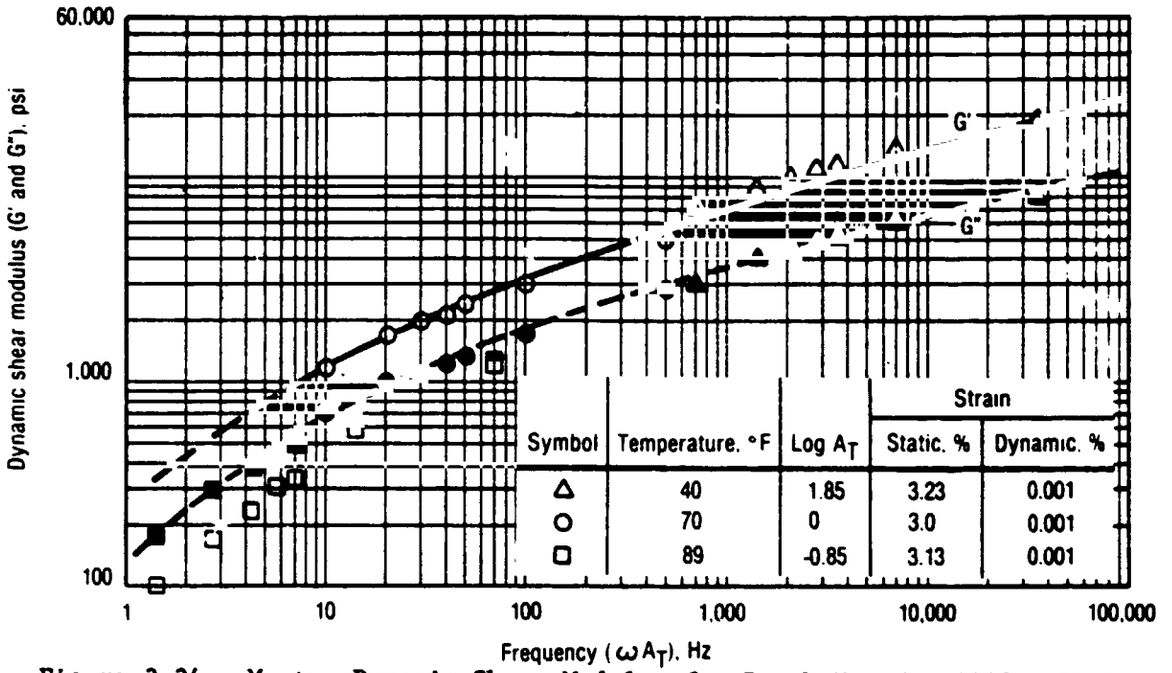

Figure 3-34. Master Dynamic Shear Modulus for Batch No. TP-H1148-9970115 at 3% Static and 0.001% Dynamic Strains

14299

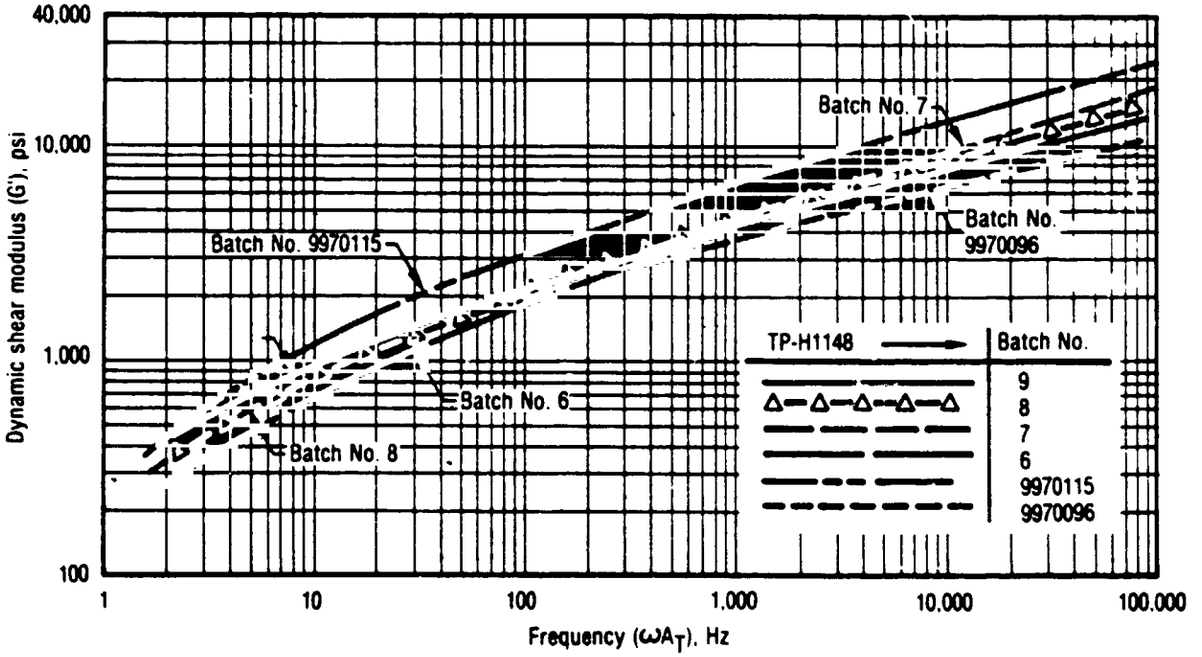

Figure 3-35. Between Batch Comparison of Propellant TP-H1148 Real Part of Dynamic Shear Modulus at 3% Static and 0.001% Dynamic Strains

14298

Batch No. 9970115 has the highest dynamic modulus with the others being close together; batch No. TP-H1148-6 is the lowest.

The real and imaginary part of the dynamic shear modulus values at 50 Hz are presented in table 3-3 for batch -9 and in table 3-4 for the other five batches. Individual values are listed along with mean values.

TABLE 3-3. REAL AND IMAGINARY DYNAMIC SHEAR MODULUS FOR BATCH NO. TP-H1148-9 COMPARED AT 50 Hz

T3182

Test	G'	G"	Test	G'	G"	Test	G'	G"	Test	G'	G"	Test	G'	G"
S 2.9%	1237	899	S 5.83%	2292	1665	S 12.52%	4544	2624	S 2.9%	312	540	S 3.15%	5727	3306
D 0.01	1202	873	D 0.01%	2228	1741	D 0.01%	4592	2651	D 0.001%	304	527	D 0.001%	5773	3333
T 72°F	1219	886	T 70°F	2287	1662	T 72°F	4724	2407	T 90°F	302	522	T 40°F	5864	3386
	1096	796		2124	1782		4945	2202		302	522		5910	3412
	1113	809		2166	1817		4929	2194		305	528		5818	3359
	1379	1002		2124	1782		4929	2194						
	1273	925		2220	1613		4787	2131						
	1273	925		2119	1655		4787	2131	S 2.9%	524	582	S 3.15%	5131	2962
	1132	822		2097	1638		4787	2131	D 0.0001%	524	582	D 0.0001%	5360	3095
	1252	909		2153	1564		4812	2142	T 88°F	524	582	T 40°F	5487	3168
Mean	1190	885		2181	1692		4784	2281		524	582		5487	3168
										524	582		5366	3098
S 2.9%	1566	904	S 5.77%	2540	1131	S 11.3%	5659	1839						
D 0.001%	1427	824	D 0.001%	2492	1110	D 0.001%	5711	1856						
T 72°F	1518	876	T 71°F	2324	1035	T 70°F	5763	1873						
	1674	966		2139	952		5763	1873	S 5.51%	827	905	S 5.73%	6326	3652
	1304	753		2514	1119		5759	1839	D 0.001%	825	917	D 0.001%	6476	3739
	1727	997		2275	1013		5804	1886	T 90°F	825	917	T 39°F	6463	3731
	1612	931		2275	1013		5649	1836		827	919		6450	3724
	1499	866		2469	1099		5649	1836		826	914		6429	3712
	1542	957		2109	939		5701	1852						
	1554	908		2334	982		5752	1869						
Mean	1542	898		2347	1039		5711	1856						
S 2.9%	1589	917	S 5.77%	2444	1088				S 11.67%	2707	1205	S 12.73%	11042	4916
D 0.0001%	1495	863	D .0001%	1965	875	S 11.6%	4480	1456	D 0.001%	2913	1297	D 0.001%	11955	5322
T 72°F	1774	1024	T .1°F	2051	1184	D 0.001%	4380	1423	T 92°F	3008	1339	T 40°F	11115	4949
	1706	985		2536	1129	T 72°F	4206	1367		3056	1361		11695	5207
	1541	890		2323	1034		4355	1415		2921	1300		11452	5098
	1696	979		2299	1023	Rerun								
	1352	780		2205	982									
	1499	866		2540	1134									
	1499	866		2163	963									
	1566	901		2279	1042									
Mean	1572	907		2282	1045									

Notes S = Static Strain
D = Dynamic Strain
T = Temperature

TABLE 3-4. REAL AND IMAGINARY DYNAMIC SHEAR MODULUS FOR OTHER BATCHES OF TP-H1148 PROPELLANT COMPARED AT 50 Hz

T3183

Notes: T = Temperature
D = Dynamic Strain
S = Static Strain

Batch -6			Batch -7			Batch -8			Batch 9970096			Batch 9970115		
Test	G'	G"	Test	G'	G"	Test	G'	G"	Test	G'	G"	Test	G'	G"
S 29%	5761	2936	S 2.9%	6252	3610	S 3.23%	6020	3067	S 3.24%	8340	3713	S 3.05%	11100	4942
D 0.001%	5511	3182	D 0.001%	6160	3556	D 0.001%	5806	2958	D 0.001%	8423	3750	D 0.001%	11183	4979
T 41°F	5729	2919	T 42°F	6009	3469	T 41°F	6260	3190	T 42°F	8455	3765	T 40°F	11108	4946
	5486	3167		5963	3442		6576	3351		8854	3942		11235	5002
	5693	2901		5963	3442		6651	3389		8912	3968		11138	4959
	5571	3216		5963	3442		6664	3396		8929	3975		11508	5123
	5589	3227		5894	3403		6651	3389		9293	4137		11077	4932
	5566	3214		5789	3342		6638	3382		8848	3939		11055	4922
	5519	3187		5778	3336		6728	3428		9374	4174		11055	4922
	5566	3214		5858	3382		6678	3402		9234	4111		10981	4889
Mean	5599	3116		5963	3442		6467	3294		8866	3947		11144	4962
S 3.00%	1230	799	S 2.89%	1317	855	S 2.89%	1490	860	S 2.9%	1561	902	S 3.00%	2176	1256
D 0.001%	1404	912	D 0.001%	1674	966	D 0.001%	1535	866	D 0.001%	1443	833	D 0.001%	2312	1335
T 73°F	1291	839	T 72°F	1447	836	T 73°F	1490	860	T 71°F	1490	861	T 70°F	2382	1375
	1212	787		1719	992		1628	940		1497	862		2419	1397
	1212	787		1447	836		1538	888		1511	873		2405	1388
	1313	853		1523	989		1595	921		1511	873		2419	1397
	1269	824		1498	973		1572	908		1497	864		2419	1397
	1173	762		1498	973		1458	842		1511	873		2428	1402
	1051	682		1564	1016		1365	788		1511	873		2475	1429
	1214	788		1527	947		1365	788		1511	873		2452	1415
Mean	1237	803		1521	938		1504	868		1504	869		2389	1379
S 2.65%	1039	1154	S 3.41%	549	756	S 3.41%	237	616	S 3.13%	345	598	S 3.13%	302	416
D 0.001%	875	972	D 0.001%	543	747	D 0.001%	266	598	D 0.001%	389	674	D 0.001%	330	455
T 89°F	875	972	T 90°F	540	744	T 91°F	273	546	T 91°F	433	751	T 89°F	334	460
	875	972		540	744		279	626		549	756		337	464
	862	958		539	742		275	618		568	782		344	473
	868	964		545	751		279	627		489	846		340	369
	850	944		539	742		288	646		502	869		350	481
	847	941		545	751		290	651		596	820		356	490
	844	937		542	746		288	646		714	793		356	490
	840	933		545	751		292	655		777	863		359	494
Mean	878	975		543	747		277	623		536	775		341	469

4.0 CONCLUSION

Selected mechanical properties of six batches of SRM solid propellant were measured using constant rate, stress relaxation, and dynamic shear test methods. Test data show very small batch-to-batch propellant variability and excellent sample-to-sample reproducibility. Stress relaxation modulus values are lower than the dynamic shear data, as expected for dynamic microstrain shear test conditions and the difference in time response. Dynamic propellant modulus values were sensitive to the static compressive strain level as well as dynamic strain. Some voids and fuel pockets were noted in the small dynamic shear test specimens which may explain the larger data variability than occurred with the larger test specimens used for the other test modes.

The test strain levels covered 0.001% to 3% and a correspondingly large modulus range. This strain range may be applicable to the Shuttle SRM dynamic loading conditions[6,7]. Specific modulus values for dynamic analysis can be selected from the available data by using the available NASTRAN computer results and defining the propellant strain range.

The compressive strain condition of the dynamic shear sample resembles the SRM motor loading during ignition as the grain will be in compression from the interior ballistic and a shear load will be applied by gravity and acceleration. This particular dynamic shear test[8,9] is more appropriate than the Gottenburg disc and other dynamic tests where the strain fields experience large gradients through the sample and are not representative of SRM conditions.

REFERENCES

1. "Constant Crosshead Rate Tensile Test," Section 4.3.5.2, ICRPG Solid Propellant Mechanical Behavior Manual, CPIA Publication No. 21, September 1963.

2. "Uniaxial Tensile Stress Relaxation Modulus Test," Section 4.3.6.1, ICRPG Solid Propellant Mechanical Behavior Manual, CPIA Publication No. 21, September 1963.

3. Williams, M. L , R. F. Landel and J. D. Ferry, "The Temperature Dependence of Relaxation Mechanisms in Amorphous Polymers and Other Glass-Forming Liquids," The Journal of The American Chemical Society, Vol. 77, July 20, 1955, pp. 3701-3707.

4. Schapery, R. A., "A Nonlinear Constitutive Theory for Particulate Composites Based on Viscoelastic Fracture Mechanics," JANNAF Operational Serviceability and Structures and Mechanical Behavior Working Groups - 1974 Combined Annual Meeting, CPIA Publication No. 253, July 1974, pp. 313-328.

5. Francis, E. C. and C. H. Carlton, "Some Aspects of Nonlinear Mechanical Behavior of a Composite Propellant," Journal of Spacecraft and Rockets, Vol. 6, No. 1, January 1969, pp. 65-69.

6. Francis E. C., R. L. Peeters and S. A. Murch, "Nonlinear Effects in Thermal Stress Analysis of a Solid Propellant Rocket Motor," Society of Engineering Science, 13th Annual Meeting, November 1976.

7. Francis E. C., R. L. Peeters and W. L. Hufferd, "Considerations in the Applications of Nonlinear Structural Materials," Second International Conference on Mechanical Behavior of Materials, Boston, Massachusetts, August 1976.

8. Miles, D. O., "Senusoidal Shear Generator For Study of Viscoelasticity," J. Appl. Phys. (33) 1962, pp. 1422.

9. Miles, D. O., G. C. Knollman and A. S. Hamamoto, "Technique for Calibration of a Dynamic Rheological Shear Apparatus" The Review of Scientific Instruments, Vol. 36, No. 2, Feburary 1965, pp. 158-161.

APPENDIX A
AUTOMATED DATA ACQUISITION SYSTEM

1.0 AUTOMATED DATA ACQUISITION SYSTEM

CSD currently interprets Instron test data using an automated data acquisition system. This results in a low cost data processing system which provides on-line acquisition of test data which is more accurate and reliable than handreduced data.

The equipment used in this automated data acquisition system is illustrated in figure A-1. The Instron is mated with a CSD-developed electrical interface package which is designed to transfer load, strain, and time information into a Wang 700 series programmable calculator. The interface system conditions the analog and digital signals from the testing machine and formats the data for correct entry into the calculator.

The test operator inserts the program into the Wang calculator using standard tape cassettes and manually inputs the test identification and test constants using the calculator keyboard. An output printer provides tabular and graphical test results and statistics in a report-type format.

The Wang calculator-interface system is used to automate the ICRPG standard rate testing and data reduction. The test data (stress and strain) are collected, reduced, and presented as E_o, σ_m, ϵ_m, σ^c_m, ϵ^c_m, and ϵ_r. User options and calculation details are summarized below.

1.1 DATA COLLECTION

A Strain

A constant crosshead rate (X) yields a simple relationship between strain (ϵ) and elapsed time (T).

$$\epsilon = XT/(\text{gage length}) \qquad \text{(A-1)}$$

The system actually measures time on a 60-cycle clock and calculates all strain using equation A-1.

B. Stress

The system collects load information at uniformly spaced strain intervals (IC). The value collected is actually a percentage (P) of a selected full-scale load range (R). The stress values are calculated by.

$$\sigma = (PR)/(\text{sample area}) \qquad \text{(A-2)}$$

C. Strain Intervals

Load information is collected at uniformly spaced strain intervals of

$$\delta\epsilon = 1.01\% \quad \text{for } X = 20 \text{ in./min} \qquad \text{(A-3)}$$
$$\delta\epsilon = 0.60\% \quad \text{for } X = 2 \text{ in./min}$$

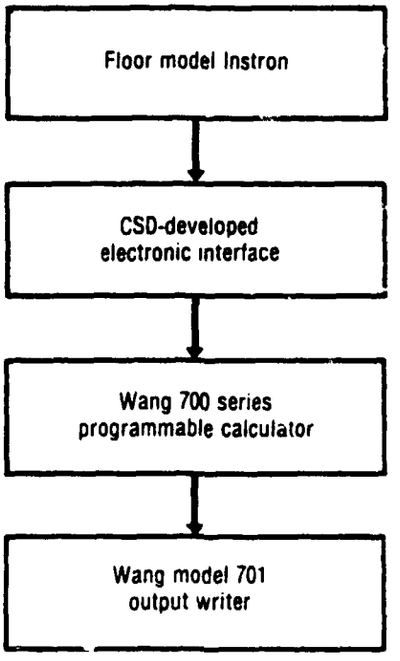

Figure A-1. CSD-Automated JANNAF Data Acquisition System

14297

The calculator storage capacity is limited to a maximum of 134 load values which correspor to a maximum strain of

$$\epsilon_{max} = 135\% \quad \text{for } X = 20 \text{ in./min} \qquad \text{(A-4)}$$
$$\epsilon_{max} = 80\% \quad \text{for } X = 2 \text{ in./min}$$

These values seem reasonable for appropriate resolution over a wide range of test conditions. Unusual propellant properties or extreme test temperatures may find $\delta\epsilon$ too large (insufficient resolution) or too small (small ϵ_{max} or δ load in the noise level). For $X < 5$ in./min, the operator can change $\delta\epsilon$ and consequently ϵ_{max} by inputting Y into register 26:

$$Y = \text{INT}\left| \frac{20\delta\epsilon}{X} - 2 \right| \qquad \text{(A-5)}$$

1.2 DATA REDUCTION

A. Initial Modulus

Three initial modulus values are listed: E, E1 and E4. The calculation of these values involves a search through the stored stress data for the maximum $\Delta\sigma$ over a certain $\Delta\epsilon$ range. The initial modulus is defined as

$$E_o = 1.05\ (\Delta\sigma/\Delta\epsilon)_{max} \qquad (A\text{-}6)$$

The three reported values differ in the $\Delta\epsilon$ (and corresponding $\Delta\sigma$) range. E, E1, and E4 are calculated over increments of $\Delta\epsilon = 2\delta$, δ'', and 4δ, respectively. Since CSD's method of discrete data collection segments the true stress strain curve, listing three values should give a better feel for the initial behavior of the curve.

B. Zero Strain Point

A zero strain point is necessary only to define other strains or at least one other strain to be used as reference. The zero strain point is indirectly located by assuming that the stress-strain curve, previous to the initial modulus E, is a linear curve. From equation A-6 E and the stress value (σ_o) at the point where E is calculated are known, so the strain (ϵ_o) at this point is

$$\epsilon_o = \sigma_o/E \qquad (A\text{-}7)$$

ϵ_o is a reference point from which all other strains are generated.

C. Maximum Stress and Strain

The maximum stress value (σ_m) is found by making a scan through the stored stress values. The strain at this point is found by counting the number of strain intervals ($\delta\epsilon$) from ϵ_o. Assuming M intervals, then,

$$\epsilon_m = \epsilon_o + M\delta\epsilon \qquad (A\text{-}8)$$

Consequently, the minimum error associated with σ_m and ϵ_m is $\delta\epsilon$.

D. Maximum Corrected Stress and Strain

The maximum corrected stress ($\sigma^C{}_m$) is defined as $[(1 + \epsilon)\sigma]_{max}$; it is found by scanning for the largest product of stress x (corresponding strain + 1). $\epsilon^C{}_m$ is defined as the strain at the maximum corrected stress and found using equation A-8. The minimum error associated with $\sigma^C{}_m$ and $\epsilon^C{}_m$ is $\delta\epsilon$.

E. Failure Strain

The failure strain (ϵ_r) is defined as the strain at the rupture point, usually when $\sigma = 0$. ϵ_r is found by using equation A-3 and is accurate to $\delta\epsilon$.

1.3 OPTIONAL OUTPUT

In addition to the standard output described above, two optional outputs are available. They are the following:

A. Tabular Printout of ϵ, E_T, σ, and σ^C

The segmented curve, consisting of the collected stress points between ϵ_o and ϵ_r intervals, with $N \leq 134$ (default) user inputed. For the first stress point to lie within each interval, the following is calculated and printed.

ϵ = strain at the first data point to lie in each interval (equation A-8)

ET = $(\Delta\sigma/\Delta\epsilon)$ with $\Delta\epsilon = 2\,\delta\epsilon$ and centered above ϵ

σ = value of first stress point to lie in each interval

$\sigma^C = (1 + \epsilon)$; using ϵ and σ from above.

The listed values will not necessarily be equally incremented in strain (due to N-dependence) but rather the strain will correspond to actual stress data points (the first point in each interval). The last point is the failure point.

B. MD-20 Output

The segmented curve between ϵ_0 and ϵ_f is divided into 24 intervals and the first data point in each interval is converted from (ϵ, σ) to (x, y) in., with chart speed = X. The conversion is

$$X = \epsilon \cdot \text{(gage length)}$$

$$Y = 10\sigma \text{ (area)/(load range)} \qquad \text{(A-9)}$$

The 25th listed point is the failure point. The corresponding printout is in a format suitable for keypunching.

The user operational keys for the Instron code are shown in table A-1; a typical printout is shown in table A-2.

TABLE A-1. USER OPERATIONAL KEYS OF INSTRON CODE T3181

Key	Function	Explanation	Note
01	Load calibration	A continuous loop is entered which displays the load in the X-register	Loop is exited by keying PRIME
03	Print heading	The heading is printed with appropriate program stops to allow manual typing	03 automatically calls 04
04	Predata	Gage length (2.7 in.), XHD SPD (2 in./min) and load range (20 lb) are entered from the Wang keyboard	04 automatically calls 08
08	Initialize series	Statistics are cleared for starting a new series	08 automatically calls 10
10	Test	A program stop allows sample width (0.375 in.) and thickness (0.5 in.) to be entered; on keying GO, the test is run and a summary printed	10 resets itself for start of a new test
12	Reject	Rejects this sample from statistics	12 automatically calls 10
13	Tabular printout	A program stop allows entry of the maximum number of data points to be printed out (default value of 134 is the maximum possible); this additional printout consists of ϵ, E, S and σ	13 automatically calls 10
14	MD-20 printout	Additional printout used as input to the MD-20 code; the format is suitable for key-punching	14 automatically calls 10
15	Statistics	The mean and standard deviation for values of nonrejected samples is printed out; a program stop allows manual paper advance to a new page; key GO initiates summary printout starting with heading and leading into predata; keying 11 will skip the heading-predata printout and list only the samples	

TABLE A-2. TYPICAL PRINTOUT

WIDTH	THICK	AREA	E	Sm	Gm	σ^c_m	G^c_n	Gr	El	EA	REMARK
.374	.500	.187	629	89.5	26.9	115.6	30.7	32.9	629	620	

G	E	S	SIGMA	G	E	S	SIGMA	G	E	S	SIGMA	G	E	S	SIGMA
7.97	599	47.8	51.3	8.73	582	52.4	56.9	9.49	582	56.6	62.0	10.25	564	61.2	67.5
11.76	388	68.9	77.1	12.52	264	71.1	80.0	14.03	229	74.5	85.0	14.79	264	76.4	87.7
16.31	176	79.9	92.9	17.06	158	81.2	95.1	17.82	141	82.3	97.0	19.34	158	84.4	100.8
20.10	141	85.8	103.0	21.61	88	87.1	106.0	22.37	70	87.9	107.6	23.88	52	88.5	109.6
24.64	52	89.0	110.9	25.40	17	89.3	111.9	26.91	00	89.5	113.6	27.67	-17	89.3	114.0
29.19	-35	89.0	115.0	29.94	-35	88.7	115.3	31.46	-970	86.3	113.5	32.98		.0	.0

MD-20 INPUT

```
.........*.........*.........*.........*.........*.........*.........*
 25,   .215,1.79,   .235,1.96,   .256,2.12,   .276,2.29,   .317,2.59,
       .338,2.66,   .358,2.73,   .399,2.86,   .419,2.94,   .440,2.99,
       .481,3.09,   .501,3.12,   .542,3.21,   .563,3.24,   .583,3.26,
       .624,3.30,   .644,3.31,   .665,3.33,   .706,3.34,   .726,3.35,
       .767,3.34,   .788,3.33,   .808,3.32,   .849,3.23,   .890,0.00,
.........*.........*.........*.........*.........*.........*.........*
```

TYPICAL PRINTOUT

The above printout consists of the following three sections:

I. Standard Printout

The first two lines contain the standard printout which is outputed with each test, it is a summary of the data reduction, including the inputed sample dimensions, three modulus values, σ_m, ε_m, σ^c_m, ε^c_m, ε_r as well as space for a remark (i.e. good break, void, reject, etc.)

II. Tabular Printout

Following the standard printout is a table of tangent modulus, stress, and corrected stress at various strains. In this case N = 24; the curve from ε_o (7.97%) to ε_r (32.98%) was broken into 23 intervals. The first 23 points in the table are the first data points in each interval. The 24th point is the failure point. Note: The table is read from left to right.

III. MD-20 Printout

The 25 (x,y) pairs, described in the text, are printed in keypunch format.

APPENDIX B

DYNAMIC SHEAR CALCULATIONS AND COMPUTER OUTPUT

1.0 DYNAMIC SHEAR CALCULATIONS AND COMPUTER OUTPUT

The dynamic shear modulus was computed for the real and imaginary parts of the complex modulus with the following equations:

$$G' = \frac{L}{A} \beta \cos \phi \qquad \text{(Real)}$$

$$G'' = \frac{L}{A} \beta \sin \phi \qquad \text{(Imaginary)}$$

where L = sample thickness in inches (nominal 0.1 in.)

A = sample area in square inches; contact area between propellant and driver plate (nominal 0.18 $in.^2$)

β = calibration factor in lb/in.

ϕ = phase angle between input and output signals.

The β calibration curve versus output voltage is obtained from stainless steel rings cut from standard tubing with the following relationship

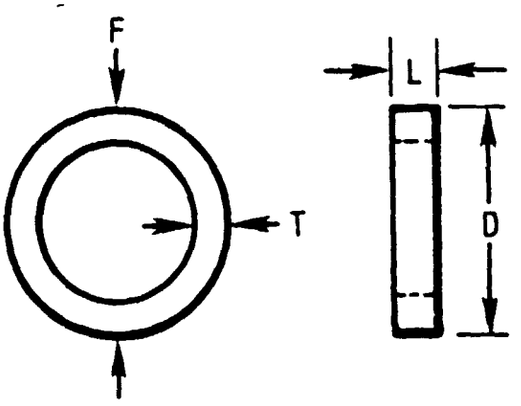

$$\Delta D = 0.224\ D^3\ F/YLT^3$$

$$\beta^2 = F/\Delta D = 4.46\ YL(T/D)^3$$

Y = Young's modulus

The rings are made from standard tubing with values of 0.25 to 0.30 in., wall thickness of 0.001 to 0.065 in., and length of 0.050 in. This provides a wide range of load calibrations.

The dynamic strain level is a linear function of the voltage applied to the driver stock of piezoelectric crystals and is calculated from

$$\epsilon = \frac{2|KV_{(o-p)}|}{L} \qquad \text{(B-3)}$$

where K = calibration constant

L = sample thickness

$V_{(o-p)}$ = applied voltage

ϵ = dynamic strain output from driver crystal.

A calibration curve is shown in figure B-1. Dynamic shear data reduction for batch No. TP-1148-9 is shown in table B-1.

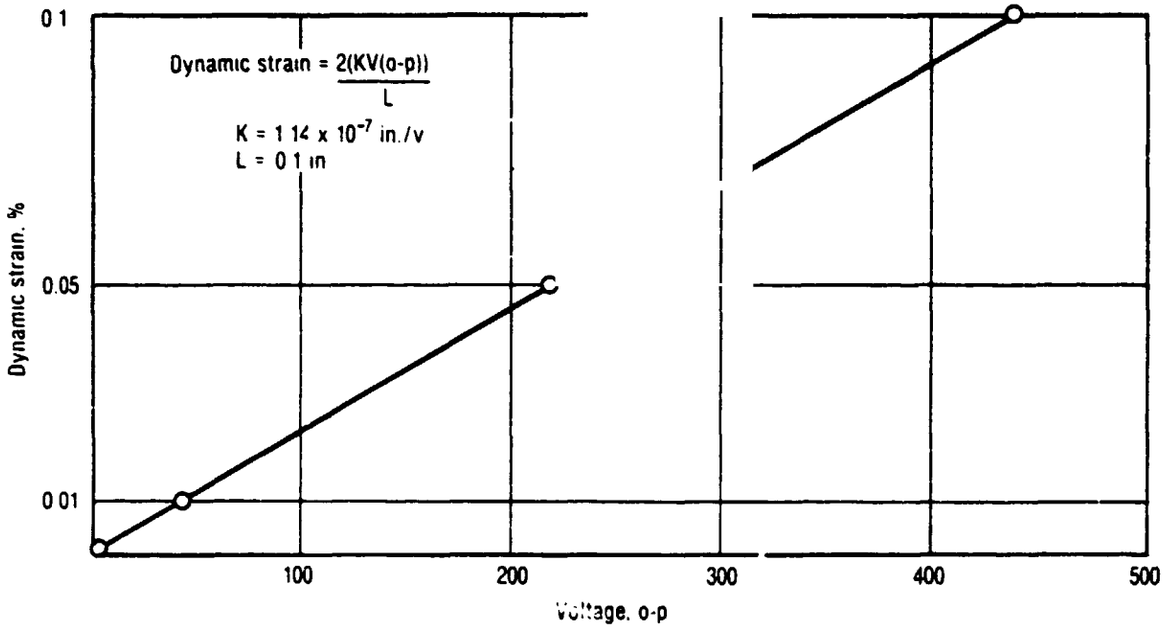

Figure B-1. Calibration Curve

14296

TABLE B-1. DYNAMIC SHEAR DATA REDUCTION FOR BATCH NO. TP-1148-9

DYNAMIC STRAIN - 0.00194
COMPRESSABILITY - 2.885%
DISPLACEMENT(Xo) -0.0031in
REFERENCE TEMP(To) - 77°F
INPUT VOLTAGE(Vo) - 0.250V
PARAMETERS FOR THE LINEAR log-log PLOT OF β vs (Vo/V): X-INTERCEPT - 4.45E-04 X-AXIS - 1.00E 02

REQUESTOR: C CARLTON
OPERATOR: VA
WOR: 2600-1100-0000
TEST DATE: 10-10-77

THE DATA REDUCTION USES THESE EQUATIONS:
BETA CURVE: β= 4.46YLt/d
DYNAMIC MODULUS: G= (To)(h/A)β(cosθ+isinθ)

Y-modulus,t-ring thickness,L-wall thickness and d-mean diameter (OD+ID)/2
G' and G'' are the real and imaginary components of G

SAMPLE # 1 72°F
AREA -0.100in²
THICKNESS -0.104in

FREQ(Hz)	PHASE(deg)	OUTPUT(mv)	G'(psi)	G"(psi)
500	30.00	7.7	3495.82	2010.31
100	30.00	4.5	2043.01	1179.53
50	30.00	3.5	1589.01	917.42
40	30.00	3.3	1498.21	864.99
30	30.00	3.0	1362.01	786.36
20	30.00	2.6	1180.41	681.51
10	30.00	2.0	908.01	524.24

SAMPLE # 2 73°F
AREA -0.100in²
THICKNESS -0.104in

FREQ(Hz)	PHASE(deg)	OUTPUT(mv)	G'(psi)	G"(psi)
500	30.00	7.1	3217.37	1857.55
100	30.00	4.2	1908.57	1005.75
50	30.00	3.3	1495.40	863.37
40	30.00	3.0	1359.45	784.88
30	30.00	2.7	1223.51	706.39
20	30.00	2.3	1042.25	601.74
10	30.00	1.8	793.01	457.85

SAMPLE # 3 71°F
AREA -0.100in²
THICKNESS -0.104in

FREQ(Hz)	PHASE(deg)	OUTPUT(mv)	G'(psi)	G"(psi)
500	30.00	8.0	3630.07	2100.90
100	30.00	4.9	2220.81	1200.80
50	30.00	3.9	1773.95	1024.19
40	30.00	3.7	1682.90	971.67
30	30.00	3.4	1523.70	879.75
20	30.00	3.0	1364.50	787.84
10	30.00	2.3	1046.10	604.01

SAMPLE # 4 71°F
AREA -0.100in²
THICKNESS -0.104in

FREQ(Hz)	PHASE(deg)	OUTPUT(mv)	G'(psi)	G"(psi)
500	30.00	8.0	3638.07	2100.90
100	30.00	4.8	2183.32	1260.54
50	30.00	3.8	1705.70	984.80
40	30.00	3.4	1546.50	892.88
30	30.00	3.1	1410.06	814.10
20	30.00	2.8	1250.86	722.19
10	30.00	2.1	932.46	538.36

ORIGINAL PAGE IS OF POOR QUALITY